DEVELOPMENT OF MULTIFUNCTIONAL CARBON NANOFIBER AGGREGATE FOR CONCRETE STRUCTURAL HEALTH MONITORING

A Dissertation

Presented to

The Faculty of the Department of Civil and Environmental Engineering

University of Houston

In Partial Fulfillment

of the Requirement for the Degree

Doctor of Philosophy

in Civil Engineering

by

Rachel N. Howser

August 2013

Development of Multifunctional Carbon Nanofiber Aggregate for Concrete Structural Health Monitoring

Rachel N. Howser

Approved:

Chairman of the Committee
Y. L. Mo, Professor,
Civil and Environmental Engineering

Committee Members:

Thomas T.C. Hsu, Moores Professor,
Civil and Environmental Engineering

Bora Gencturk, Assistant Professor,
Civil and Environmental Engineering

Gangbing Song, Professor,
Mechanical Engineering

Shin-Shem Pei, Professor,
Electrical Engineering

Suresh Khator, Associate Dean,
Cullen College of Engineering

Kasper Willam, Professor and Chairman,
Civil and Environmental Engineering

ACKNOWLEDGMENTS

I would like to express my genuine gratitude to Dr. Y. L. Mo for his guidance and encouragement during the course of this research. Additionally, I would like to offer my appreciation to Dr. Y. L. Mo, Dr. Thomas T.C. Hsu, Dr. Bora Gencturk, Dr. Gangbing Song, and Dr. Shin-Shem Pei for serving on my dissertation committee.

I would like to thank the National Science Foundation and the American Society of Civil Engineers for funding this research and Master Builders Inc. (USA) for generously donating chemical admixtures for this study.

I gratefully acknowledge my friends and fellow graduate students Y. Jeannot Ahossin, Christiana Chang, Yuping Liu, and Ivan Prestini for helping me carry out experimental work in the laboratory. I would also like to thank the laboratory technician, Gerald McTigret. I would also like to thank the researchers at Tongji University, especially Dr. Liang Lu, for their collaboration on this project.

Lastly, I would like to thank my friends and family for being continually supportive, especially my fiancé, Craig Roberts, who has helped me with the many projects I have brought home with me. Most of all I would like to thank God, without whom none of this would be possible.

DEVELOPMENT OF MULTIFUNCTIONAL CARBON NANOFIBER AGGREGATE FOR CONCRETE STRUCTURAL HEALTH MONITORING

An Abstract

of a

Dissertation

Presented to

The Faculty of the Department of Civil and Environmental Engineering

University of Houston

In Partial Fulfillment

of the Requirement for the Degree

Doctorate of Philosophy

in Civil Engineering

by

Rachel N. Howser

August 2013

ABSTRACT

Fiber research in concrete construction is an ongoing field and the use of carbon nanofibers (CNFs) will be examined in this study. Short-fiber composites are a class of strain sensor based on the concept of short electrically conducting fiber pull-out that accompanies slight and reversible crack opening. For a fiber composite to have strain sensing ability, the fibers must be more conducting than the matrix in which they are embedded, of diameter smaller than the crack length, and well dispersed. Their orientations can be random, and they do not have to touch one another. The electrical conductivity of the fibers enables the DC electrical resistivity of the composites to change in response to strain damage, hydration level, or temperature, allowing sensing.

Because of the high cost associated with CNFs, a CNF aggregate (CNFA) was developed. The CNFA is a 16.39 cm^3 (1.00 $in.^3$) cubic specimen of CNF mortar. The CNF mortar is self-sensing and can be used to determine the hydration level, damage, or temperature in the multifunctional CNFAs. The CNFAs can be embedded in reinforced or prestressed concrete structures and used to monitor early strength, determine the localized damage, or measure the temperature in a structure.

TABLE OF CONTENTS

LIST OF FIGURES

LIST OF TABLES

LIST OF ABBREVIATIONS

ACI	American Concrete Institute
CNF	Carbon Nanofiber
CNFA	CNF Aggregate
CNT	Carbon Nanotube
CSH	Calcium-Silicate-Hydrate
DC	Direct Current
EMI	Electromagnetic Interference
ERV	Electrical Resistance Variation
FEA	Finite Element Analysis
HRWR	High-Range Water Reducer
LET	Liquid Electrical Tape
LVDT	Linear Voltage Differential Transformer
LS	LeakSeal
MWCNT	Multi-Wall CNT
OpenSees	Open System for Earthquake Engineering Simulation
PCI	Precast/Prestressed Concrete Institute
SAC	Siliconized Acrylic Caulk
SCC	Self-Consolidating Concrete
SCCNFC	Self-Consolidating CNF Concrete
SCRC	Self-Consolidating Reinforced Concrete

SCSFC	Self-Consolidating Steel Fiber Concrete
SEM	Scanning Electron Microscope
SWCNT	Single-Wall CNT
TU	Tongji University
UH	University of Houston
UM	University of Michigan
VMA	Viscosity Modifying Agent

CHAPTER 1

INTRODUCTION

1.1 Overview of Research

The use of fibers to reinforce brittle materials can be traced back to ancient times when straw was added to mud bricks (ACI Committee 544 1996). The modern development of the use of fibers in construction began in the 1960s with the addition of steel fibers to reinforced concrete structures. This was closely followed by the addition of polymeric fibers, glass fibers and carbon fibers in the 1970s, 80s and 90s, respectively (Li 2002).

Fibers improve brittle materials such as concrete by enhancing tensile strength, ductility, toughness, and conductivity (Chen and Chung 1993a; Gao et al. 2009; Li et al. 2004; Li, Zhang, et al. 2007; Shah and Naaman 1976). In concrete, they enhance the material properties by arresting cracks. The cracking process within concrete begins with the onset of isolated nanocracks. These nanocracks grow together to form localized microcracks, which in turn grow together to form macrocracks. These macrocracks widen to form cracks visible with the naked eye. Fibers arrest these cracks by forming bridges across them. With increasing tensile stress, a bond failure eventually occurs, and the fiber will pull out of the concrete allowing the crack to widen.

Short-fiber composites are a class of strain sensor based on the concept of short electrically conducting fiber pull-out that accompanies slight and reversible crack opening. For a fiber composite to have strain sensing ability, the fibers must be more conducting than the matrix in which they are embedded, of diameter smaller than the crack length, and well dispersed. Their orientations can be random, and they do not have to touch one another (Chen and Chung 1996; Chung 1995). The electrical conductivity of the fibers enables the direct current (DC) electrical resistivity of the composites to change in response to strain damage or temperature, allowing sensing (Bontea et al. 2000; Chen and Chung 1996; Chung 1995; Gao et al. 2009; Li et al. 2004). Fig. 1.1 shows the bridging action of fibers across micro and macrocracks in concrete. An ideal concrete in terms of strength, ductility, toughness, and sensing would include nano, micro and macrofibers; however, this concrete is not currently economically feasible.

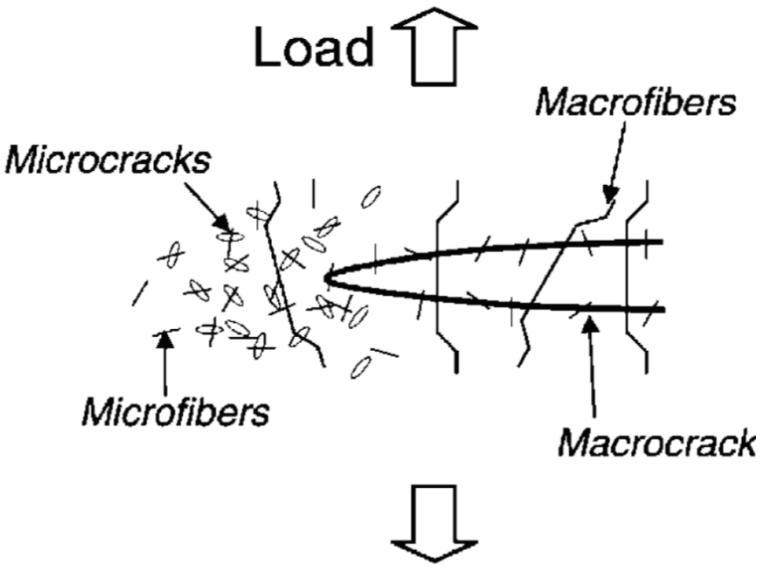

Fig. 1.1 Bridging Action of Fibers Across Micro and Macrocracks (Shah 2009)

Fiber research in concrete construction is an ongoing field and the use of carbon nanofibers (CNFs) is examined in this study. Because of past success at the University of Houston (UH) demonstrating that self-consolidating CNF concrete (SCCNFC) can be used as a strain sensor (Gao et al. 2009; Howser et al. 2011), a CNF aggregate (CNFA) was developed that can be used to determine localized damage in concrete structures. The development of a CNFA is significant because it is possible to use the strain sensing capabilities of SCCNFC with a greatly reduced cost since only the CNFAs placed in the structure would contain CNFs. The CNFA is self-sensing and can be used to monitor early strength, determine the localized damage, and measure the temperature of the structure in which it is embedded. The CNFAs can be embedded in reinforced or prestressed concrete structures.

The developed CNFA is 2.54 cm x 2.54 cm x 2.54 cm (1.00 in. x 1.00 in. x 1.00 in.) so that it is roughly the same size as a normal aggregate found in the concrete matrix. Fig. 1.2 shows a schematic of the CNFA using the four-probe method for the measurement of electrical resistance.

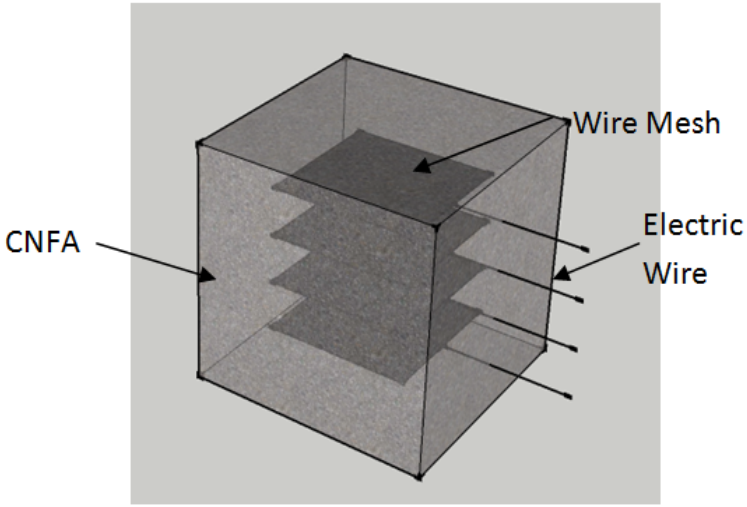

Fig. 1.2 CNFA Schematic

1.2 Objectives of Research

The objectives of this research can be summarized as follows:

1) To develop CNFAs with self-sensing capabilities for embedment in full-scale reinforced and prestressed concrete specimens.
2) Investigate the effects of water on CNFAs.
3) Investigate the effects of temperature on CNFAs.
4) Investigate the effects of strain on CNFAs.
5) Embed and test CNFAs in small- and large-scale infrastructure for structural health monitoring.

1.3 Outline of Dissertation

This dissertation is divided into nine chapters. Chapter 1 introduces an overview and the objectives of the research in addition to an outline of this dissertation. Chapter 2 presents a literature review of the past relevant work in self-consolidating and carbon nanofiber concrete research. Chapter 3 describes the development of the CNFAs. Chapter 4 presents a temperature study and shows how the CNFAs can be used as a temperature sensor in the absence of varying strain. Chapter 5 presents the effects of water and fresh concrete on CNFAs and their suitability for early strength monitoring. Chapter 6 includes a strain study in which CNFAs are tested monotonically and cyclically embedded in concrete cylinders. Chapter 7 presents a small-scale test in which CNFAs are embedded in the tension and compression regions of a reinforced concrete modulus of rupture beam. Chapter 8 includes a full-scale column tests in which the CNFAs are embedded. Chapter 9 presents the conclusion of the study and suggests future work.

CHAPTER 2
LITERATURE REVIEW

2.1 Introduction

Fiber research in concrete construction is an ongoing field and the use of carbon nanofibers (CNFs) is examined. Fibers improve brittle materials such as concrete by enhancing tensile strength, ductility, toughness, and conductivity. Short-fiber composites are a class of strain sensor based on the concept of short electrically conducting fiber pull-out that accompanies slight and reversible crack opening. For a fiber composite to have strain sensing ability, the fibers must be more conducting than the matrix in which they are embedded, of diameter smaller than the crack length, and well dispersed. Their orientations can be random, and they do not have to touch one another. The electrical conductivity of the fibers enables the direct current (DC) electrical resistivity of the composites to change in response to strain change or temperature, allowing sensing.

2.2 Nanotechnology in Concrete

Despite the fact that nanotechnology is a relatively recent development in scientific research, the introduction of the concept is credited to Nobel Prize winner Richard Feynman from his 1959 lecture, “There’s Plenty of Room at the Bottom” (Feynman 1960). Feynman considered the possibility of direct manipulation of individual atoms as a powerful form of synthetic chemistry. Decades later, Feynman’s concept morphed into the field of nanotechnology. According to the National Science Foundation and National

Nanotechnology Initiative, the definition of nanotechnology includes three elements (Roco 2007):

- The size range of the material structures under consideration should be approximately 100 nanometers;
- The nanotechnology should have the ability to measure or transform at the nanoscale;
- There should be properties that are specific to the nanoscale as compared to the macro or micro scale.

Following this definition, in the past 25 years nanotechnology has expanded from Feynman's idea and now finds applications in fields ranging from medical devices to nano-reinforced concrete (Howser et al. 2011; Narayan et al. 2004).

To date, the awareness and application of nanotechnology in the construction industry are increasing; however, progress is uneven in the current early stages of its practical exploitation. Bartos (Bartos 2006) presents three reasons for this phenomenon:

- The nature of the construction industry differs greatly from other industries doing research in nanotechnology. The final products coming from the construction industry are not mass-produced and require relatively long service lives, differentiating it from the products from the microelectronics, information technology, and automotive industries.
- Historically, there is a very low level of investment in construction research and development.

- Research in nano-related research and development requires very high initial capital investment

Despite these difficulties, there have been significant advances in nanoscience of cementitious materials with an increase in the understanding of basic phenomena in cement at the nanoscale. These include structural and mechanical properties of the hydrate phases, origins of cement cohesion, cement hydration, interfaces in concrete, and mechanisms of degradation (Mondal et al. 2007; Sanchez and Sobolev 2010). A major nanotechnology application is the inclusion of nano-sized reinforcement in cement-based materials such as carbon nanotubes or nanofibers.

2.3 Fiber Reinforced Concrete

Concrete, composed of fine and coarse aggregates held together by a hydrated cement binder, is one of the most important construction materials and is used in diverse project areas including foundations, high rise tower components, highways, and dams. Hydrated cement is a brittle material that is an order of magnitude stronger in compression than in tension. To compensate for this weakness, reinforcement consisting typically of rebar or fibers is added to the concrete.

The use of fibers to reinforce brittle materials can be traced back to ancient times when straw and horse hair was added to mud bricks, adobe, mortar, and plaster (ACI Committee 544 1996). The modern development of the use of fibers in construction began with the addition of steel fibers to reinforced concrete structures in the 1960s,

followed by the addition of polymeric, glass, and carbon fibers in the 1970s, 80s and 90s, respectively (V. Li 2002).

Fibers improve material properties in brittle materials such as concrete by enhancing tensile strength, ductility, toughness, and conductivity (Chen and Chung 1993b; Gao et al. 2009; Iijima 1991; Konsta-Gdoutos et al. 2010a; Li et al. 2004, 2006; Li, Zhang, et al. 2007; Naaman 1985; Shah and Naaman 1976). Fibers are typically used in two forms: short randomly dispersed fibers in a cementitious matrix or a continuous mesh of fibers used in thin sheets. This dissertation will focus on randomly dispersed fibers used to arrest cracks. The cracking process within concrete begins with the onset of isolated nanocracks. These nanocracks grow together to form localized microcracks, which in turn grow together to form macrocracks. These macrocracks widen to form cracks visible with the naked eye. Fibers arrest these cracks by forming bridges across them. With increasing tensile stress, a bond failure eventually occurs, and the fiber will pull out of the concrete allowing the crack to widen (Shah 2010). Fig. 2.1 shows the bridging action of fibers across micro and macrocracks in concrete. Fig. 2.2 shows carbon nanotubes (CNTs) bridging a crack in a scanning electron microscope (SEM) image.

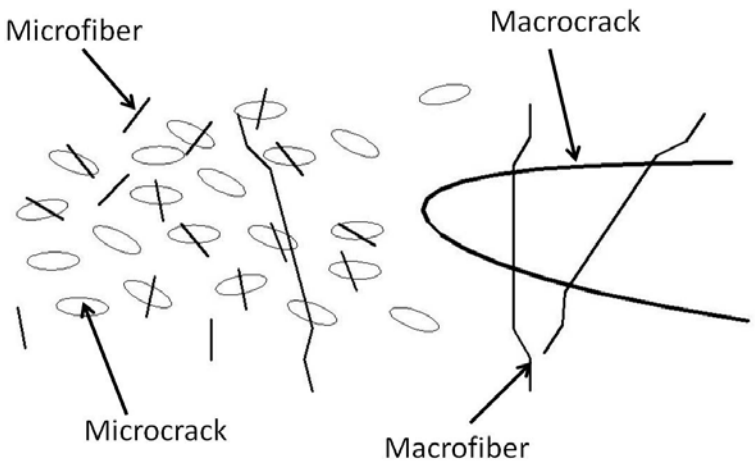

Fig. 2.1 Bridging Action of Fibers Across Micro and Macrocracks

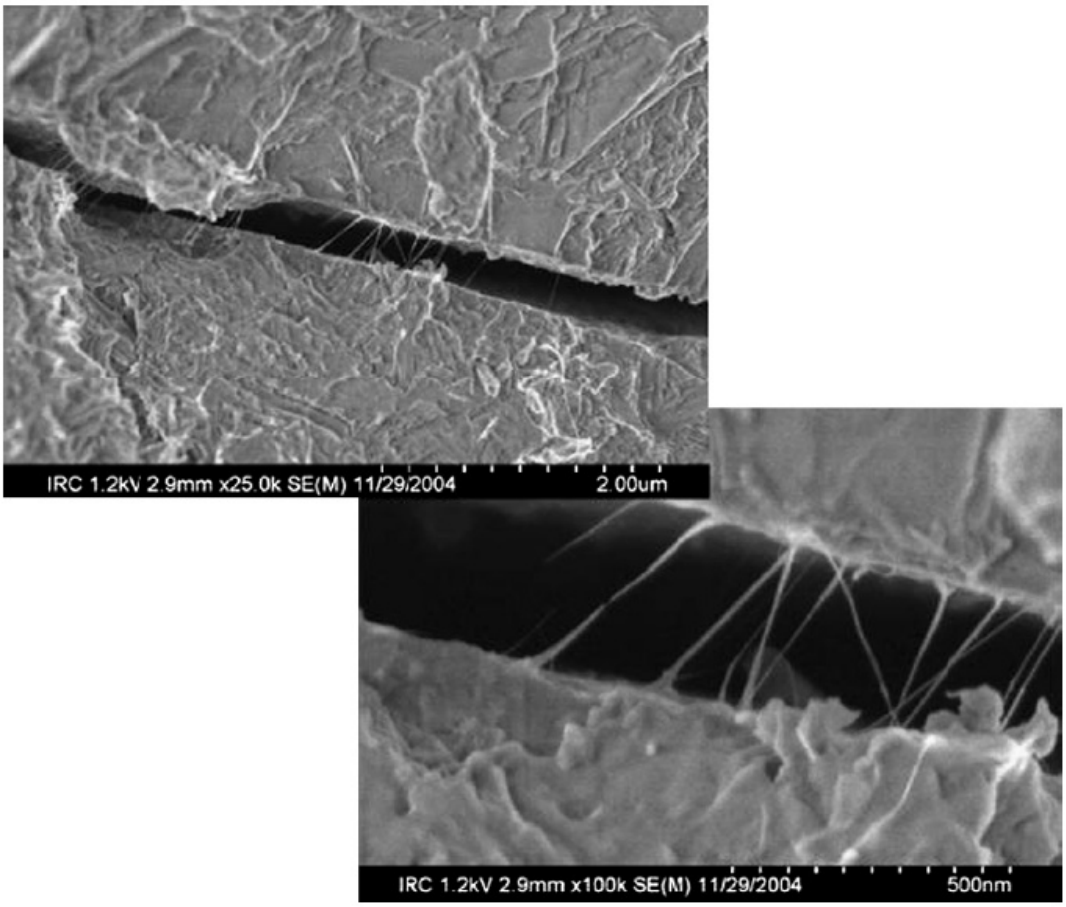

Fig. 2.2 Crack Bridging in Cement-CNT Composites (Makar et al. 2005)

2.4 Nanoreinforcement in Cement-Based Materials

Since the discovery of CNTs in 1991 (Iijima 1991), researchers have desired to implement the unique mechanical, thermal, and electronic properties of CNTs and CNFs in cement-based composites. Single-wall CNTs (SWCNTs), multi-wall CNTs (MWCNTs), and CNFs are graphene ring-based materials with aspect ratios greater than 1000 with high surface areas (Li et al. 2005; Li, Wang, et al. 2007; Sanchez and Sobolev 2010). CNTs and CNFs have moduli of elasticity in the range of terrapascals and tensile strength on the order of gigapascal (Makar and Beaudoin 2004; Salvetat et al. 1999; Sanchez and Sobolev 2010). SWCNTs consist of a single graphene sheet wrapped into a seamless cylinder, while, as the name suggests, MWCNTs inhere of multiple concentric sheets of graphene wrapped around a hollow core. CNFs are cylindrical nanostructures with graphene layers arranged as stacked cones, cups, or plates. CNFs are advantageous because their stacked structure presents exposed edge planes not present in CNTs that introduce increased surface area and better bond characteristics. Fig. 2.3 shows the structural differences of a CNT and CNF. Because of their structure, CNFs are easier to produce and cost 100 times less than SWCNTs (Kang et al. 2006). Because of the increased bond surface and lower cost, CNFs are more attractive than CNTs for application in cement-based composites.

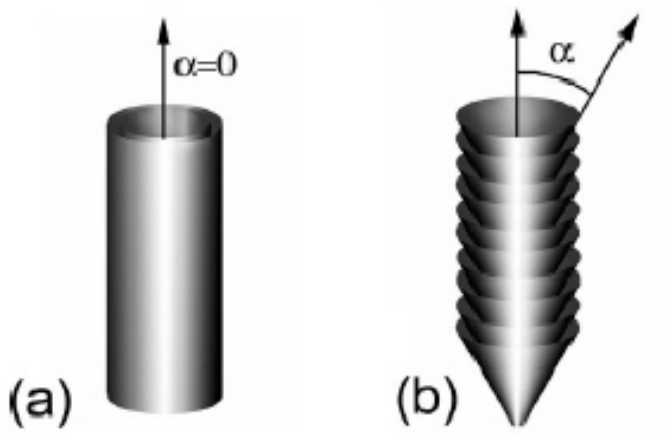

Fig. 2.3 Structure of (a) CNT and (b) CNF (Dume 2007)

2.5 CNT and CNF Dispersion

The majority of nanoreinforced composite research has been completed on polymers containing CNTs or CNFs (Coleman et al. 2006; Makar et al. 2005; Sanchez and Sobolev 2010). One of the main reasons for this is because uniform dispersion is difficult in cement-based materials. Well dispersed CNFs results in uniform calcium-silicate-hydrate (CSH) gel formation, which improves the structural and electrical properties of the concrete (Chung 2005). CNTs and CNFs are inherently hydrophobic and are attracted to one another due to Van der Waals forces, causing the fibers to tend to agglomerate hindering their dispersion in solvants (Baughman et al. 1999, 2002; Hilding et al. 2003; Makar and Beaudoin 2004; Tzeng et al. 2004).

Several solutions have been proposed to solve this issue including dispersing the fibers through milling, ultrasonication, high shear flow, elongational flow, functionalization, in addition to surfactant and chemical dispersement systems (Hilding et al. 2003; Konsta-Gdoutos et al. 2010b; Woo et al. 2005; Yu and Kwon 2012). These

methods primarily fall into two categories: mechanical and chemical dispersion. The mechanical dispersion methods, such as ultrasonification, while effective in seperating the fibers, can fracture them decreasing their aspect ratio. Chemical methods use surfactants or functionalization to make the fibers less hydrophobic, reducing their tendancy to agglomerate. However, many of the chemicals used can digest the fibers causing the fibers to become less effective. The surfactants also often cause bubbles to form in the composite negatively effecting the strength of the material.

Chen et al. (Chen and Chung 1993b; Chen et al. 1997) studied the dispersion of carbon microfibers in cement paste. It was argued that the use of microscopy to assess the degree of fiber dispersion is tedius, difficult, and ineffective. Instead, Chen et al. proposed studying the mechanical and electrical properties since both properties are negatively effected by poor dispersion. They studied the mechanical and electrical properties of cement containing carbon microfibers when methylcellulose, methylcellulose plus silica fume, and latex where each in turn added to the paste. Chen et al. (Chen and Chung 1993b; Chen et al. 1997) discovered that the addition of methylcellulose and silica fume enhanced both the electrical and mechanical properties of the material thus aiding in the dispersion of the carbon microfibers.

Gao et al. (Gao et al. 2009) proposed a dispersion method specifically used for CNF/CNT dispersion in cement-based materials that eliminates the beforementioned drawbacks. In this method, a high-range water reducer (HRWR) is used to create a self-consolidating concrete (SCC). The American Concrete Institute (ACI) Committee 237 Self-Consolidating Concrete offers the following definition for SCC (ACI Committee 318 2011):

Self-consolidating concrete (SCC) is highly flowable, non-segregating concrete that can spread into place, fill the formwork, and encapsulate the reinforcement without any mechanical consolidation.

SCC is a product of technological advancements in the area of underwater concrete technology where the mixtures must ensure high fluidity and high resistance to washout and segregation. Okamura originally advocated SCC in 1986, and the first success with SCC occurred in 1988 (PCI TR-6-03 2003). The use of SCC has gained wide acceptance for savings in labor costs, shortened construction time, a better finish, and an improved work environment (Gaimster and Foord 2000; Khayat et al. 1999; Okamura and Ozawa 1995; Tanaka et al. 1993).

Advancement in SCC technology were primarily possible due to the introduction of new chemical admixtures that improved and controlled the SCC rheological properties. Better performing SCC mixes were produced due to the advent of melamine, naphthalene, polycarboxylate, and acrylic based HRWR superplasticizers and viscosity modifying agents (VMAs).

Gao et al. (Gao et al. 2009) proposed adding CNF to SCC because acceptable SCC is not only highly flowable, but is also highly stable and homogenious on a macro scale. The Precast/Prestressed Concrete Institute (PCI) stipulates the following criteria for SCC (PCI TR-6-03 2003):

- Filling ability – The property that determines how fast SCC flows under its own weight and completely fills intricate spaces with obstacles, such as reinforcement, without losing its stability.

- Passing ability – the ability of SCC to pass through congested reinforcement and adhere to it without application of external energy.
- Stability – the ability of SCC to remain homogenous by resisting segregation, bleeding and air popping during transport and placing as well as after placement.

Gao et al. (Gao et al. 2009) studied SCC containing CNFs to see if the same effect was present on the nano scale. In Gao et al.'s mixing procedure, HRWR, water, and CNFs are mixed in a laboratory-grade blender. Simultaneously, fine aggregate, course aggregate, and cement are combined in a centrifugal mixer. The CNF mixture is then slowly added to the mixer to gain a homogenous mix. The fresh concrete was used to create cylinders that were tested in compression. After the test, pieces of the cylinders were observed under a SEM. The SEM showed significant CNF clumping in specimens made of normal CNF concrete and uniform distribution in SCC containing CNFs, as shown in Fig. 2.4 and Fig. 2.5, respectively.

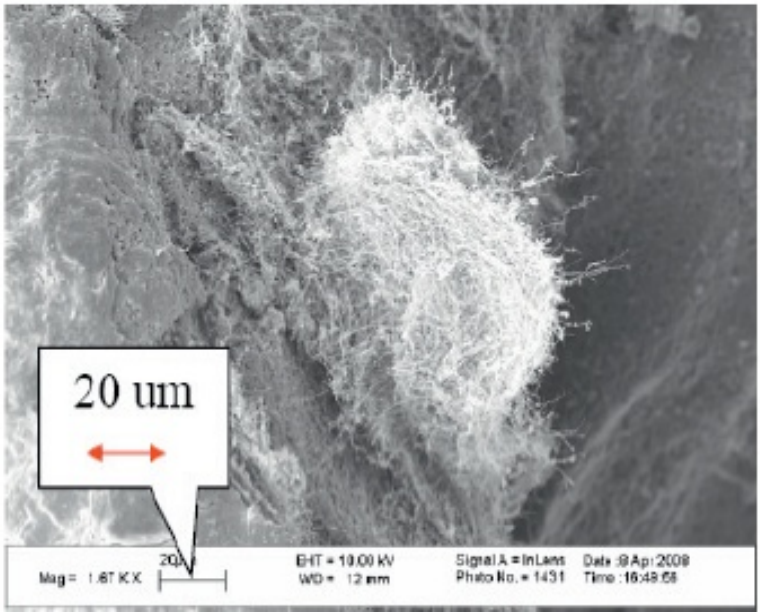

Fig. 2.4 Scanning Electron Microscope Image of CNFs Clump in Normal Cement (1670x Magnification)

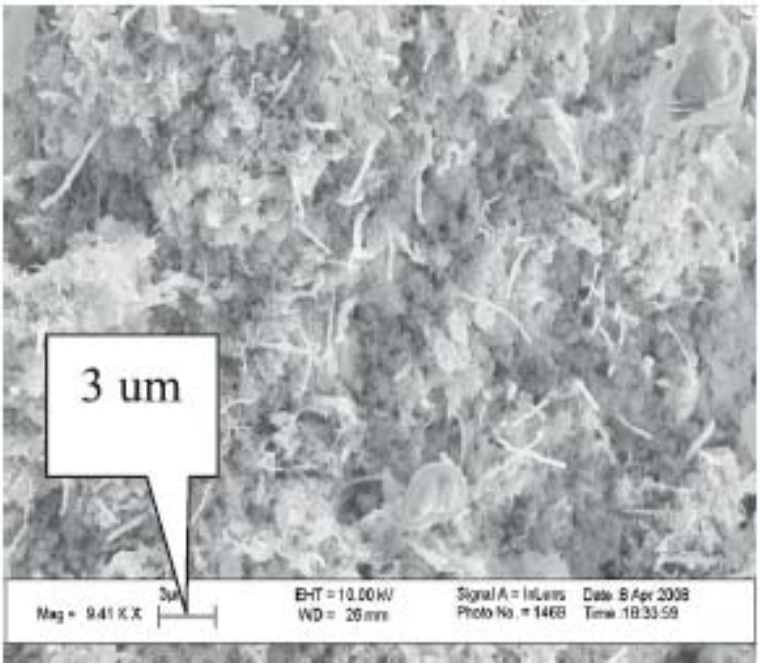

Fig. 2.5 Scanning Electron Microscope Image of Well Dispersed CNFs in a Uniform Self-Consolidating Cement (9410x Magnification)

2.6 Strain Sensing Ability of CNT/CNF Cement-Based Materials

Smart materials are materials that sense their environment and respond to changes in strain, temperature, moisture, pH, and/or electric or magnetic fields. CNT/CNF composites qualify as smart materials since they can be used to measure strain and temperature (Chung 1995, 2000; Gao et al. 2009; Howser et al. 2011; Li, Wang, et al. 2007; Li et al. 2004; Yang and Chung 1992). There are two types of strain sensing, reversible and irreversible. The measurement of irreversible strain allows structural health monitoring, while the sensing of reversible strain permits dynamic load monitoring. Structural health monitoring is the process of implementing a damage detection and characterization strategy for engineering structures. Dynamic load monitoring can detect loads on structures as they are applied and removed in real time. These are important technologies because they gauge the ability of a structure to perform its intended function despite aging, degradation, or disasters. Typically, monitoring reversible strain is more difficult because it can only be monitored in real time. Additionally, reversible strain tends to be smaller than irreversible strain (Chen and Chung 1996).

Strain sensing refers to the ability to measure an electrical or optical response corresponding to a strain. Chen and Chung (Chen and Chung 1996) give the following requirements for a structural sensor:

a) Wide strain/stress range of detection (from small strains up to failure)
b) Response being reversible upon stimulus removal (necessary for repeated use of the sensor)

c) Ease of measuring the response (without the need of expensive peripheral equipment)

d) Presence of the sensor having no negative effect on the structural properties of the structure

e) Chemical stability and durability

f) Low cost

Current commonly used strain sensors include strain gages, fiber optic sensors, and piezoelectric sensors, which all suffer from high cost, poor durability, and the need for expensive peripheral equipment including electronics and lasers. Because of this, the use of sensors in civil structures is uncommon (Chen and Chung 1996). CNT/CNF composites could become a better option as a strain sensor because the above-mentioned points a) through e) are applicable. CNTs and CNFs are currently fairly expensive, CNTs more so than CNFs; however, technology may provide a way to make them more cheaply in the future.

CNT and CNF cement-based materials exhibit properties necessary for reversible strain monitoring and electromagnetic interference (EMI) shielding. Short-fiber composites were found to be a class of strain sensor based on the concept of short electrically conducting fiber pull-out that accompanies slight and reversible crack opening. For a CNT/CNF composite to have strain sensing ability, the fibers must be more conducting than the matrix in which they are embedded, of diameter smaller than the crack length, and well dispersed. Their orientations can be random, and they do not have to touch one another (Chung 1995, 1998, 2000). The electrical conductivity of the fibers enables the DC electrical resistivity of the composites to change in response to

strain damage or temperature, allowing sensing (Chung 1995, 1998, 2000; Gao et al. 2009; Howser et al. 2011; Li et al. 2004; Yang and Chung 1992).

2.7 Carbon Fiber Cement and Mortar Self-Sensing Applications

Around the same time that CNTs were discovered, researchers were adding carbon microfibers to cement-based materials and studying their mechanical properties. In 1992 while studying the mechanical properties of carbon microfibers dispersed in mortar, Yang and Chung (Yang and Chung 1992) noted that the electrical resistivity of mortar containing these fibers dramatically decreased by up to several orders of magnitude.

This idea of electrically conducting concrete led to Chen and Chung proposing an intrinsically smart concrete containing carbon microfibers (Chen and Chung 1993a). Chen and Chung prepared mortar cubes containing carbon microfibers and tested them cyclically. They discovered that the electrical resistivity of the concrete increased irreversibly upon compressive loading up to approximately 1/3 the compressive strength of the mortar. After this point, the resistance reversibly increased and decreased upon loading and unloading of the specimens. Chen and Chung concluded that carbon fiber reinforced concrete can serve as a smart structural material. Chen and Chung followed this experiment with a more detailed cyclic experiment on carbon microfiber mortar under cyclic loads (Chen and Chung 1996), as shown in Fig. 2.6. After this test, they concluded that the initial irreversible behavior is due to permanent damage associated with the fiber/matrix interface weakening. They attributed the reversible behavior to crack opening with fiber pull-out and crack closing with fibers pushing back in.

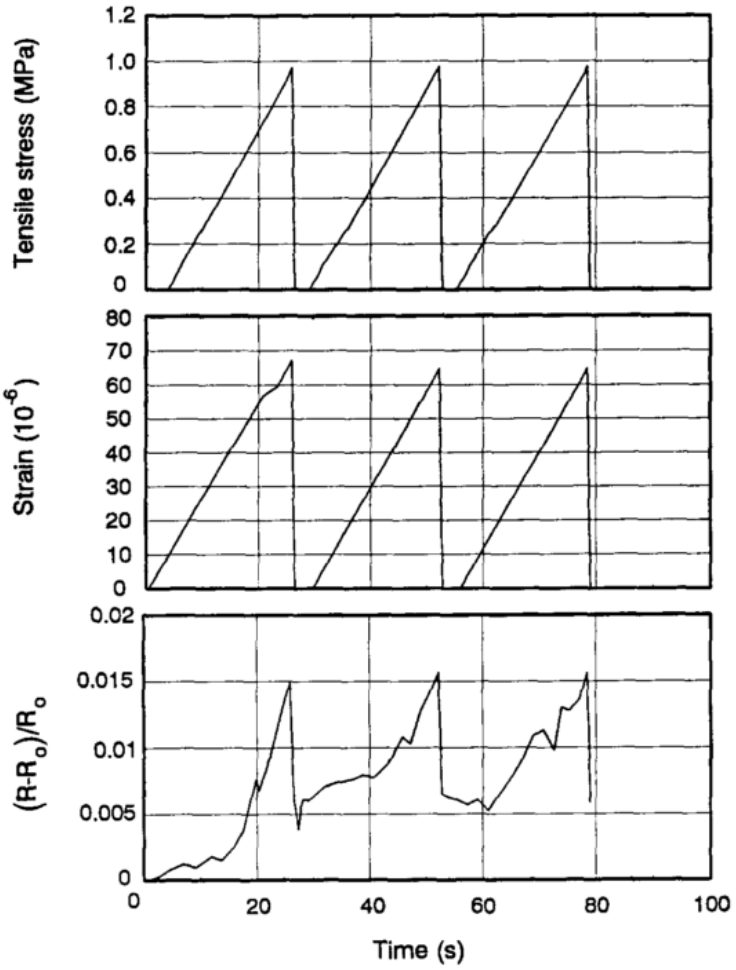

Fig. 2.6 Stress, Strain, and Electrical Resistance Variation of a Carbon Microfiber Mortar Composite (Chen and Chung 1996)

In addition to monitoring strain, Chung (Chung 2000) used a carbon microfiber silica fume cement paste to sense temperature through the thermoresister effect. A thermoresister is a thermometric device consisting of a material, typically a semiconductor, whose electrical resistivity decreases with a rise in temperature. Over a limited temperature range from approximately 45°C (113°F) to 1°C (34°F), there was an increase in resistance of nearly 800%, as shown in Fig. 2.7. This proves that a cement-based carbon fiber composite can be used as a multifunctional sensor.

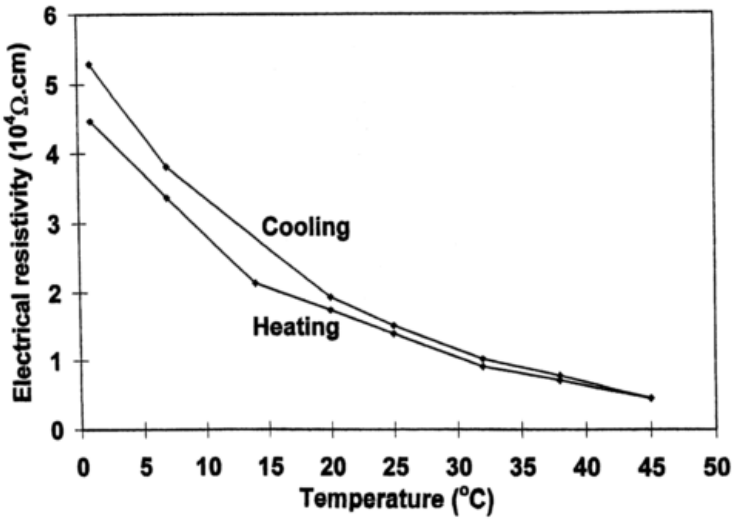

Fig. 2.7 Electrical Behavior during the Heating and Cooling of a Carbon Microfiber Silica Fume Cement Paste (Chung 2000)

CNTs are the most conductive fibers presently known and are, therefore, more ideal for electrical applications than their micro-scale counterparts (Thess et al. 1996; Wei et al. 2001). CNTs and CNFs are also attractive for use in cement-based composites because of strength and high aspect ratios (Makar and Beaudoin 2004; Salvetat et al. 1999; Sanchez and Sobolev 2010). Li et al. proposed adding MWCNTs to mortar for improved mechanical properties (Li, Wang, et al. 2007). Li et al. confirmed that the flexural and compressive strength of the concrete was enhanced, but they did not study the electrical properties. The same group later studied the electrical volume resistivity of cement paste containing CNTs measured using the four-probe method (Narayan et al. 2004). They applied a cyclic compressive load to a 40.0 mm by 40.0 mm by 160.0 mm (1.575 in. by 1.575 in. by 6.30 in.) rectangular prism made of the material. The fractional change in the volume resistivity oscillated up to approximately 10% with the oscillation of the compressive load.

2.8 Damage Detection of CNF Concrete Columns

Gao et al. expanded the work on self-sensing cement-based materials by studying 152.4 mm by 305 mm (6.00 in. by 12.00 in.) cylinders made of concrete, rather than cement or mortar, containing CNFs (Gao et al. 2009). Gao et al. crushed the cylinders monotonically and studied the electrical resistance variation. They observed electrical resistance variations up to 80% and concluded that concrete containing CNFs can be used for self-structural health monitoring.

Howser et al. continued Gao et al.'s work and extended it to a full scale reinforced concrete column containing CNFs (Gao et al. 2009; Howser et al. 2011). A self-consolidating CNF concrete (SCCNFC) column was built and tested under a reversed cyclic load. The structural behavior and the self-sensing ability were examined. The results were compared to the structural and self-sensing ability of a traditional self-consolidating reinforced concrete (SCRC) and a self-consolidating steel fiber concrete (SCSFC) specimen.

All of the columns were 508 mm (20.0 in.) tall with cross-sections of 305 mm by 305 mm (12.00 in. by 12.00 in.). Each specimen contained six #8 (25.4 mm or 1.00 in. diameter) rebar, which corresponded to 3.27% longitudinal steel by volume of concrete. The SCRC and SCCNFC columns contained #2 stirrups with a spacing of 120.7 mm (4.75 in.) providing transverse reinforcement of 0.287% by volume of concrete. Since the columns were designed to be shear critical, the maximum reinforcement spacing was chosen based on the ACI 318 specifications (ACI Committee 318 2011). See Fig. 2.8 for the cross-section used for the SCRC and SCCNFC columns. The SCSFC column contained no transverse reinforcement, as shown in Fig. 2.9. Each of the columns was

rigidly connected to similar foundations. See Fig. 2.10 for the elevation view of the SCRC and SCCNFC columns and foundations. The SCSFC column is identical to that shown in Fig. 2.10, except it does not contain transverse reinforcement. Fig. 2.11 shows the experimental set-up.

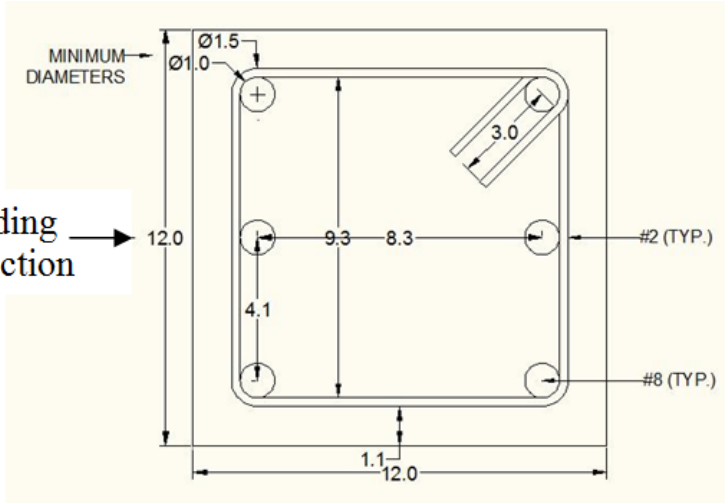

Fig. 2.8 Cross-Section of SCRC and SCCNFC Columns (dimensions in inches)

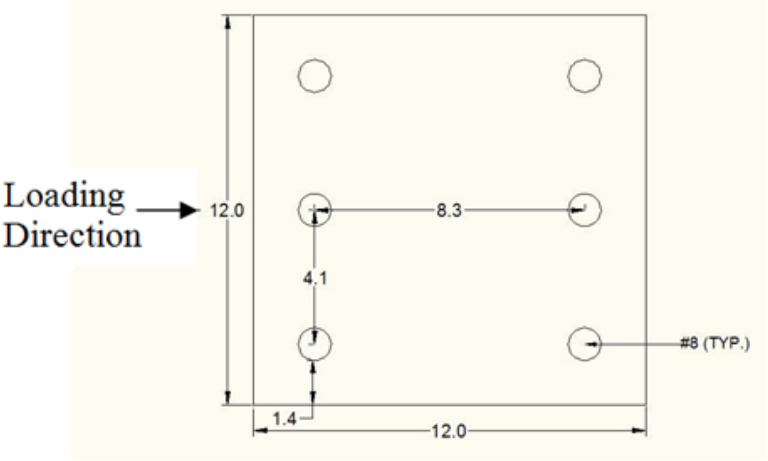

Fig. 2.9 Cross-Section of SCSFC Column (dimensions in inches)

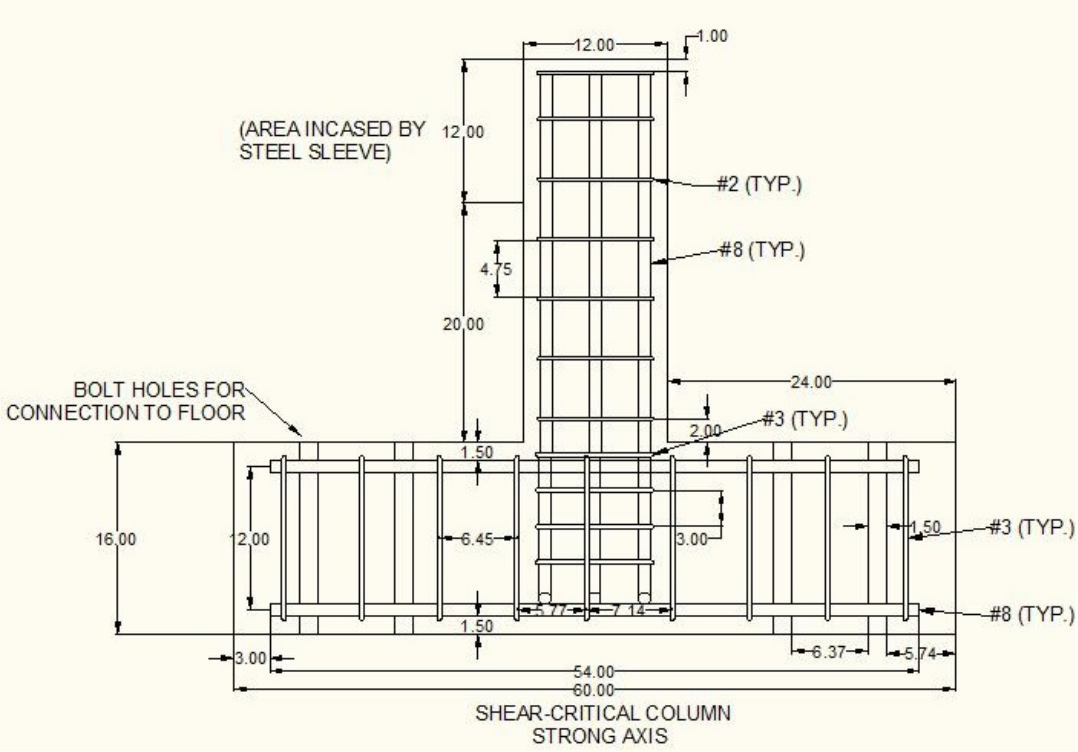

Fig. 2.10 Elevation View of the Strong Axis of the Shear-Critical SCRC and SCCNFC Columns and Foundations (dimensions in inches)

Fig. 2.11 Experimental Set-Up

The properties of the materials used for the three mixes were as follows:

a) Cement: The cement used in all mixtures was ASTM Type III Portland cement.

b) Fly Ash: Class C fly ash was used for the SCSFC mix and Class F fly ash was used for the SCRC mix.

c) Coarse Aggregate: Crushed limestore with a maximum diameter of ¾" was used in the SCCNFC column. River rock with a maximum diameter of ¾" was used in the other columns.

d) Fine Aggregate: Natural river sand with a fineness modulus of 2.71 was used in all mixes.

e) High Range Water Reducer (HRWR): Glenium® 3200HES was used in the SCCNFC column and Glenium® 3400 HES was used in the other columns. Both chemicals were polycarboxylate admixtures from BASF Chemical Co.

f) Viscosity Modifying Agent (VMA): RHEOMAC® VMA 450 was used in the specimens and also supplied by BASF Chemical Co.

g) Steel Fibers: Dramix® ZP305 fibers were used in the SCSFC mix. This was a hooked fiber with a specific gravity of 7.85. The diameter of the fiber is 0.55 mm (0.0217 in.) and the length is 30 mm (1.18 in.) resulting in an aspect ratio of 55.

h) Carbon Nanofibers: Pyrograf Products, Inc. PR-19-XT-LHT-OX fibers were used in this study. The specific gravity of the fibers was 0.0742. The diameter of the fibers was 149 nm (5.87e-6 in.) and the length was 19 μm (7.48e-4 in.) resulting in an aspect ratio of 128.

The mix proportions used for the three columns can be seen in Table 2.1. One percent fiber by volume was used for both of the fiber columns chosen based on literature review. It was discovered by Gao et al. that CNFs have an optimal dosage of approximately 1% by volume (Gao et al. 2009). It was found by many researchers that increased steel fiber concentrations increases concrete properties; however, after a percentage of 1% fibers by volume, the concrete becomes increasingly less workable which could cause problems in construction such as honeycombing (Aoude et al. 2009; Narayan et al. 2004; Padmarajaiah and Ramaswamy 2002).

Table 2.1 Mix Proportions in kg/m^3 (lb/yd^3) of Concrete

Material	SCRC Mix	SCSFC Mix	SCCNFC Mix
Cement	446 (752)	446 (752)	457 (771)
Fly Ash (Class C)	-	299 (504)	-
Fly Ash (Class F)	299 (504)	-	-
Fine Aggregate	937 (1580)	937 (1580)	898 (1514)
Coarse Aggregate (Limestone)	-	-	859 (1448)
Coarse Aggregate (River Rock)	491 (827)	491 (827)	-
Water	224 (377)	224 (377)	182 (307)
Glenium® 3400HES	2.81 (4.73)	2.81 (4.73)	-
Glenium® 7700HES	-	-	2.34 (3.94)
REHEOMAC® VMA 450	5.69 (9.59)	5.69 (9.59)	-
Steel Fibers	-	79.8 (134)	-
Carbon Nanofibers	-	-	3.23 (5.45)

The main goal of testing the SCCNFC column was to prove that concrete containing CNFs can be used as a sensor. To test the electrical properties of the concrete, wire meshes were constructed and embedded in each of the columns. The wire meshes were made of 12.7 mm (0.5 in.) hardware cloth with 14 gauge copper wire soldered to it. The wire extended outside of the column. The four-probe method for measuring resistance was implemented, and the meshes were placed in the column as shown in Fig. 2.12. A power supply was attached to the top mesh that provided a current of approximately 31 V

DC. An ammeter was attached to the bottom mesh and connected back to the power supply to complete a circuit. The current measured by the ammeter was recorded continuously during the tests by hand. Additional voltmeters were attached to the two middle meshes on both the north and south sides of the column to measure voltage. The voltage readings were also recorded continuously throughout the test.

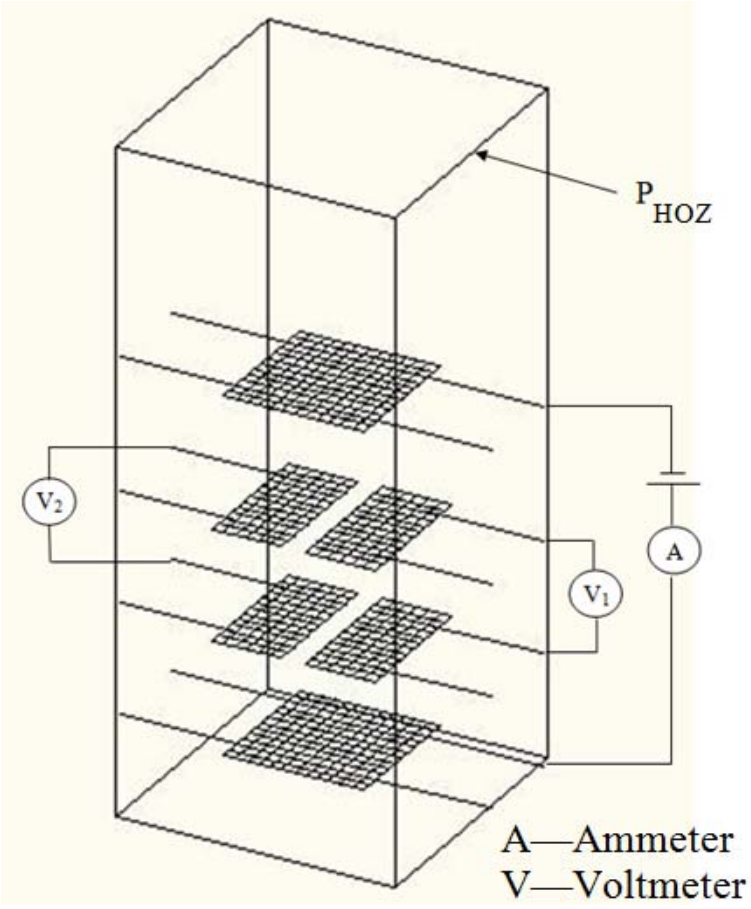

Fig. 2.12 Four Probe Method of Resistance Measurement

The first step of the load program was to apply an axial load that would remain constant during the course of the test. The axial load equaled one-tenth of each of the columns calculated axial capacity. The axial capacity is dependent on the compressive strength of the concrete, so the axial force for each specimen varied.

After the application of the axial load, a reversed-cyclic load was added using a 649 kN (146 kip) capacity actuator. The intended load path was to use force-control to complete two cycles each of ±89 kN (20 k), ±178 kN (40 k), and ±267 kN (60 k). A positive force denotes a push by the actuator while a negative force represents a pull. At the point of longitudinal steel yielding, the test switched to displacement-control and completed two cycles each at a displacement ductility of 2, 3, 4, etc. Once failure occurred, a descending branch on the load versus displacement curve was obtained in displacement-control mode.

The load path followed for the SCRC column specimen can be seen in Fig. 2.13 with the first cracks, switch to displacement-control and failure marked. The first crack on the south side of the column occurred at -178 kN (-40 k). The first shear crack formed on the column during the first -178 kN (-40 k) cycle at -178 kN (-40 k) on the west side. The column failed in shear and crushing of concrete at 276 kN (62 k). The west side of the column exhibited crushing of the concrete struts with large shear cracks. The east side exhibited local crushing at the actuator connection. The maximum displacement at the top of the column (drift) was 12.7 mm (0.50 in.).

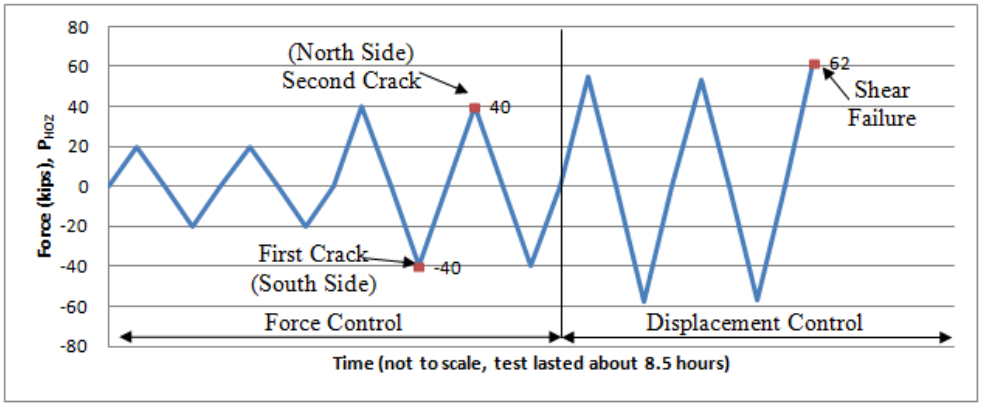

Fig. 2.13 SCRC Column Load Path

The load path followed for the SCSFC column can be seen in Fig. 2.14 with the first cracks and failure marked. The first shear and flexural cracks formed on the column during the second 178 kN (40 k) cycle at 178 kN (40 k) on the west and north sides, respectively. The second flexural crack formed on the south side during the second -178 kN (-40 k) cycle at -178 kN (-40 k). The column failed suddenly in shear and crushing at 347 kN (78.0 k) on the west side of the column before the rebar yielded. The maximum displacement was 8.38 mm (0.33 in.).

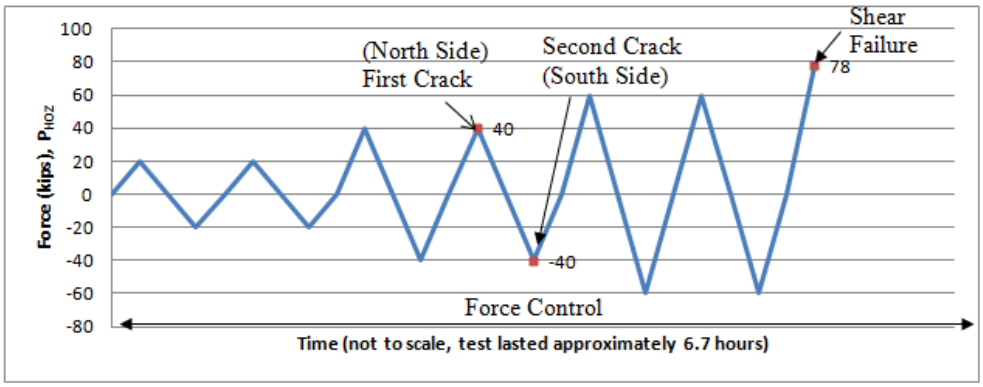

Fig. 2.14 SCSFC Column Load Path

The actual load path followed for the SCCNFC column can be seen in Fig. 2.15. The pump shut down during the test, and the actuator unloaded during the fifth cycle of the test. The pump was turned back on and the test resumed. The first flexural crack formed on the column at 160 kN (36 k) on the east, west and north sides. The second flexural crack formed on the east, west and south sides at a load of -158 kN (-35.6 k). The column failed in the combined modes of shear and concrete crushing due to flexure at 298 kN (67 k) on the west side of the column. The maximum displacement was 10.16 mm (0.4 in.).

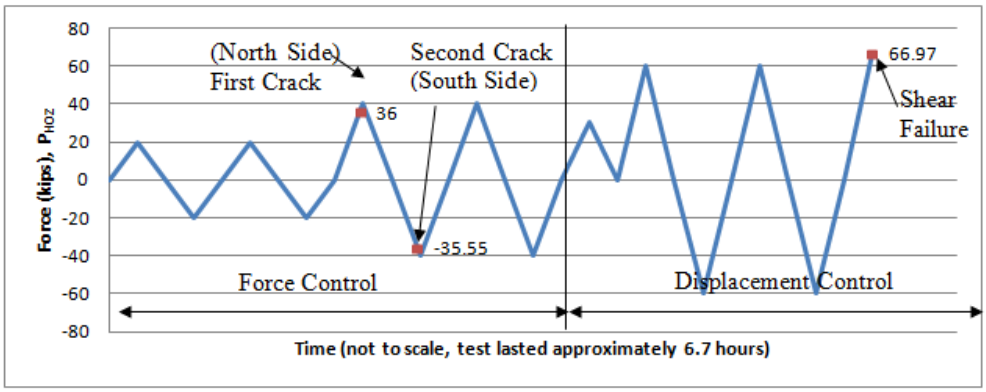

Fig. 2.15 SCCNFC Column Load Path

During each of the column tests, the electrical resistance was determined to check the self-sensing ability of the concrete. The electrical readings showed a great correlation between the peaks in the applied horizontal force, strain, and resistance plots for the SCCNFC column but little correlation between the resistance plots and the force or strain plots for the SCRC or SCSFC column. Fig. 2.16 shows the relationship between the SCRC column's horizontal force, linear voltage differential transformer (LVDT) strain and electrical resistance versus time on the north side of the column. There is no relationship between the peaks and valleys in the electrical resistance and the load or strain on the north side of the column.

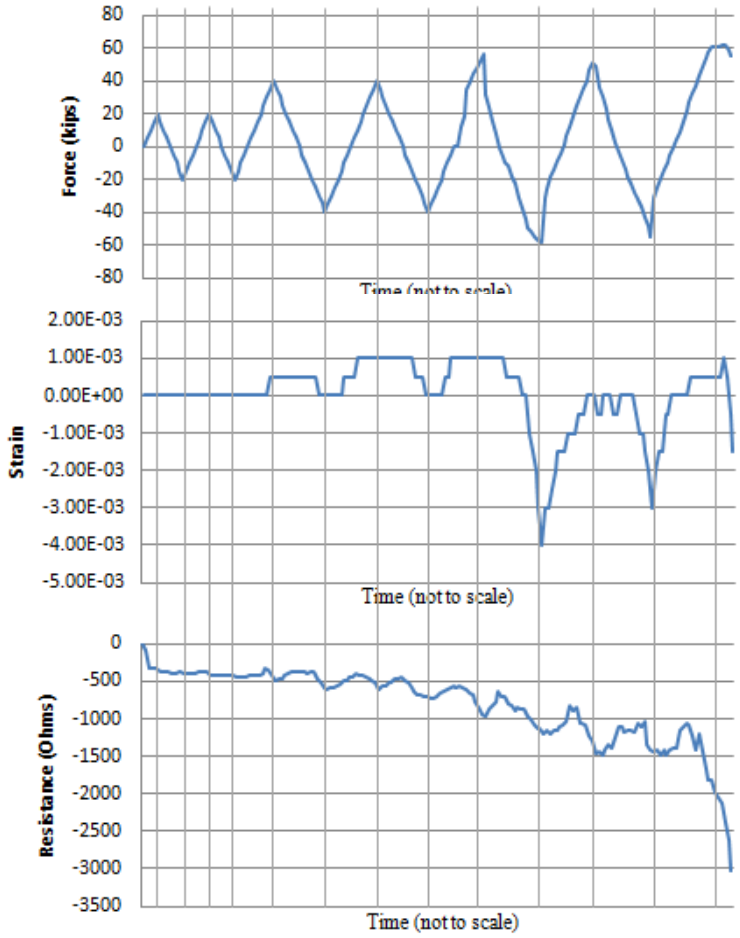

Fig. 2.16 SCRC Column Comparison of Horizontal Force, LVDT Strain, and Electrical Resistance on North Side

Fig. 2.17 shows the SCSFC column's force, strain, and resistance versus time on the north side of the column. As shown by the grey vertical lines, there is not a relationship between the peaks and valleys in the resistance and load or strain until major cracking began to occur. After major cracking began to occur, the peaks and valleys in the electrical resistance began to correspond with the load and strain peaks and valleys. This point is shown by the dashed line in Fig. 2.17.

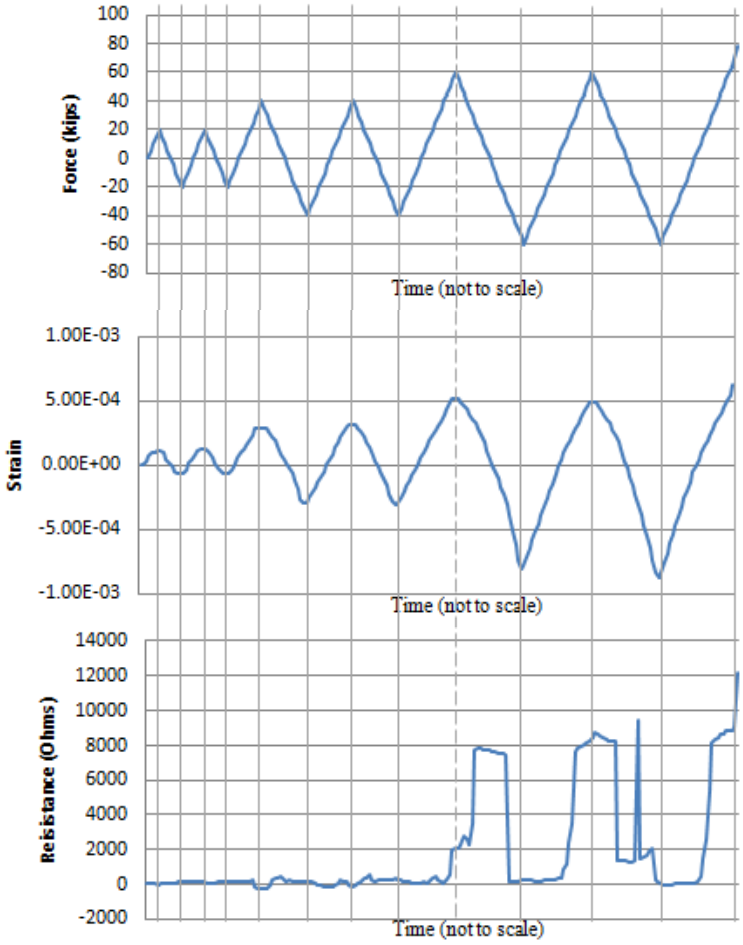

Fig. 2.17 SCRC Column Comparison of Horizontal Force, LVDT Strain, and Electrical Resistance on North Side

Fig. 2.18 shows the relationship between the SCCNFC column's horizontal load, LVDT strain, and electrical resistance versus time on the north side of column. As shown by the vertical lines in the grid, there is very good correlation between the force, strain, and resistance. The peaks and valleys in the data matched until the point that the column was greatly damaged.

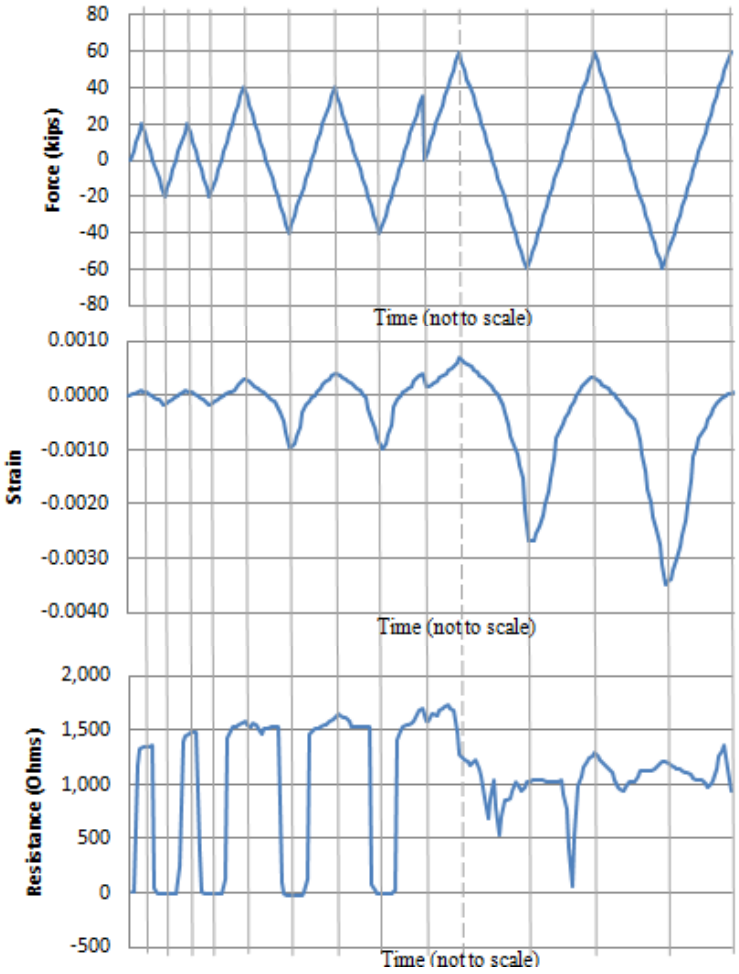

Fig. 2.18 SCCNFC Column Comparison of Horizontal Force, LVDT Strain, and Electrical Resistance on North Side

Because of the strong correlation found between the horizontal load, LVDT strain, and electrical resistance versus time graphs for the SCCNFC column, the electrical resistance variation (ERV) was calculated and compared to the deflection at the top of the column. ERV is the measured electrical resistance minus the initial electrical resistance quantity divided by the initial electrical resistance. Fig. 2.19 shows the relationship between the ERV and deflection at the top of the column for the first five cycles of the test. It is obvious from Fig. 15 that the column shows major damage at approximately a deflection of 2.03 mm (0.08 in.). This corresponds to the steel yielding in the SCCNFC

column. This proves that SCCNFC can be used as a type of self-structural health monitoring system.

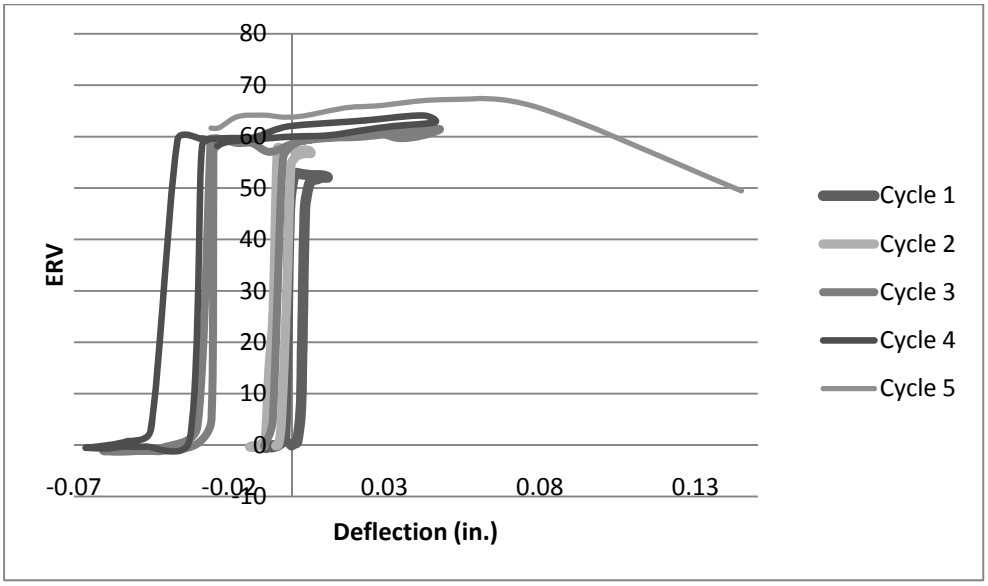

Fig. 2.19 SCCNFC Column ERV versus Horizontal Deflection

2.9 Summary

Self-consolidating carbon nanofiber concrete (SCCNFC) follows the definition for nanotechnology set forth by the National Science Foundation and National Nanotechnology Initiative (Roco 2007). The size range of the carbon nanofibers (CNFs) is approximately 100 nanometers, the SCCNFC is able to measure damage in the composite, and the CNFs have properties that are specific to the nanoscale.

Well-dispersed CNFs improves the strength and stiffness of concrete. Excess concentration leads to poorly dispersed CNF clumps inside the concrete and has a negative effect on both strength and electrical sensitivity. Highly workable and stable

self-consolidation concrete (SCC) can maintain its workability and stability with the addition of fibers. SCC greatly increases the dispersion of CNFs (Gao et al. 2009).

As proven by Gao et al. (Gao et al. 2009) and Howser et al. (Howser et al. 2011), SCCNFC can be used as a reversible strain sensor. In Howser et al.'s test, the peaks and valleys in the electrical resistance readings of the SCCNFC match the peaks and valleys of the applied force and the strain in the concrete. While the peaks and valleys in the electrical resistance readings of the self-consolidating reinforced concrete and self-consolidating steel fiber concrete specimens occasionally matched, there was not enough correspondence to safely assume that these concretes could be used as a reversible strain sensor. It was concluded that when an appropriate dosage of CNFs is used, SCCNFC can be used for self-structural health monitoring.

CHAPTER 3
DEVELOPMENT OF THE CARBON NANOFIBER AGGREGATE

3.1 Introduction

Because of past success at the University of Houston (UH) demonstrating that self-consolidating carbon nanofiber concrete (SCCNFC) can be used as a strain sensor (Gao et al. 2009; Howser et al. 2011), a carbon nanofiber aggregate (CNFA) was developed to determine localized strain in concrete structures. The development of a CNFA is significant because it is possible to use the strain sensing capabilities of SCCNFC with a greatly reduced cost since only the CNFAs placed in the structure would contain carbon nanofibers (CNFs). SCCNFC costs nearly 20 times as much as normal concrete. This chapter describes the optimization of both the CNFA configuration and the mortar design. Fig. 3.1 shows previous CNFA configurations.

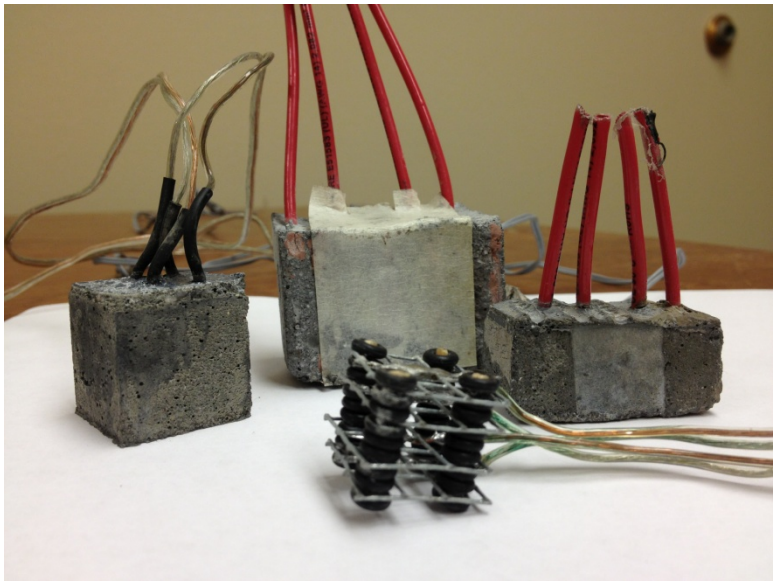

Fig. 3.1 Previous CNFA and Mesh Configurations

3.2 Electrical Resistance Measurement Technique

The four-probe method was chosen to measure the electrical resistance in the CNFA specimens. In this method, current is supplied to a pair of current leads (1 and 4) and the voltage drop can be measured across the inner connections (2 and 3) as shown in Fig. 3.2. Since the resistance of CNFAs is much higher than the resistance of the wires, this method is quite accurate for determining the electrical resistance variation of the CNFAs.

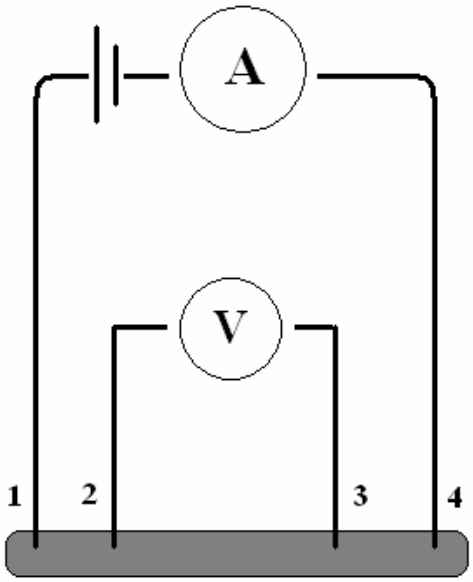

Fig. 3.2 Four Probe Method for Determining Electrical Resistance

The calculations required for this method are quite simple. One can determine the resistance using Ohm's Law,

$$V = RI \,, \qquad \textbf{Equation 3.1}$$

where:

V: Voltage (V),

R: Resistance (Ω),

I: Currant (A).

The electrical resistance variation (ERV) can be determined as

$$ERV = \frac{R_i - R_0}{R_0}, \qquad \textbf{Equation 3.2}$$

where:

ERV: Electrical Resistance Variation,

R_i: Resistance at Step I,

R_0: Initial Resistance.

The four-probe method was accomplished by creating four steel meshes and embedding them inside of the CNFAs. Fig. 3.3 shows a schematic showing the CNFA with the four embedded meshes.

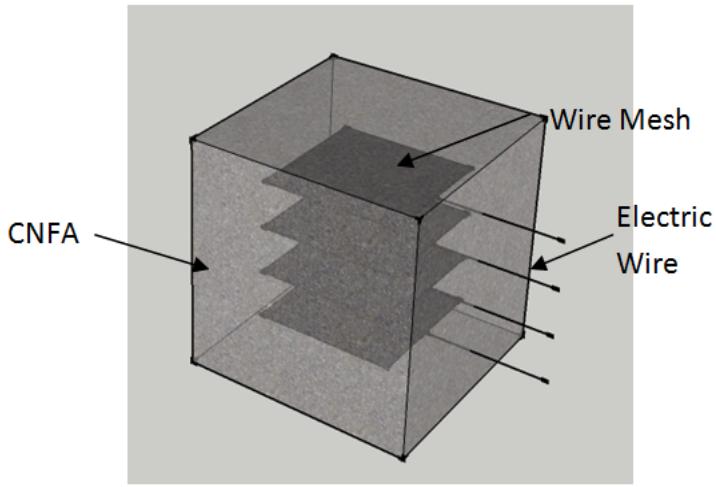

Fig. 3.3 CNFA Schematic

3.3 CNFA Size

For size optimization, the CNFA needed to be large enough that the meshes required for the four-probe method could be easily constructed and placed within the aggregate without touching one another; however, it had to be appropriately sized so that it did not cause casting problems when it was embedded in a larger structure.

According the American Concrete Institute (ACI) (ACI 318 2008), the nominal maximum size of course aggregates should not be larger than:

a) 1/5 the narrowest dimension between sides of forms
b) 1/3 the depth of slabs
c) 3/4 the minimum clear spacing between individual reinforcing bars or wires, bundles of bars, individual tendons, bundled tendons, or ducts

However, these rules are not absolute in that the code allows that a licensed design professional may chose to use larger aggregates if the workability of the concrete and method of consolidation are adequate to eliminate honeycombing and voids.

The optimal CNFA size chosen was 2.54 cm by 2.54 cm by 2.54 cm (1.00 in. by 1.00 in. by 1.00 in). This allowed for both reasonable construction limitations as outlined by points a) through c) above and manageable space in which to place the four wire meshes needed for the four probe method.

3.4 Mesh Construction

The meshes were made from 6.35 mm by 6.35 mm (0.25 in. by 0.25 in.) 23 gauge welded galvanized steel hardware cloth. The hardware cloth was cut into 19.05 mm by 19.05 mm (0.75 in. by 0.75 in.) squares with four prongs extending, as illustrated in Fig. 3.4. Gauge 24 copper wire was soldered to one of the prongs that was used to reinforce the wire extending from the CNFA. This was the most vulnerable place for the wire to break. Two of the extended prongs were inserted into holes drilled in the formwork to hold the bottom of the meshes in place during casting, as shown in Fig. 3.5. The sides of

the formwork were assembled around the meshes, and the prongs extending from the top of the meshes were slid into grooves cut in the top pieces of the formwork, as shown in Fig. 3.6. This ensures that the correct spacing was maintained as the concrete was cast. The spacing of the meshes is shown in Fig. 3.7.

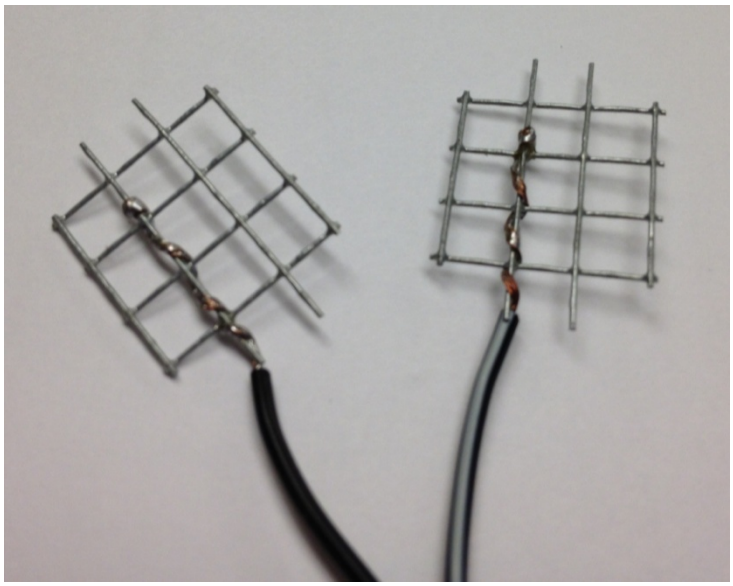

Fig. 3.4 Two Meshes with Soldered Wires

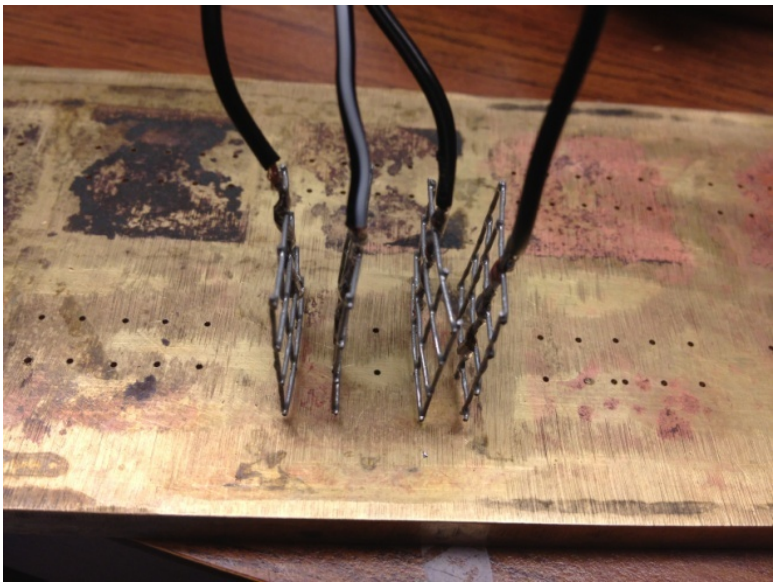

Fig. 3.5 Meshes Inserted into Bottom of Formwork

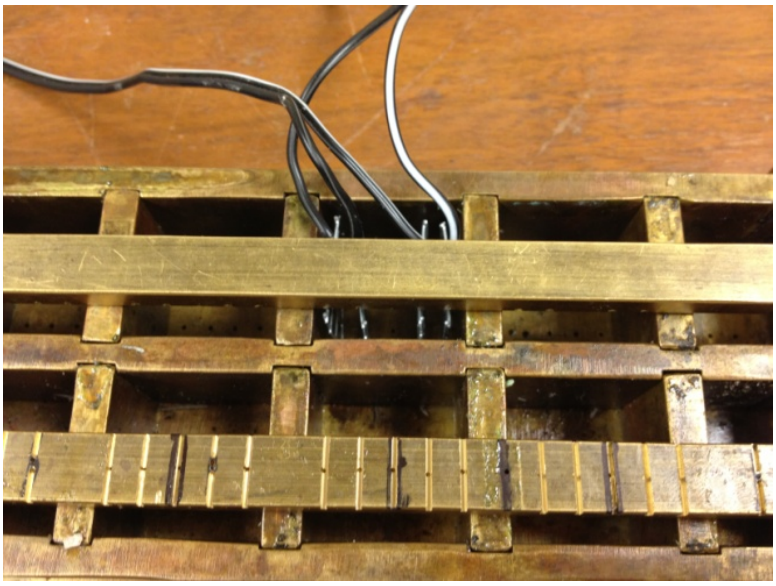

Fig. 3.6 Meshes Inserted into Complete Formwork

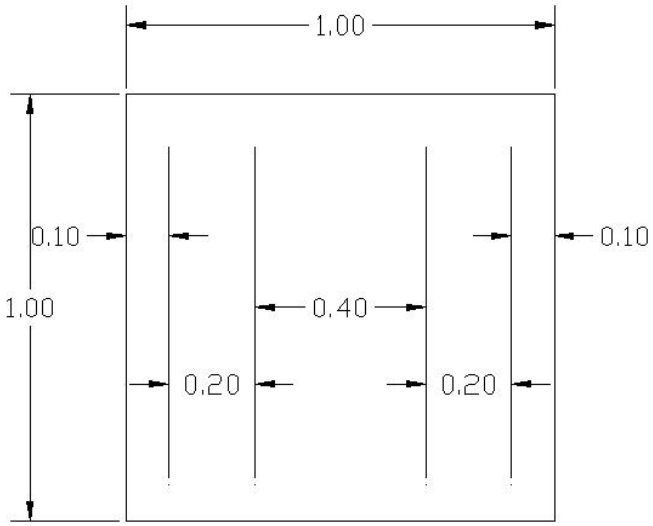

Fig. 3.7 Mesh Spacing (units in.)

3.5 Mortar Mix Design

The CNFA consists of a CNF mortar mix. In addition to the typical mortar ingredients of cement and fine aggregate, admixtures were added. A study was carried out to determine the optimal mix design. The first admixture was a high-range water

reducer (HRWR). It was proven by Gao et al. (Gao et al. 2009) that a HRWR capable of creating self-consolidating concrete (SCC) also aids in the dispersion of fibers. The mortar needed to be self-consolidating so that it would flow under its own weight, flowing around the meshes without creating voids with no mechanical vibration. The second admixture was silica fume. Chen et al. (Chen and Chung 1993b; Chen et al. 1997) proved that silica fume also increases the dispersion of fibers in cement-based materials. The third admixture was the CNFs, which allow the mortar mixture to become self-sensing. The properties of the materials used in the mix are as follows:

a) Cement: The cement used was ASTM Type III Portland cement. Type III was chosen for its decreased curing time for quicker CNFA manufacturing.
b) Fine Aggregate: The fine aggregate used was Quikrete® Premium Play Sand, which is a washed, dried, and screened fine sand.
c) High–Range Water Reducer (HRWR): Glenium® 3400 HES is a polycarboxylate admixture from BASF Chemical Co.
d) Silica Fume: Rheomac® SF100 is a dry, densified silica fume admixture from BASF Chemical Co.
e) Carbon Nanofibers: Pyrograf Products, Inc. PR-19-XT-LHT-OX fibers were used in this study. The specific gravity of the fibers is 0.0742. The diameter of the fibers is 149 nm (5.87e-6 in.) and the length is 19 μm (7.48e-4 in.) resulting in an aspect ratio of 128. Gao et al. (Gao et al. 2009) completed an extensive study on various CNFs and found PR-19-XT-LHT-OX fibers to have the best self-sensing behavior in concrete. Fig. 3.8 shows clumps of CNFs with no magnification.

Fig. 3.8 Carbon Nanofibers

Several researchers have studied CNF concentrations in cement-based mixtures. Chen and Chung (Chen and Chung 1993a) studied the electrical and mechanical properties of carbon microfibers in concentrations of 0.5% by weight of cement. They saw a decrease in electrical resistivity of up to 83% when compared to normal concrete. Chen and Chung (Chen and Chung 1996) later studied carbon microfibers in concentrations of 0 to 4% by weight of cement in mortar and 0.5 to 3% by weight of cement in concrete. Their results showed that carbon microfibers in concrete and mortar created a reversible damage sensor by measuring the ERV. They found that increasing the fiber content in the mortar did not have appreciable effects on the change in ERV. In concrete, they found that increasing the fiber content increased the ERV. Gao et al. (Gao et al. 2009) found that increasing the fiber content in CNF concrete by more than 0.7% by

weight of cement caused fiber clumping. They found 0.7% by weight of cement was the optimal concentration. Howser et al. successfully used 0.7% CNFs by weight of cement in a reinforced concrete column test (Howser et al. 2011).

A study on the fiber concentration in mortar was carried out to discover the optimal concentration (Howser and Mo 2013). Over 100 CNFAs with varying percentages of CNFs were tested in compression, and the ERV was measured to find the optimal percentage. Before the test began, the CNF dispersion, or lack thereof, could be observed at some concentrations with the naked eye. Fig. 3.9 shows a series of CNFAs with different CNF concentrations (i.e., 0.00%, 0.25%, 0.50%, 0.75%, 1.00%, 1.25%, 1.50%, and 1.75% by weight of cement). It can easily be seen that the color of the mortar becomes darker with each increase of CNF concentration up to 1.75%. This was caused by severe clumping of CNFs in the mortar mixture at 1.75%. At this concentration, fiber clumping was observed during the casting procedure as shown in Fig. 3.10. The CNFAs containing 1.75% by weight of cement were damaged before testing due to the clumping as shown in Fig. 3.11. Visible clumps were observed in tested CNFAs containing 1.00% CNFs by weight of cement as seen in Fig. 3.12. From this visual inspection, it was clear that the optimal concentration was likely less than 1.00% CNFs by weight of cement.

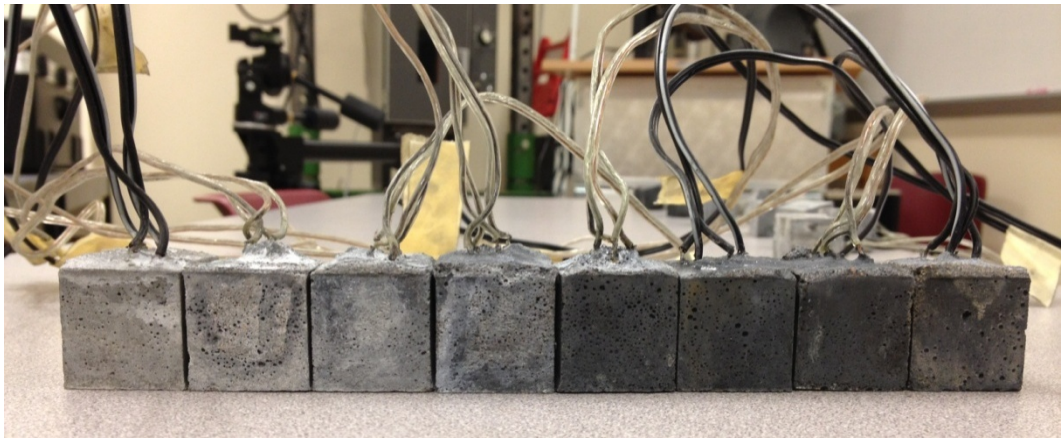

Fig. 3.9 Color Gradation of CNF Mortar Mixes (0.00%, 0.25%, 0.50%, 0.75%, 1.00%, 1.25%, 1.50%, and 1.75% CNFs by Weight of Cement)

Fig. 3.10 CNF Clumps in Mortar Containing 1.75% CNFs by Weight of Cement

Fig. 3.11 Severe Damage in CNFA Containing 1.75% CNFs by Weight of Cement due to Clumping Before Testing

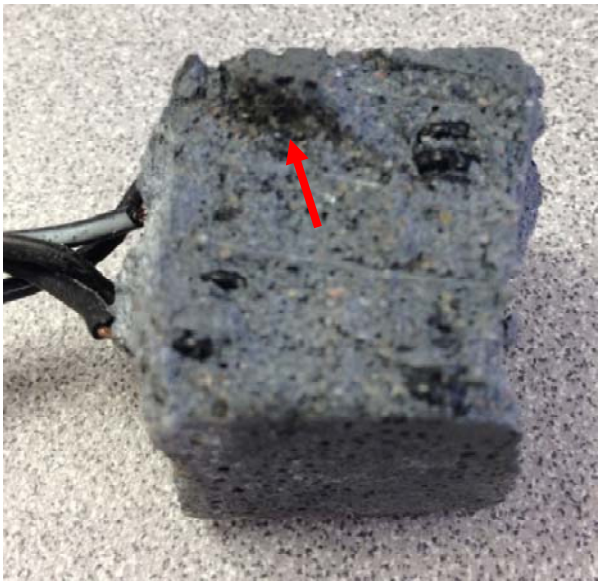

Fig. 3.12 CNF Clump in Tested CNFA Containing 1.00% CNFs by Weight of Cement

After casting, each of the specimens was cured for 28 days. After 28 days, the specimens were air dried for 24 hours. To remove all access moisture, they were oven dried for 24 hours at 100°C (212°F).

The test setup used is shown in Fig. 3.13. Each CNFA was placed in a loading frame with a 44.5 kN (10 kip) capacity. A lead sheet was placed above and below the aggregate to ensure an even contact surface. A steel plate was placed on top of the upper lead sheet with two linear variable differential transformers (LVDTs) connected to measure the average displacement of the CNFAs during the test. The CNFAs were tested in compression at a constant displacement rate of 0.0254 mm/min. (0.001 in./min.) until failure. The electrical resistance was measured using the four-probe method and a Keithley Source Meter. Fig. 3.14 shows a tested CNFA that exhibited extensive cover spalling.

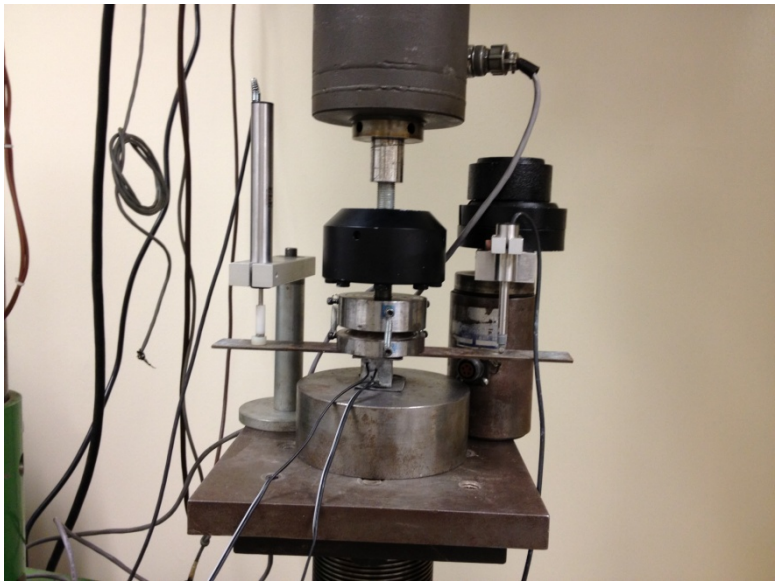

Fig. 3.13 Optimal CNF Concentration Test Setup

Fig. 3.14 Tested CNFA in Compression

Over the course of a year over 100 CNFAs were tested in compression. The manufacturing techniques used evolved over time, so the results from the tests are not completely comparable; however, there is a clear trend between the concentration of CNFs per weight of cement and the maximum ERV recorded, as show in Fig. 3.15. The maximum ERVs recorded for each CNF concentration were averaged and the standard deviations were calculated. Fig. 3.15 shows the average ERV plus and minus one standard deviation. Some of the variance in the results is due to the change in manufacturing practices. A CNF concentration with respect to the weight of cement of 0.70% exhibited the largest change in ERV, which matched the results found by Gao et al. (Gao et al. 2009).

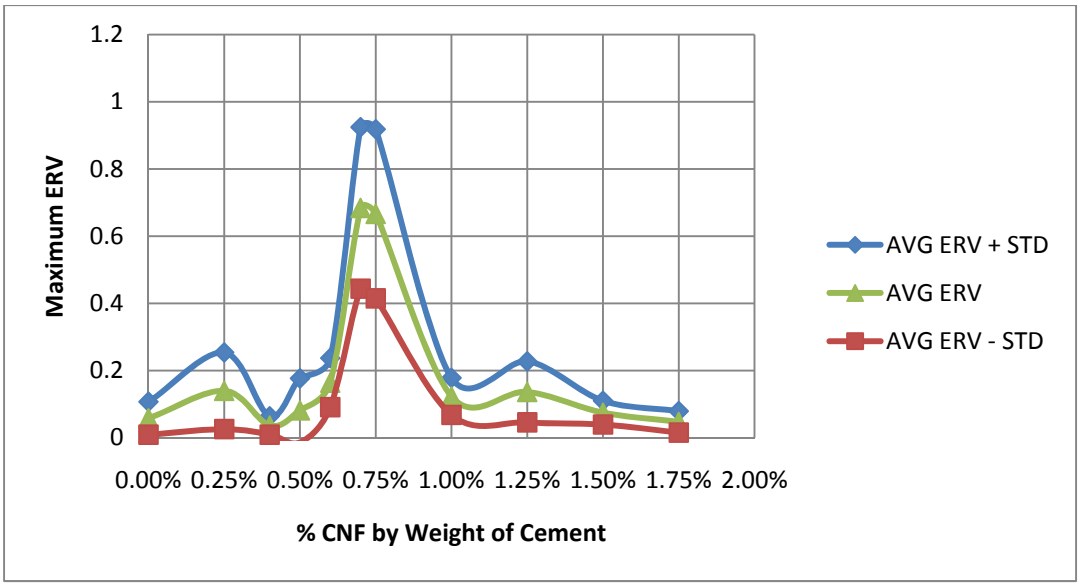

Fig. 3.15 Relationship between CNF Percentage and ERV

Five CNFAs with the final construction practices were tested containing 0.70% CNFs by weight of cement. The stress versus strain diagram for the five specimens is shown in Fig. 3.16. It can be seen that there is quite a bit of variation in the stress strain curves of the specimens despite the fact that the specimens were all cast at the same time using the same mix and cured under the same conditions. This is likely due to the fact that the specimens are quite small, and any type of local damage has great effect on the global specimen. Larger specimens have a more smeared global response despite the inclusion of local phenomenon.

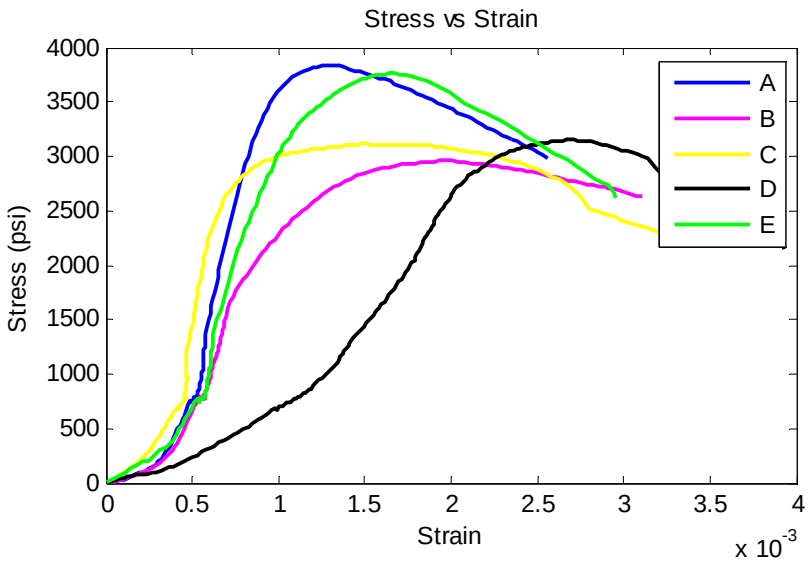

Fig. 3.16 CNFAs with 0.70% CNFs by Weight of Cement Stress versus Strain

Fig. 3.17 shows the ERV versus strain data for the specimens. From the figure, a strong trend is evident in all of the specimens as shown by the S-shape. While the CNFAs are compressed, initially there is very little damage and very little change in ERV. When the mortar begins to crush, the CNFs come in better contact with each other, causing the electrical resistance to decrease. As cracks form in the CNFAs, the fibers pull out, causing the change in ERV to lessen. These three phenomenon cause the S-shape.

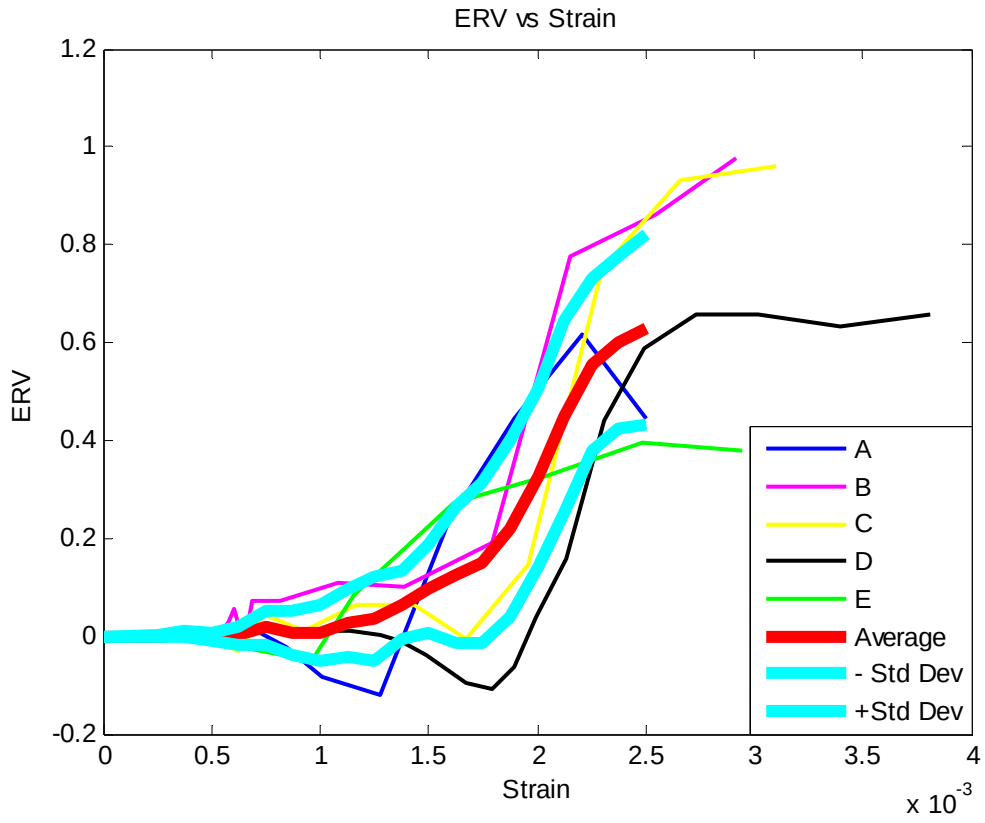

Fig. 3.17 CNFAs with 0.70% CNFs by Weight of Cement ERV versus Strain

Based on results from the tests completed to determine the optimal CNF dosage, a mix design was developed to optimize the material and electrical properties. See Table 3.1 for the final CNFA mix design proportioned by the total weight of the mortar.

Table 3.1 CNFA Mix Design

Material	Percentage of Total Mortar Weight
Fine Aggregate	52.9%
Cement	28.6%
Water	12.14%
Silica Fume	4.29%
HRWR	1.957%
CNFs	0.200%

3.6 Mortar Mixing Procedure

The mixing procedure used for the CNFAs is a hybrid of the mixing procedure proposed by the University of Michigan (UM) for a high performance self-consolidating steel fiber reinforced concrete mix (Liao et al. 2006) and the mixing procedure proposed by the University of Houston (UH) for a self-consolidating CNF concrete (Gao et al. 2009). In the UM mixing procedure, the water and chemical admixtures were premixed and added to the cement, fly ash, and fine aggregates in several steps to create a homogenous paste before adding the coarse aggregate and fibers. In the UH mixing procedure, the water, chemical admixtures, and CNFs were premixed and added to the cement, fly ash, fine aggregates, and coarse aggregates in one step. The mixing procedure is appropriate for small mortar mixes. The newly proposed hybrid mixing procedure is as follows.

1) Pour the water, HRWR, and CNFs into a laboratory grade blender and blend for 30 seconds.
2) Remove the mixture and place into a separate container. Fig. 3.18 shows the water, HRWR, and CNF mixture.

Fig. 3.18 Water, HRWR, and CNF Mixture

3) Pour one half of the sand, all of the cement, the silica fume, and the rest of the sand into the blender. Dry mix for 30 seconds.

4) Remove the blender from the stand. Use a long thin tool to scrape the sides and bottom of the blender. Place back onto the stand mix for 30 more seconds. Fig. 3.19 shows the sand and cement mixture after the first dry mix. Fig. 3.20 shows the sand and cement mixture after the second dry mix. It is easily seen that the mixture is much more homogenous after the second mix.

Fig. 3.19 Sand and Cement after First Dry Mix

Fig. 3.20 Cement and Sand after Second Dry Mix

5) Pour approximately one half of the original water, HRWR, and CNF mixture to the sand, silica fume, and cement mixture. Mix for 30 seconds. Fig. 3.21 shows the mortar mixture after mixing. It can be seen that liquid is concentrated in the middle while the outside is mostly dry. Repeat Step 4. Fig. 3.22 shows the mixture after mixing the second time. The consistency of the mixture should be approximately that of wet granulated sugar.

Fig. 3.21 Mortar Mixture after First Mixing of Step 5

Fig. 3.22 Mortar Mixture after Second Mixing of Step 5, Wet Granulated Sugar Stage

6) Pour approximately one half of the remaining water, HRWR, and CNF mixture (one quarter of the total mixture) in to the mortar mixture. Mix for 30 seconds. Fig. 3.23 shows the mortar mixture after mixing. It can be seen that liquid is concentrated in the middle. Repeat Step 4. Fig. 3.24 shows the mixture after

mixing the second time. The consistency of the mixture should be approximately that of dough.

Fig. 3.23 Mortar Mixture After First Mixing of Step 6

Fig. 3.24 Mortar Mixture After Second Mixing of Step 6, Dough Stage

7) Pour the remaining water, HRWR, and CNF mixture (one quarter of the total mixture) in the mortar mixture. Mix for 30 seconds. Fig. 3.25 shows the mortar mixture after mixing. It can be seen that liquid is concentrated in the middle.

Repeat Step 4. Fig. 3.26 shows the mixture after mixing the second time. The consistency of the mixture should be approximately that of syrup.

Fig. 3.25 Mortar Mixture After First Mixing of Step 7

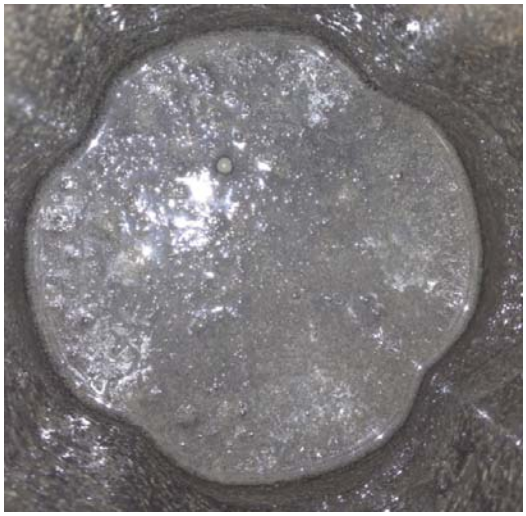

Fig. 3.26 Mortar Mixture After Second Mixing of Step 7, Syrup Stage

8) If the mixture is too stiff, add a very small amount of water and repeat Step 4 until the mixture is the consistency of syrup. A low viscosity level is needed so

that the mortar is self-consolidating. It has to flow under its own weight around the already placed meshes without creating any voids.

9) If upon visual inspection there are higher concentrations of CNFs in some areas as shown in Fig. 3.27, additional mixing may alleviate the issue. However, if the concentration of CNFs in the mixture is too high, the fibers will clump and additional mixing will not have an effect.

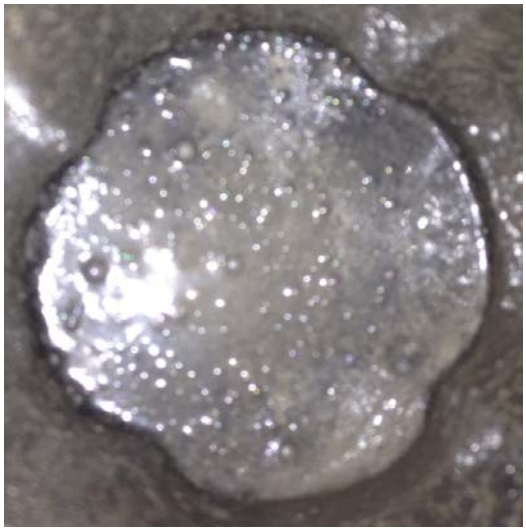

Fig. 3.27 Disproportionate Distribution of CNFs in Mortar

10) Pour the mortar into the assembled formwork with the meshes in place. The self-consolidating mortar requires no mechanical vibration. Vibrations may cause the meshes to misalign. Fig. 3.28 shows fresh mortar poured into the formwork.

Fig. 3.28 Fresh Mortar Poured into CNFA Formwork

3.7 Summary and Future Work

A carbon nanofiber aggregate (CNFA) was developed with self-sensing capabilities. The CNFA is a 2.54 cm by 2.54 cm by 2.54 cm (1.00 in. by 1.00 in. by 1.00 in) cube of mortar contain 0.70% carbon nanofibers (CNFs) by weight of cement. The electrical resistance is measured in the CNFAs through the embedment of four steel meshes and the use of the four-probe method.

The next steps in the development of the CNFA include:

- It is very difficult to align the meshes in the current formwork and the meshes sometimes become misaligned during casting. A better design would have vertical grooves cut into the side plates of the formwork. The meshes would slide down into the vertical grooves and be held perfectly aligned. This would result in a more consistently constructed CNFA.
- Other, more conductive, electrode materials should be explored for the meshes. These materials could include such materials as copper or nickel.

- Scanning electron microscope (SEM) pictures should be taken of the microstructure of the CNFAs. These should include pictures of the fibers post-testing to capture the pull-out behavior and pictures of the mesh-fiber interaction.
- Mortar was used as the material for the CNFA development so that the material properties matched the properties of the material in which it was embedded; however, cement based materials have some of the most variable material properties of any construction material. This variability translates to the electrical properties, making sensing difficult. Another material, such as a polymer, with similar elastic material properties may have better sensing capabilities due to more consistent material behavior.
- CNFAs should be exposed and calibrated to other stresses besides axial stress. If the study shows that their dominant behavior is in the axial-direction, than the use of CNFAs oriented in three principal directions should be explored.

CHAPTER 4
CARBON NANOFIBER AGGREGATE TEMPERATURE STUDY

4.1 Introduction

In addition to strain sensing, carbon fiber composites have been used to monitor temperature (Chung 2000) and create self-heating composites (Chang et al. 2009; Chung 2004). Because of the high cost associated with carbon nanofibers (CNFs), a CNF aggregate (CNFA) was developed. The CNFA is a 16.39 cm^3 (1.00 $in.^3$) cubic specimen of CNF mortar. The CNF mortar is self-sensing and can be used to determine the temperature in the CNFAs. The CNFAs can be embedded in reinforced or prestressed concrete structures and used to determine the internal temperature of the structure.

4.2 Thermistors

Discovered by Michael Faraday in 1833, a thermistor is a resistor whose resistance varies with temperature (McGee 1988). Since the 1930s, thermistors have commonly been used as temperature sensors. They differ from other temperature sensors such as resistance temperature detectors and thermocouples because of their material. Resistance temperature detectors and thermocouples are constructed of metals while thermistors are typically constructed of semiconductors. This study evaluates the use of a CNFA as a thermistor.

4.3 Specimen Construction

The goal of the experiment was to measure how the electrical resistance of an embedded CNFA varies with temperature. Six CNFAs were embedded in 7.62 cm (3 in.) by 15.24 cm (6 in.) cylinders. Type K thermocouples, as shown in Fig. 4.1, were

embedded in three of the cylinders. A hole was drilled in the center of the cylinder moulds to allow the CNFA and thermocouple wires to exit the concrete. Each mould was filled halfway with self-consolidating concrete (SCC), the CNFA was placed in the fresh SCC, and more SCC was placed on top. If the cylinder also contained a thermocouple, the thermocouple was epoxied to the top of the CNFA. SCC was used because it required no mechanical vibrations. Vibrations may cause the CNFA's orientation to change and the cylinder could not have been used for future strain monitoring tests. Fig. 4.2 shows an uncoated CNFA and thermocouple placed in fresh SCC.

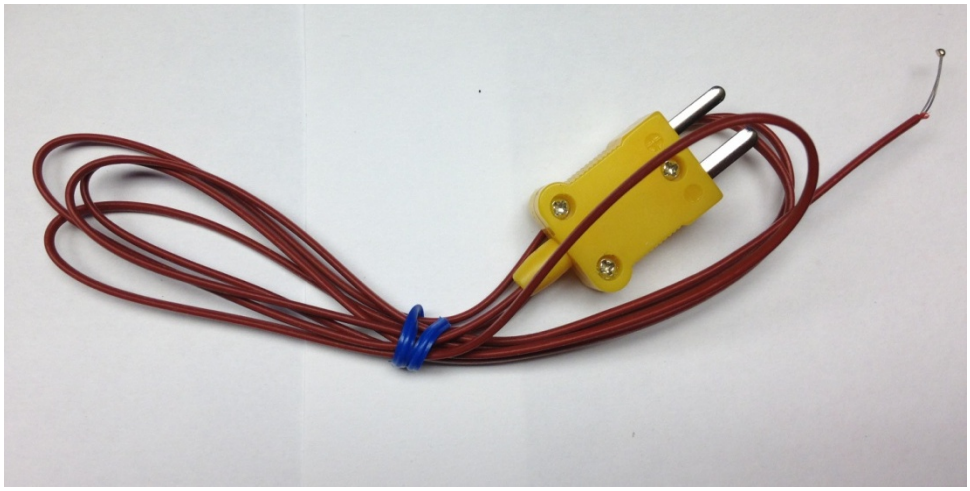

Fig. 4.1 Type K Thermocouple

Fig. 4.2 CNFA and Thermocouple in Fresh SCC

4.4 Experimental Setup and Results

Type III cement was used to make the SCC, which has a curing time of seven days. After curing, the temperature study commenced. The initial resistance was measured at the ambient temperature of 21.7°C (71.1°F). Six specimens were placed in a freezer capable of reaching -20°C (-4°F), as shown in Fig. 4.3. The specimens were monitored as they were frozen to the minimum temperature and returned to the ambient temperature outside of the freezer. The specimens were then placed in an oven capable of reaching 90°C (194°F), as shown in Fig. 4.4. The specimens were monitored as they were heated to the maximum temperature and returned to the ambient temperature outside of the oven; therefore, the specimens were monitored through one complete cooling and heating cycle. Fig. 4.5 shows the electrical resistance variation (ERV), defined as the change in electrical resistance divided by the initial electrical resistance, versus the temperature.

The initial resistance was taken as the resistance corresponding to 20°C (68°F). It is obvious from the figure that the ERV heating and cooling behavior is quite reversible and repeatable across multiple CNFAs.

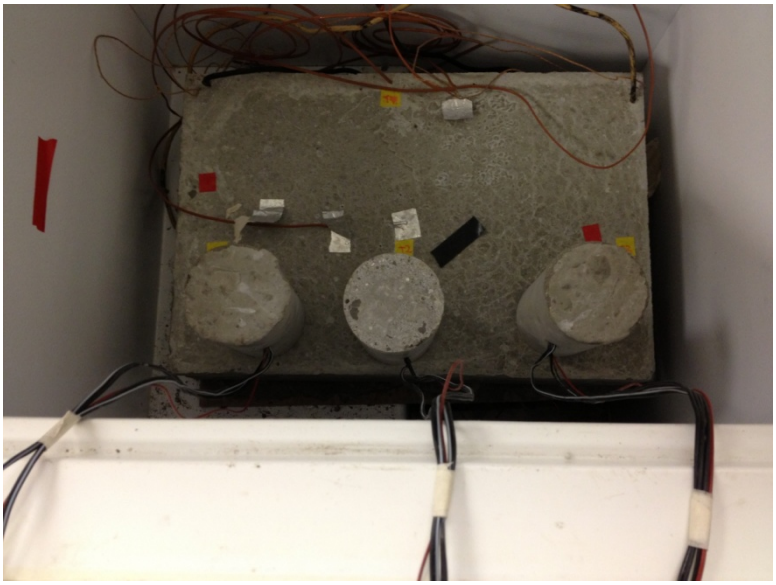

Fig. 4.3 Three Cylinders inside Freezer

Fig. 4.4 Six Cylinders inside Oven

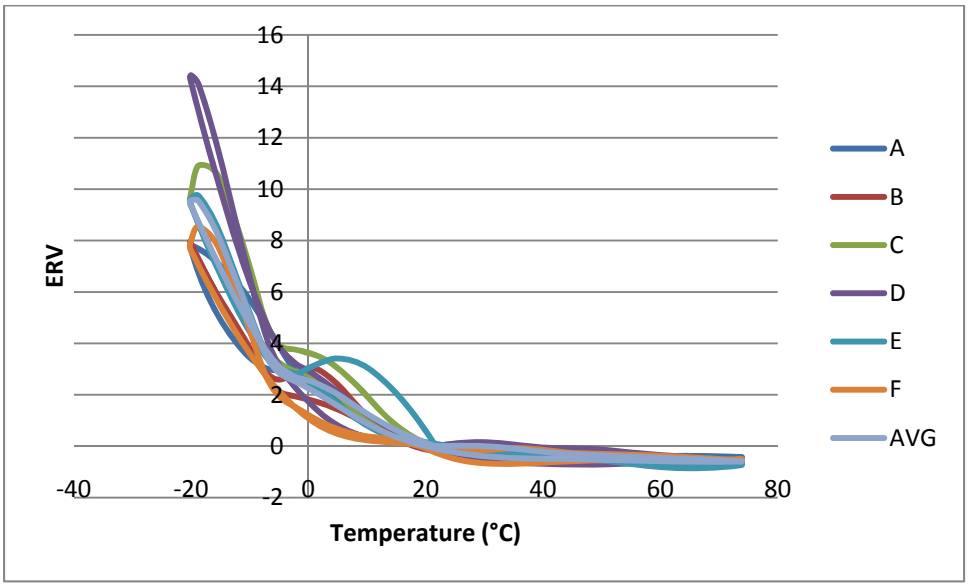

Fig. 4.5 Temperature versus ERV for Six Embedded CNFA and Their Average

4.5 Modeling of Thermal Behavior

The Steinhart-Hart equation (Steinhart and Hart 1968) is a nonlinear model widely used for the approximation of the resistance/temperature curve of thermistors,

$$\frac{1}{T} = A + B\ln(R) + C\ln(R)^3, \qquad \textbf{Equation 4.1}$$

where:

T: Temperature in Kelvin,

R: Resistance in Ohms,

A, B, C: Steinhart-Hart coefficients.

Often the inverse of the equation is useful,

$$R = \exp\left(\sqrt[3]{x-y} - \sqrt[3]{x+y}\right), \qquad \textbf{Equation 4.2}$$

where:

R: Resistance in Ohms,

x: $\sqrt{\left(\frac{B}{3C}\right)^3 + y^2}$,

y: $\frac{A - \frac{1}{T}}{2C}$,

T: Temperature in Kelvin,

A, B, C: Steinhart-Hart coefficients.

To find the Steinhart-Hart coefficients, at least three operating points are needed denoted by subscripts 1, 2, and 3,

$$A + B\ln(R_1) + C\ln(R_1)^3 = \frac{1}{T_1},$$
$$A + B\ln(R_2) + C\ln(R_2)^3 = \frac{1}{T_2}, \qquad \textbf{Equation 4.3}$$
$$A + B\ln(R_3) + C\ln(R_3)^3 = \frac{1}{T_3},$$

where:

T_1, T_2, T_3: Three different temperatures in Kelvin,

R_1, R_2, R_3: Resistance in Ohms corresponding to T_1, T_2, and T_3,

A, B, C: Steinhart-Hart coefficients.

Using the relationships and definitions shown in Equation 4.3, the Steinhart-Hart coefficients can be derived,

$$L_1 = \ln(R_1),$$
$$L_2 = \ln(R_2), \qquad \textbf{Equation 4.4}$$
$$L_3 = \ln(R_3),$$

$$Y_1 = \frac{1}{T_1},$$
$$Y_2 = \frac{1}{T_2}, \qquad \textbf{Equation 4.5}$$
$$Y_3 = \frac{1}{T_3},$$

$$\gamma_2 = \frac{Y_2 - Y_1}{L_2 - L_1},$$
$$\gamma_3 = \frac{Y_3 - Y_1}{L_3 - L_1}, \qquad \textbf{Equation 4.6}$$

$$C = \left(\frac{\gamma_3 - \gamma_2}{L_3 - L_2}\right)(L_1 + L_2 + L_3)^{-1}, \qquad \textbf{Equation 4.7}$$

$$B = \gamma_2 - C(L_1^2 + L_1L_2 + L_2^2), \qquad \textbf{Equation 4.8}$$

$$A = Y_1 - \left(B + L_1^2 C\right) L_1 . \qquad \textbf{Equation 4.9}$$

Several different operating temperatures were tried in the equations to optimize the fit. The chosen operating temperatures were -10.3°C (13.5°F), 21.7°C (71.1°F), and 73.9°C (165.0°F). The Steinhart-Hart coefficients A, B, and C were determined to be 3.60E-3, 2.19E-4, and 8.16E-5, respectively. Therefore, the best fit equation is:

$$\frac{1}{T} = 3.60 \times 10^{-3} + 2.19 \times 10^{-4} \ln\left(R\right) + 8.16 \times 10^{-5} \ln\left(R\right)^3 , \quad \textbf{Equation 4.10}$$

where:

T: Temperature in Kelvin,

R: Resistance in Ohms.

The coefficient of determination (R^2) value for the fit was calculated to be 0.555. The resistance values determined using Equation 4.10 were converted to ERV values by assuming that the resistance associated with 20°C (68°F) was the initial resistance. Fig. 4.6 shows a comparison of the Steinhart-Hart equation (S-H) and the average measured ERV (AVG) temperature versus ERV relationship. The Steinhart-Hart equation models the behavior for temperatures warmer than about -3°C (27°F).

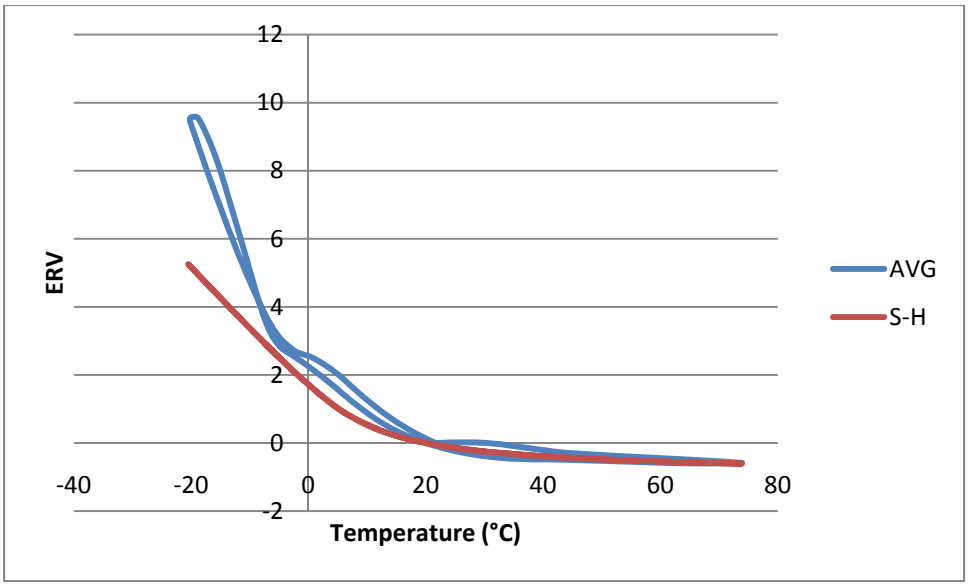

Fig. 4.6 Comparison of the Steinhart-Hart Equation and Average Measured ERV versus Temperature Data for Embedded CNFAs

To increase the accuracy of the fit, Steinhart and Hart (Steinhart and Hart 1968) suggest adding a fifth-order term to their third-order equation. Adding a fifth-order term would greatly complicate the equation and make it impractical for use. Cornell's Creative Machines Lab developed a free mathematical software, Eureqa, which determines mathematical equations that describe sets of data in their simplest form (Schmidt and Lipson 2009). The average ERV and temperature data were entered into Eureqa and Equation 4.11 was developed. Equation 4.11 is both much simpler than Equation 4.10 and fits the data better with a coefficient of determination of 0.927. Fig. 4.7 repeats Fig. 4.6 with the addition of the Eureqa best fit equation (FIT). The equation developed using Eureqa fits the data nearly perfectly. Therefore; the suggested model for the thermal behavior of CNFAs is:

$$ERV = 2.54\exp(-0.0681T) - 0.578, \qquad \textbf{Equation 4.11}$$

where:

ERV: Electrical resistance variation,

T: Temperature in Celsius.

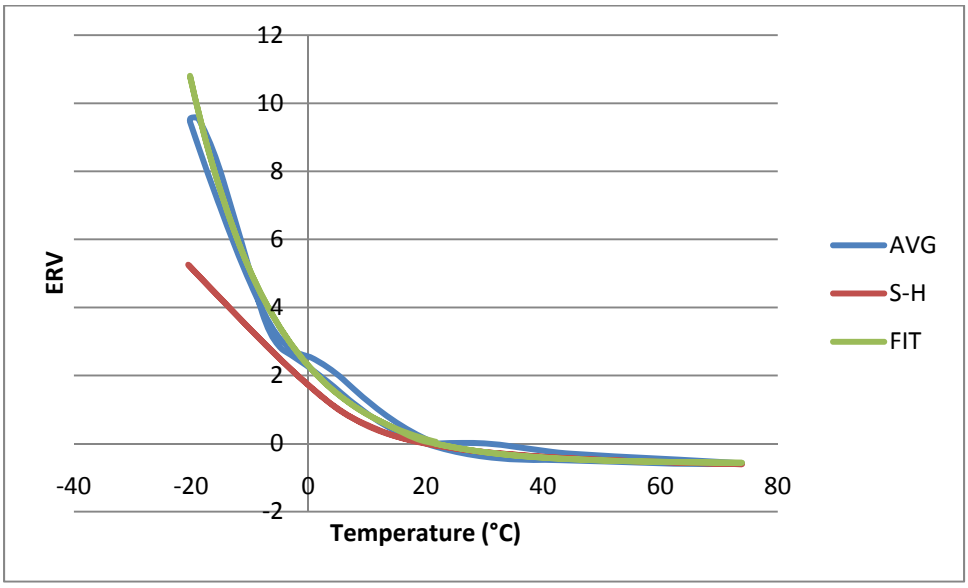

Fig. 4.7 Comparison of the Eureqa Fit, Steinhart-Hart Equation, and Average Measured ERV versus Temperature Data for Embedded CNFAs

4.6 Summary and Future Work

The response of embedded carbon nanofiber aggregates (CNFAs) was studied as they were exposed to varying temperatures. It was determined that CNFAs are a type of thermistor, a semiconductor that is capable of temperature sensing, and two models were derived that predict the thermal behavior of CNFAs. Future work includes testing many more specimens to make sure that the proposed model is appropriate. A wider temperature range should also be explored.

CHAPTER 5
CARBON NANOFIBER AGGREGATE HYDRATION STUDY

5.1 Introduction

Nearly all concrete comes in contact with water and the concrete hydration process is dependent on water. It stands to reason that the resistivity of a carbon nanofiber concrete composite would change with water content, but very little research has been done on the topic. Chen et al. (Chen et al. 2004) studied the effects of hydration and relative humidity on carbon fiber reinforced cement-based composites with inconclusive results. Han et al. (Han et al. 2010) studied the change in ERV of cement based materials containing carbon fibers and carbon black during the hydration process. An experiment was set up to see how the electrical resistance of the developed carbon nanofiber aggregates (CNFAs) react to water, if CNFAs can be used to monitor concrete hydration, and if a waterproof coating is practical with the use of a CNFA.

5.2 Experimental Setup

During the experiment, three parameters were explored:

- Coating: Half of the CNFAs were coated in a waterproof coating while half were left uncoated
- Embedment: Half of the CNFAs were embedded in a 7.62 cm (3 in.) by 15.24 cm (6 in.) cylinder while half were not

- Environment: Half of the CNFAs were submerged in water while half were left in normal room conditions

To adequately test the three parameters, eight test groups were formed as shown in the test matrix in Table 5.1. The test matrix is shown graphically in Fig. 5.1 Three CNFAs were tested in each group and the experiment was designed to run for 28 days.

Table 5.1 Hydration Test Matrix

Group	Uncoated	Coated	Not Embedded	Embedded	In Air	In Water
A	X		X		X	
B		X	X		X	
C	X		X			X
D		X	X			X
E	X			X	X	
F		X		X	X	
G	X			X		X
H		X		X		X

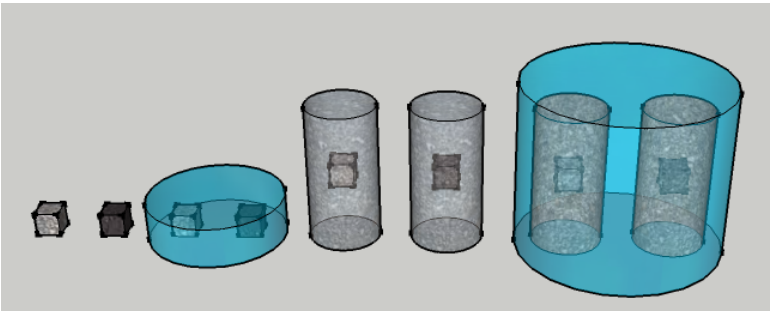

Fig. 5.1 Hydration Test Setup (From Left to Right, Groups A through H)

The purposes of the different test groups were as follows:

- Groups A and B: Groups A and B were the control groups. Hypothetically, their resistances should not have changed during the experiment. The experiment tested the stability of the resistance in the CNFAs.

- Groups C and D: Groups C and D were the extreme environment groups. For practical use, the CNFAs will be embedded in larger structures, so they were protected to some extent by the concrete around them after the concrete has set. The purpose of these groups was to test the waterproof coating in the worst-case environment.
- Groups E and F: Groups E and F acted as the typical environment for the CNFAs. The CNFAs became wet during the casting process as they were installed in fresh concrete. The concrete then formed around them and went through the hydration process. During this time, the excess water combines with the cement. Group E was especially interesting in this case to see if the uncoated CNFAs were capable of monitoring the hydration process.
- Groups G and H: Groups G and H were the extreme environment case for the embedded CNFA. Since the concrete is immersed in water, the pores in the concrete should have remained saturated.

5.3 Waterproof Coating and CNFA Preparation

Three waterproof coatings were considered during the course of the study. The first waterproof coating was Gardner Bender® Liquid Electrical Tape (LET). LET is a commonly available commercial product whose purpose is to provide waterproof insulation and protection for electrical splices and connections. The second product examined was Rust-Oleum® LeakSeal Flexible Rubber Coating (LS). LS is a rubberized protective utility coating whose primary purpose is to provide a waterproof seal for leaks

and cracks. The third coating examined was Ace® 35 Year Siliconized Acrylic Caulk (SAC). The purpose of SAC is to provide a waterproof seal on windows and doors.

In preparation for the experiment, all of the CNFAs were cured for seven days, which is appropriate for Type III cement. After 7 days, the specimens were air dried for 24 hours. To remove all excess moisture, they were oven dried for 24 hours at 100°C (212°F). Several coats of waterproof coating were applied to the CNFAs and cured as directed. The entire CNFA and approximately 7.62 cm (3 in.) of the wires nearest the CNFA were coated. The LET coating was applied with a small brush. It was very difficult to apply the coating evenly. Brush strokes were apparent in the coating leaving some areas with a very thin coat. To compensate for this problem and try to establish an even coating, the coats were applied in perpendicular directions. The LS comes in an aerosol can. The material was directly sprayed onto the aggregates. The material had a foamy consistency that left bubbles in the coating. Several coats were applied to compensate for the bubbles. The SAC was described as paintable in the manufacturer's directions, so it was painted on the CNFAs using a small paintbrush. The SAC appeared to be the most substantial, evenly coated material of the three.

After the directed curing time required for the waterproof coatings, the CNFAs in Groups E through H were embedded in 7.62 cm (3 in.) by 15.24 cm (6 in.) cylinders. A hole was drilled in the center of the cylinder moulds to allow the wires to exit the concrete. The moulds were filled halfway with self-consolidating concrete (SCC), the CNFA was placed in the fresh SCC, and more SCC was placed on top. SCC was used because it required no mechanical vibrations. Vibrations may have caused the CNFA's

orientation to change, and the cylinder could not have been used for future strain monitoring tests. Fig. 5.2 shows an uncoated CNFA placed in fresh SCC.

Fig. 5.2 Uncoated CNFA in Fresh SCC

5.4 Experimental Results

The initial experiment used the LET as a waterproof coating. The electrical resistance was measured using the four probe method and a Keithley Source Meter. The experiment was aborted after it was obvious that the waterproof coating failed. Fig. 5.3 shows the electrical resistance variation (ERV), defined as the change in electrical resistance divided by the initial electrical resistance, for the means of Groups C and D monitored over a 48 hour period. All of the CNFAs were submerged in water at approximately 26 hours into the monitoring time. Both Groups C and D behaved exactly the same immediately plunging to an ERV of -100% when exposed to water, despite the fact that Group D was coated in a supposedly waterproof substance.

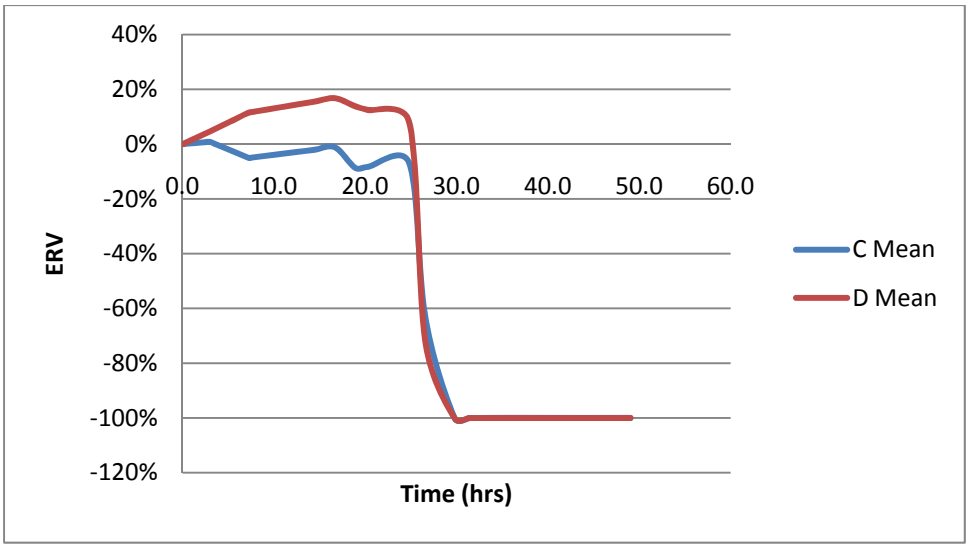

Fig. 5.3 ERV versus Time for Groups C and D with LET Waterproof Coating

The experiment was repeated using LS as the waterproofing agent. Unfortunately, this waterproof coating also failed. When Group D was exposed to water at about 30 hours, the ERV immediately dropped to -84%. After being exposed to water for roughly 6 hours, the ERV was -100%, exactly like the uncoated specimens in Group C. This experiment was also aborted.

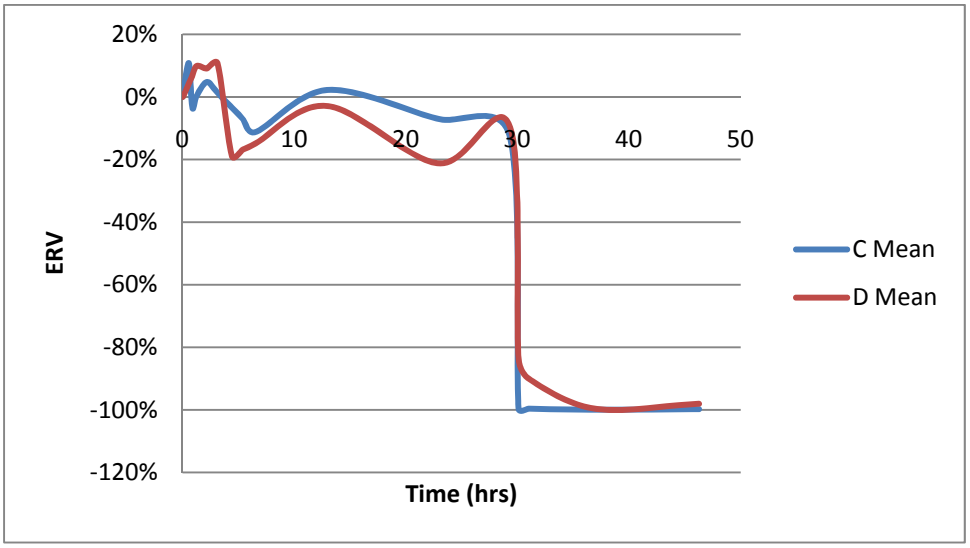

Fig. 5.4 ERV versus Time for Groups C and D with LS Waterproof Coating

The experiment with the SAC waterproof coating ran for the intended 28 day duration. Several observations could be made about each of the test groups.

5.4.1 Experimental Results—Groups A and B

Groups A and B consisted of uncoated and coated dry specimens, respectively, that were not embedded in concrete. It was expected that their ERV would not have a significant change; however, that was not the case. It was observed that it took the CNFAs in these groups about three weeks to reach a stable electrical reading that did not change. The sinusoidal behavior observed is likely due to temperature changes since the behavior was observed in all six CNFA. At the time of the test, no temperature studies had been completed, and the temperature was not recorded because it was not assumed to have a large effect on ERV. It was found that cool temperatures do have a significant effect on ERV. This experiment was completed in February, and the temperature variation in the testing environment was great enough to affect the ERV.

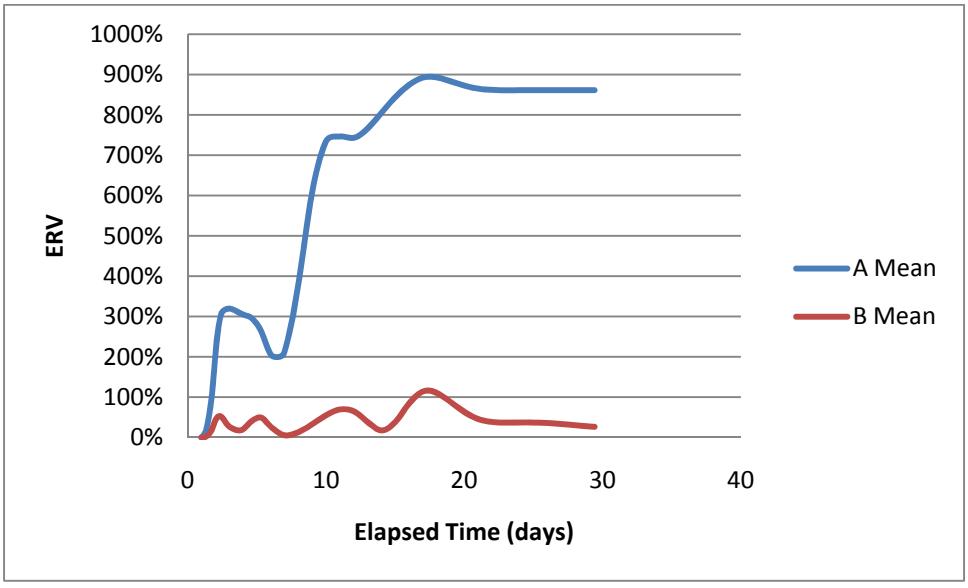

Fig. 5.5 ERV versus Time for Groups A and B with SAC Waterproof Coating

5.4.2 Experimental Results—Groups C and D

Groups C and D consisted of uncoated and coated specimens, respectively, that were not embedded in concrete and were placed in water. It was expected and observed that Group C would immediately have an ERV of -100% upon immersion in water. If the SAC waterproof coating worked, it was expected that there would be no change in ERV. The SAC coating worked to an extent for approximately 16 days before it had started to be visually washed away in the water, as shown in Fig. 5.6. By the 19th day, the ERV stabilized at about -94%.

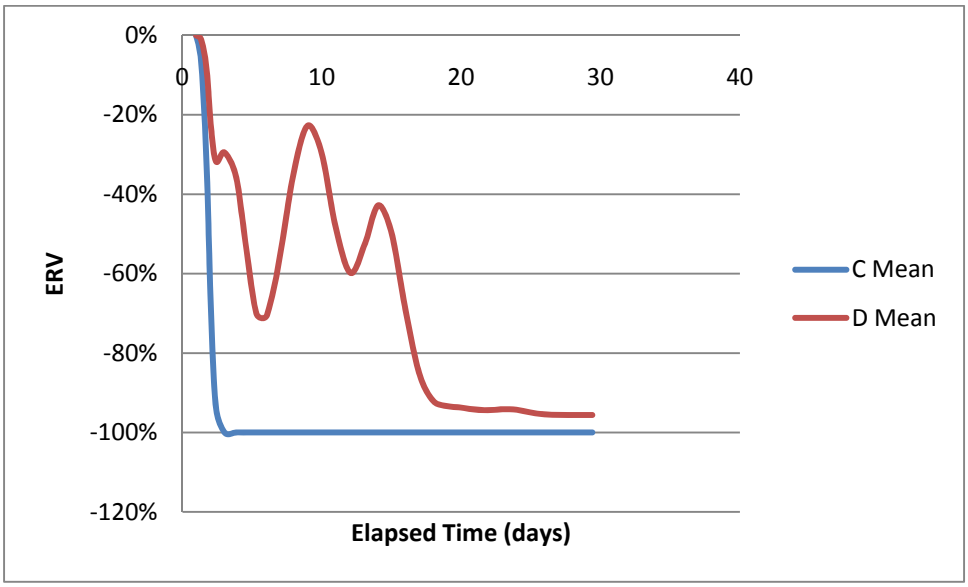

Fig. 5.6 ERV versus Time for Groups C and D with SAC Waterproof Coating

5.4.3 Experimental Results—Groups E and F

Groups E and F consisted of uncoated and coated specimens, respectively, that were embedded in concrete and were not placed in water. It was expected and observed that Group E would immediately have an ERV of -100% upon embedment. If the SAC waterproof coating worked, it was expected that there would be no change in ERV. However, as observed in Fig. 5.7, the ERV immediately dropped to -77% upon

embedment. Over the next 5 days, the ERV reached -100%. It then rose to and maintained -97%. Since this behavior was more severe than Group D's behavior, despite the fact that Group D was in a harsher environment, it is likely that water entered the CNFA via the uncoated portion of the wire.

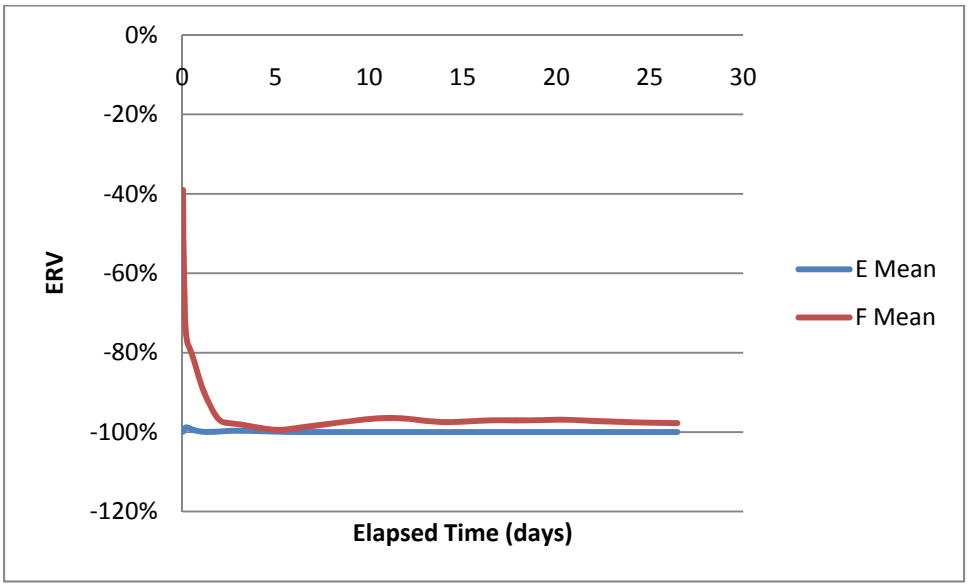

Fig. 5.7 ERV versus Time for Groups E and F with SAC Waterproof Coating

5.4.4 Experimental Results—Groups G and H

Groups G and H consisted of uncoated and coated specimens, respectively, that were embedded concrete and placed in water. It was expected and observed that Group G would immediately have an ERV of -100% upon embedment. If the SAC waterproof coating worked, it was expected that there would be no change in ERV. Group H behaved similarly to Group F. Group H's ERV dropped considerably immediately and reached -100% after about 5 days.

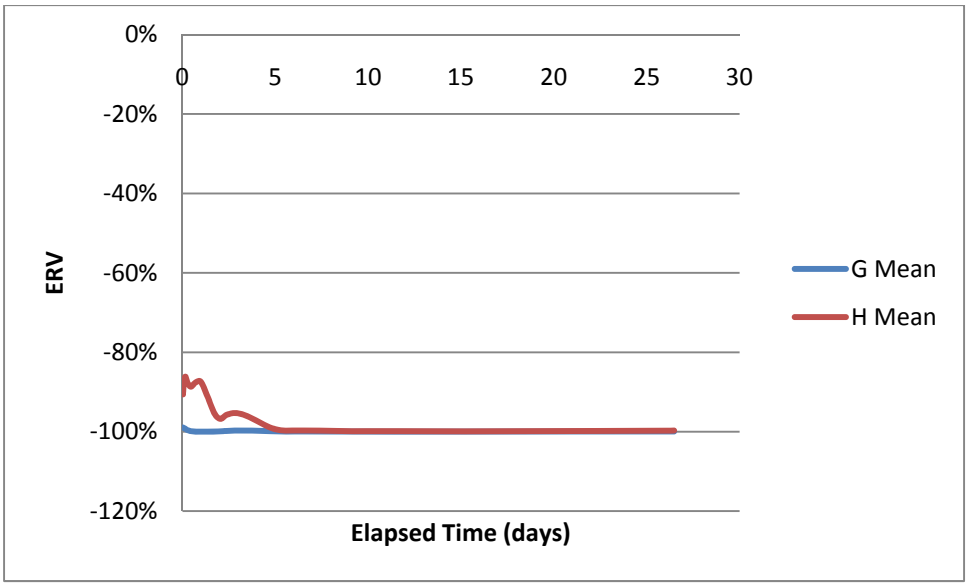

Fig. 5.8 ERV versus Time for Groups G and H with SAC Waterproof Coating

5.4.5 Additional Observations

In carbon fiber composites, the ERV is typically recorded because the initial resistances of the specimens are not the same. Using the ERV instead of the actual resistance normalizes the results. Because there was such a significant difference between the oven dried CNFA resistance (on the order of 10 MΩ) and the freshly embedded CNFA resistance (on the order of 5 kΩ), the ERV versus time graphs simply show a flat line with an ERV of -100%. However, there was an interesting phenomenon that occurred when the resistances were observed in Groups E and G, which were the embedded uncoated aggregates in air and water, respectively. All six CNFA in these two groups behaved almost identically. The averages of the two groups can be observed in Fig. 5.9. The sinusoidal behavior observed through the fifth day is likely due to temperature effects. After the fifth day, the resistances of all six CNFA became very stable and almost identical in resistance. Up until 28 days, the resistances of the CNFA had only increased slightly. When they were tested in compression one month after this

test, their resistances were all in the range of 3 to 5 kΩ. These results imply that embedded CNFA have a very stable resistance despite the presence of water or humidity on the concrete surface.

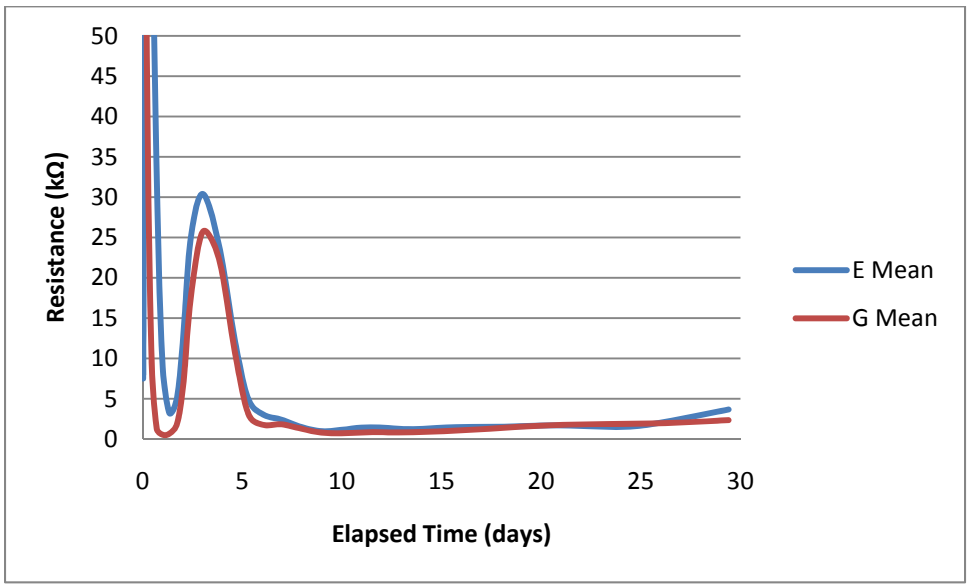

Fig. 5.9 Resistance versus Time for Groups E and G

5.5 Follow-Up Experiment Introduction

From the hydration study, it was concluded that after the CNFAs were embedded, the behavior of the CNFAs was the same whether the outer concrete was exposed to water or air. A certain amount of water was trapped inside the CNFAs, causing the resistances to drop from approximately 10 MΩ to approximately 5 kΩ. The CNFAs then maintained a resistance on the order of 5 kΩ whether or not the concrete it was embedded in was exposed to additional water.

A follow-up experiment consisting of monitoring three uncoated CNFAs embedded in 7.62 cm (3 in.) by 15.24 cm (6 in.) cylinders was devised for two purposes:

- Check the necessity of oven drying the CNFAs: Logically, if uncoated CNFAs will be saturated with water during the casting process, there is no need to oven dry the CNFA. In this experiment, the CNFA were not oven dried, and the resistances were measured before and after casting.
- Monitor Temperature Effects: Thermocouples were embedded in the cylinders during casting to measure temperature during the course of the test.

5.6 Follow-Up Experimental Setup

Before casting, the resistances of the three CNFAs were measured to be 13.36 kΩ, 12.61 kΩ, and 13.07 kΩ for CNFAs A, B, and C, respectively. Since the resistances were on the order of kilo-Ohms rather than mega-Ohms, the resistances could be measured automatically using a data acquisition system rather than manually using the Keithly Source Meter used in the previous experiment. To measure the resistance, the outer wires of the three CNFAs were connected in series with a 5.6 kΩ resistor and a 10 V power supply, as shown in blue in Fig. 5.10. The voltage drops across the inner wires of the CNFAs and resistor were measured using the data acquisition system dSpace, as shown in red in Fig. 5.10. There was an impedance problem within the data acquisition system, so differential amplifiers were placed between each component of the circuit and the data acquisition system, as shown in Fig. 5.10. A differential amplifier is a circuit that computes the differences of two voltages and multiplies it by a constant. The differential amplifier circuit is shown in Fig. 5.11.

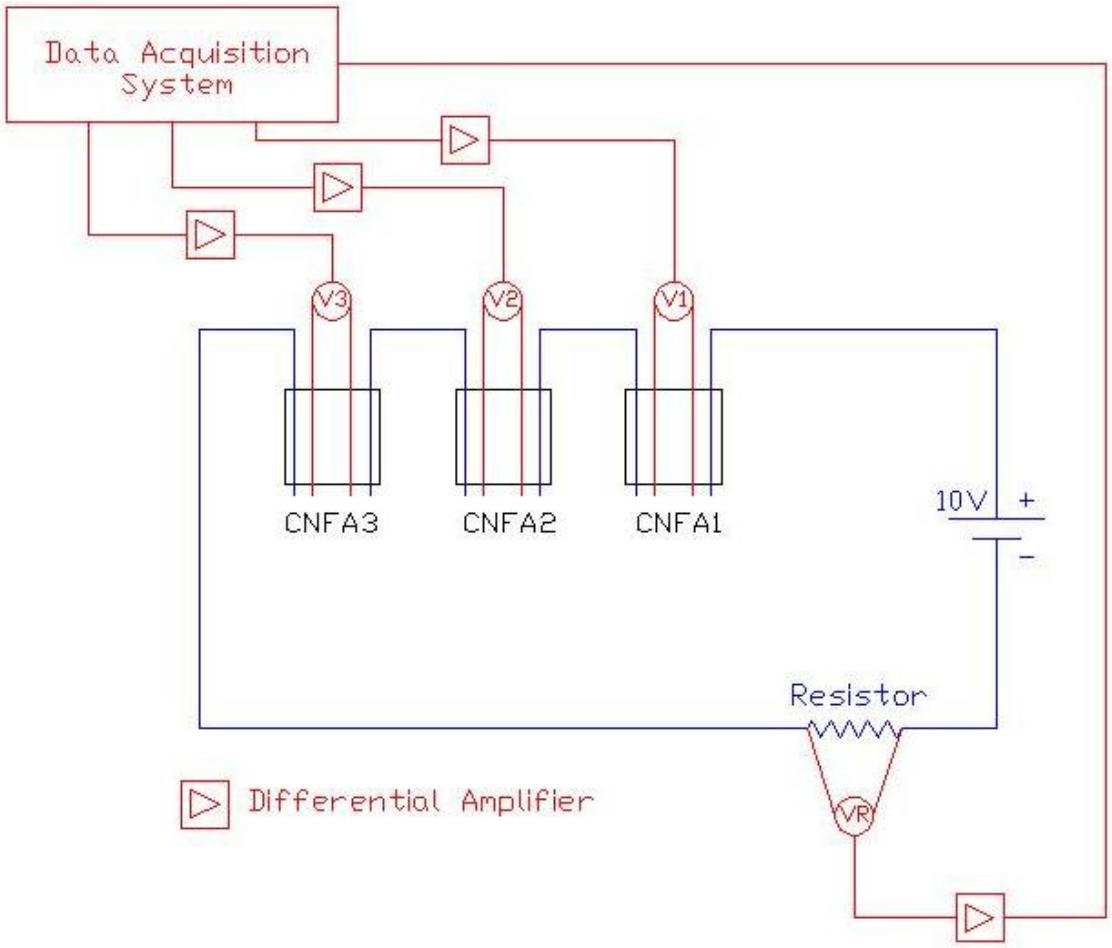

Fig. 5.10 Electrical Circuit and Connection to Data Aquisition System for Follow-Up Experiment

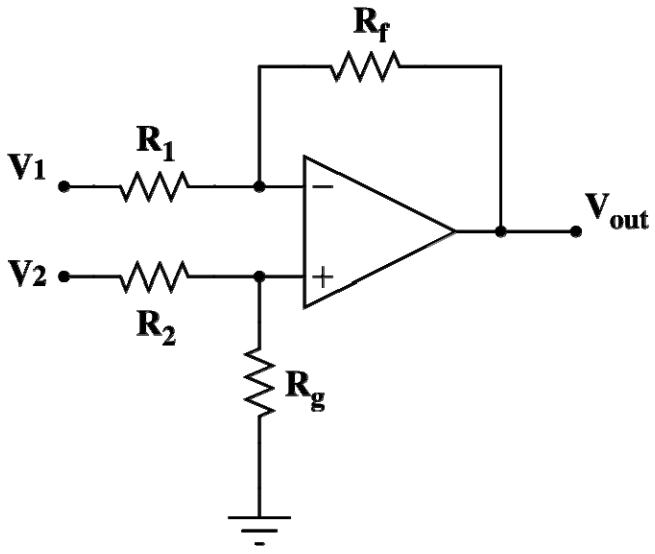

Fig. 5.11 Differential Amplifier Circuit

The output voltage is computed as:

$$V_{out} = \frac{(R_f + R_1)R_g}{(R_g + R_2)R_1} V_2 - \frac{R_f}{R_1} V_1, \qquad \textbf{Equation 5.1}$$

where:

V_{out}: Output Voltage,

V_1: Input Voltage 1,

V_2: Input Voltage 2,

R_1: Resistor Connected to Voltage 1,

R_2: Resistor Connected to Voltage 2,

R_f: Feedback Resistor,

R_g: Grounding Resistor.

If all four of the resistors have equal resistances, the output voltage equals the difference of the two input voltages,

$$V_{out} = V_2 - V_1 . \qquad \textbf{Equation 5.2}$$

The differential amplifiers, consisting of all equal resistors and 741 operational amplifiers, are shown in Fig. 5.12.

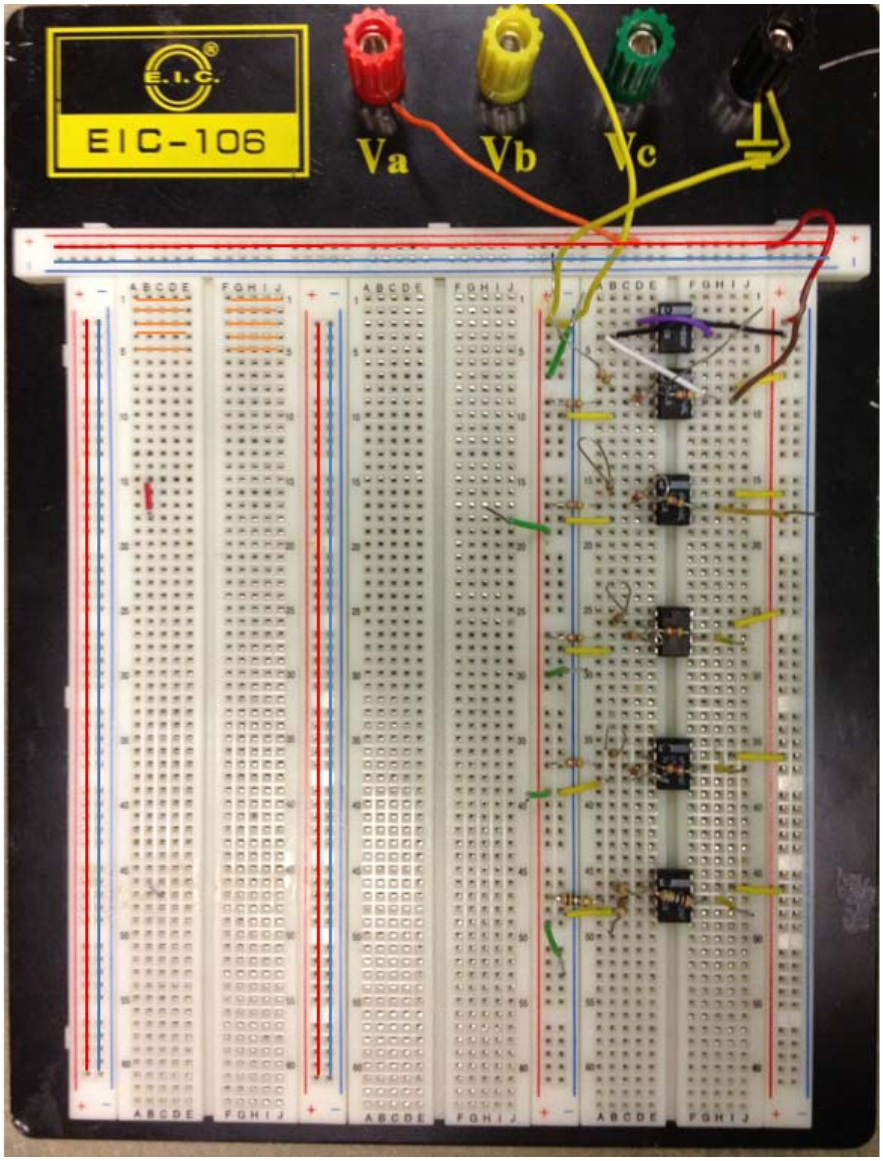

Fig. 5.12 Differential Amplifiers

A Type K thermocouple, as shown in Fig. 5.13, was embedded in one of the cylinders. A hole was drilled in the center of the cylinder moulds to allow the CNFA and

thermocouple wires to exit the concrete. Each mould was filled halfway with SCC, the uncoated CNFAs (and thermocouple when applicable) were placed in the fresh SCC, and more SCC was placed on top. The SCC was made using Type III cement so that the majority of the hydration process would occur in seven days. Fig. 5.14 shows an uncoated CNFA and thermocouple placed in fresh SCC.

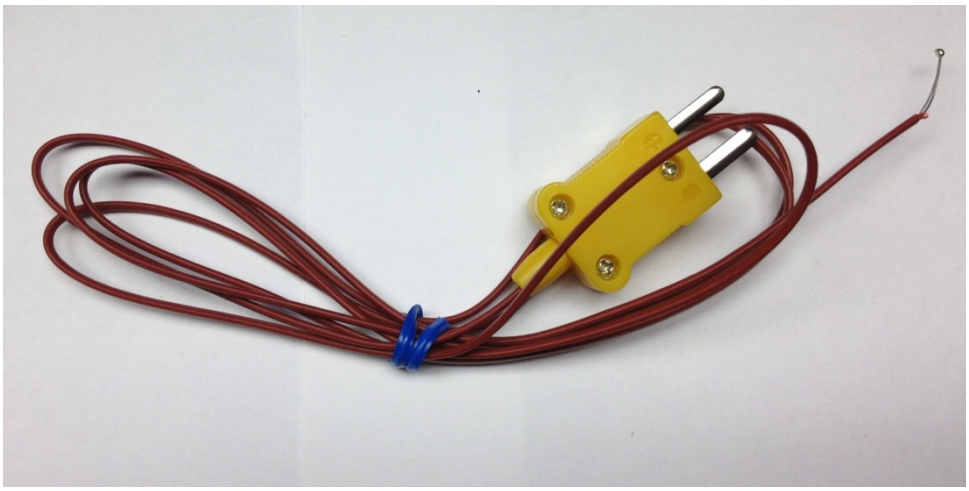

Fig. 5.13 Type K Thermocouple

Fig. 5.14 Uncoated CNFA and Thermocouple in Fresh SCC

5.7 Follow-Up Experiment Results

The resistance and temperature of the three CNFAs were monitored for seven days after they were embedded, as shown in Fig. 5.15. It is clear that with the exception of the heat of hydration, which occurred within the first day, the temperature stayed relatively constant throughout the test and the cyclic behavior observed in the previous test did not occur. The final resistances measured for CNFAs A, B, and C were 5.44 kΩ, 3.63 kΩ, and 5.97 kΩ, respectively. These resistances were consistent with the final resistances found in the previous test; therefore, it is acceptable to not oven dry the CNFAs before embedment. All three CNFAs reached a stable ERV within one to two days after embedment. This leads one to believe that early strength monitoring could likely be achieved by monitoring the ERV of embedded CNFAs in a full-scale concrete structure.

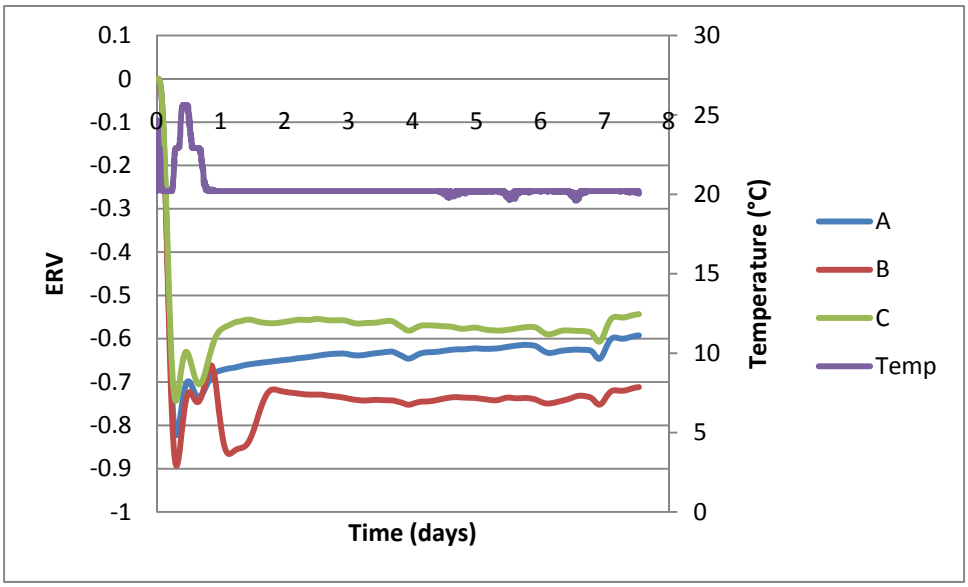

Fig. 5.15 Follow-Up Experiment ERV and Temperature versus Time

5.8 Summary and Future Work

The response of carbon nanofiber aggregates (CNFAs) was studied as CNFAs were exposed to water. The following conclusions were drawn from experimental data:

- Three waterproof coatings were tested for use with CNFAs. It was discovered that all three waterproof coatings failed, allowing water in the CNFAs. Later, when the waterproofed CNFAs were tested inside of concrete cylinders, the bond behavior was poor and the CNFAs could not be used for strain sensing.
- It was discovered that uncoated aggregates embedded in cylinders had the same behavior whether or not the cylinder was exposed to water. Since the uncoated CNFAs embedded in concrete are not sensitive water, it was deemed that the waterproof coating was unnecessary.
- It was discovered that it was not necessary to oven dry the CNFAs before embedment since the uncoated CNFAs would become saturated with water upon embedment. The final resistances after embedment were on the same order of magnitude whether or not the CNFAs were oven dried before embedment.
- The electrical resistance variation (ERV) of the CNFAs becomes stable one to two days after embedment. Initial set occurs roughly one day after casting, so this phenomenon may be useful for early-age monitoring of concrete.

Future work in this area of research includes:

- Although it appears that waterproofing is not necessary, other waterproofing agents such as epoxies can be explored. These materials should have similar elastic properties to that of concrete so the sensor can still be used for strain monitoring.
- A more detailed, systematic study should be completed on the effects of moisture on the CNFAs.
- The early properties of embedded CNFAs should be tested with the purpose of observing any correlation between early strength and ERV.

CHAPTER 6
CARBON NANOFIBER AGGREGATE COMPRESSIVE STRAIN STUDY

6.1 Introduction

The primary purpose for developing carbon nanofiber (CNF) composites in this study is for strain monitoring. Because of the high cost associated with CNFs, a CNF aggregate (CNFA) was developed. The CNFA is a 16.39 cm^3 (1.00 $in.^3$) cubic specimen of CNF mortar. The CNF mortar is self-sensing and can be used to determine the damage in the CNFAs. The CNFAs can be embedded in reinforced or prestressed concrete structures and used to determine the localized damage in a structure. For the purpose of compressive strain monitoring, the CNFAs were embedded in concrete cylinders and tested in compression to determine a relationship between compressive strain and electrical resistance.

6.2 Specimen Construction

The goal of the experiment was to measure how the electrical resistance of an embedded CNFA varies with strain. The CNFAs were embedded in 7.62 cm (3 in.) by 15.24 cm (6 in.) cylinders. Type K thermocouples, as shown in Fig. 6.1, were embedded in the cylinders. A hole was drilled in the center of the cylinder moulds to allow the CNFA and thermocouple wires to exit the concrete. Each mould was filled halfway with self-consolidating concrete (SCC), the CNFA was placed in the fresh SCC, and more SCC was placed on top. A thermocouple was epoxied to the top of the CNFAs. SCC

was used because it required no mechanical vibrations. Vibrations may cause the orientation of the CNFA to change. Fig. 6.2 shows a CNFA and thermocouple placed in fresh SCC.

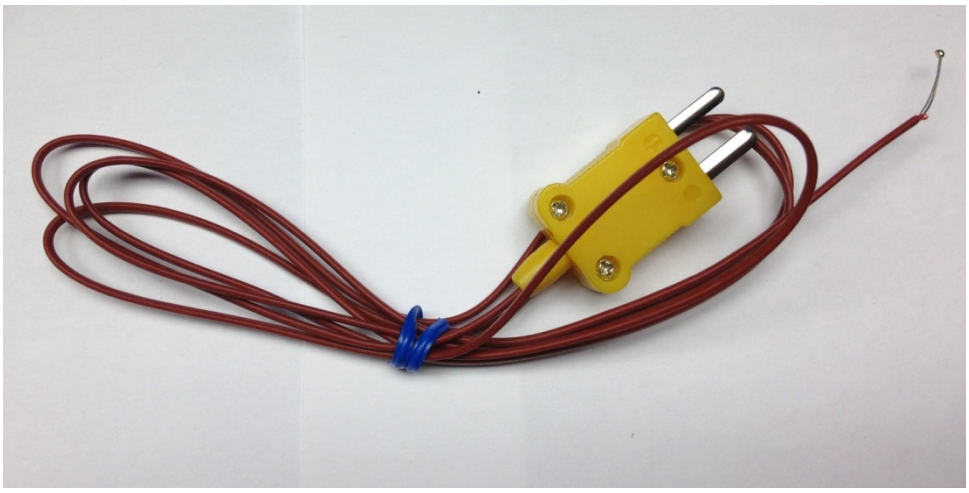

Fig. 6.1 Type K Thermocouple

Fig. 6.2 CNFA and Thermocouple in Fresh SCC

6.3 Experimental Setup

To measure the electrical resistance, the outer wires of the CNFA were connected in series with a 5.6 kΩ resistor and a 10 V power supply, as shown in blue in Fig. 6.3. The voltage drops across the inner wires of the CNFA and resistor were measured using the data acquisition system dSpace, as shown in red in Fig. 6.3. There was an impedance problem within the data acquisition system, so differential amplifiers were placed between each component of the circuit and the data acquisition system, as shown in Fig. 6.3.

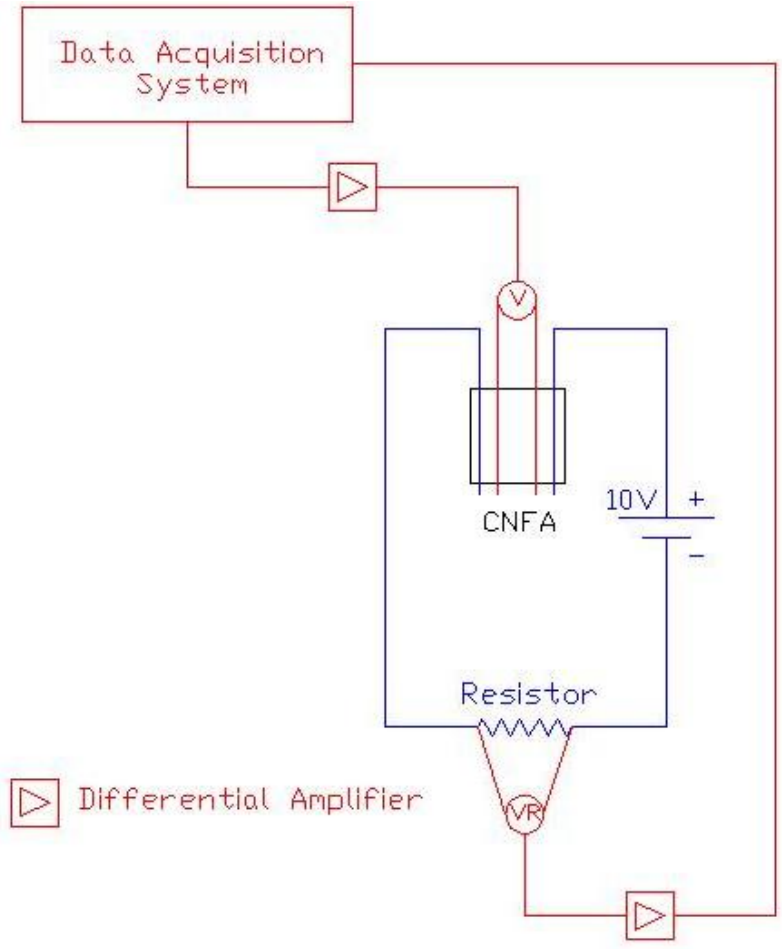

Fig. 6.3 Electrical Circuit and Connection to Data Aquisition System for Cylinder Compression Experiments

The differential amplifier circuit is shown in Fig. 6.4. A differential amplifier is a circuit that computes the differences of two voltages and multiplies it by a constant. If all four of the resistors have equal resistances, then the output voltage will equal the difference of the two input voltages. The differential amplifiers, consisting of all equal resistors and 741 operational amplifiers, are shown in Fig. 6.5.

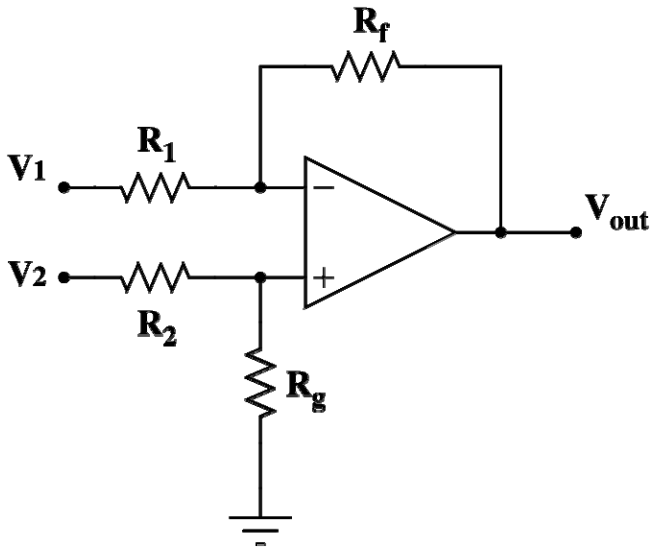

Fig. 6.4 Differential Amplifier Circuit

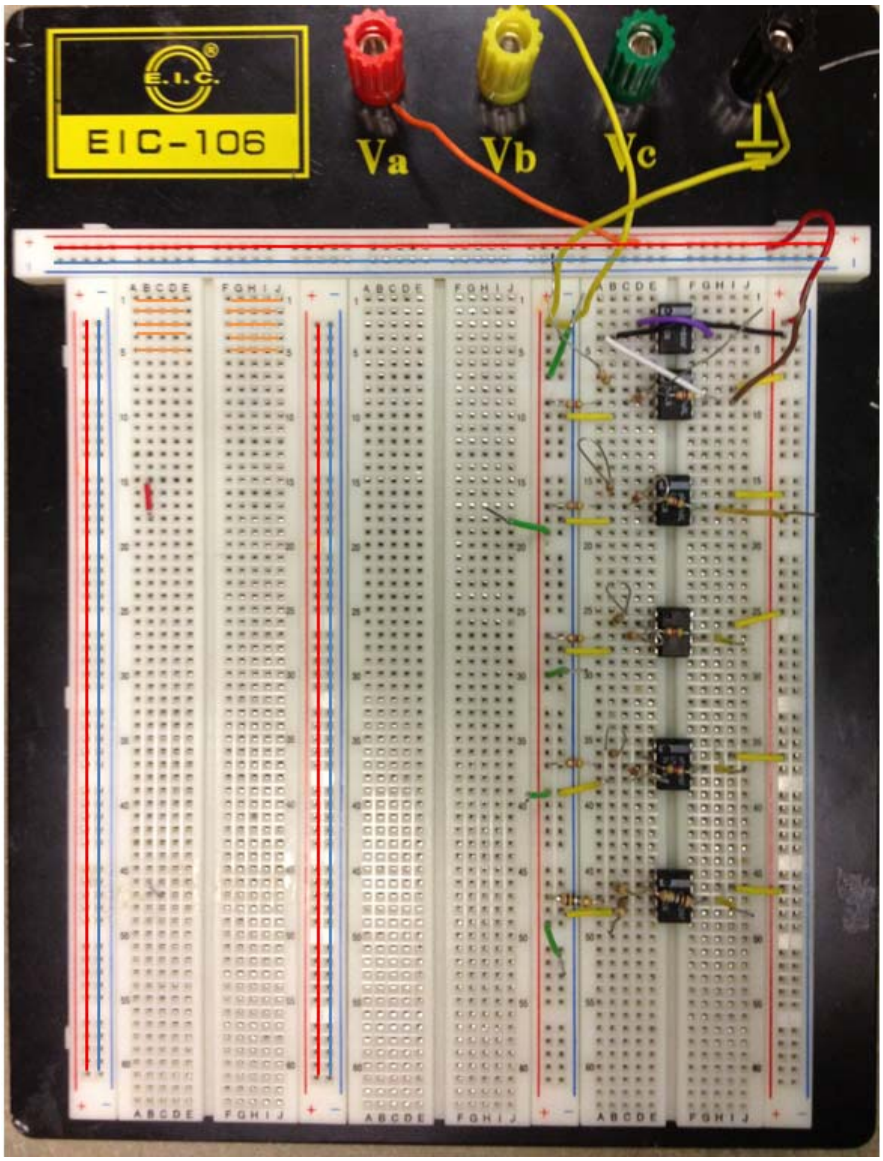

Fig. 6.5 Differential Amplifiers

The cylinders were tested in a Tinius Olsen Hydraulic Tester. The force was measured from the Tinius Olsen Hydraulic Tester. The strain was monitored using an extensometer, shown in green in Fig. 6.6. The extensometer measured the smeared strain across the center 50.8 mm (2.00 in.) of the cylinder. To ensure the failure occurred in this region, steel pipe clamps were used to confine each cylinder 25.4 mm (1.00 in) from the top and bottom, as shown in Fig. 6.6.

Fig. 6.6 Cylinder Compression Experimental Setup

6.4 Experimental Results

Three different experimental groups were tested in this experiment as shown in Table 6.1.

Table 6.1 Cylinder Compression Experimental Groups

Group	Temperature Range	Load Type
Group 1	Room Temperature	Monotonic Compression
Group 2	Frozen	Monotonic Compression
Group 3	Room Temperature	Cyclic Compression

6.4.1 Group 1 Experimental Results

Group 1 consisted of 12 cylinders tested in monotonic compression at room temperature. The electrical resistance variation (ERV), defined as the change in electrical resistance divided by the initial electrical resistance, showed several definite trends across

all of the cylinders. Typical stress versus time, strain versus time, ERV, and voltage variation (VV) versus time relationships for three cylinders are shown in Fig. 6.7. VV is defined as the change in voltage divided by the original voltage. From the ERV curves, it is apparent when each cylinder began loading as the ERV increases from 0 simultaneously with the stress and strain. The maximum ERV occurs near a strain of 0.001 for each case. From the VV curves, failure is clearly shown by a sudden drastic change in the negative direction.

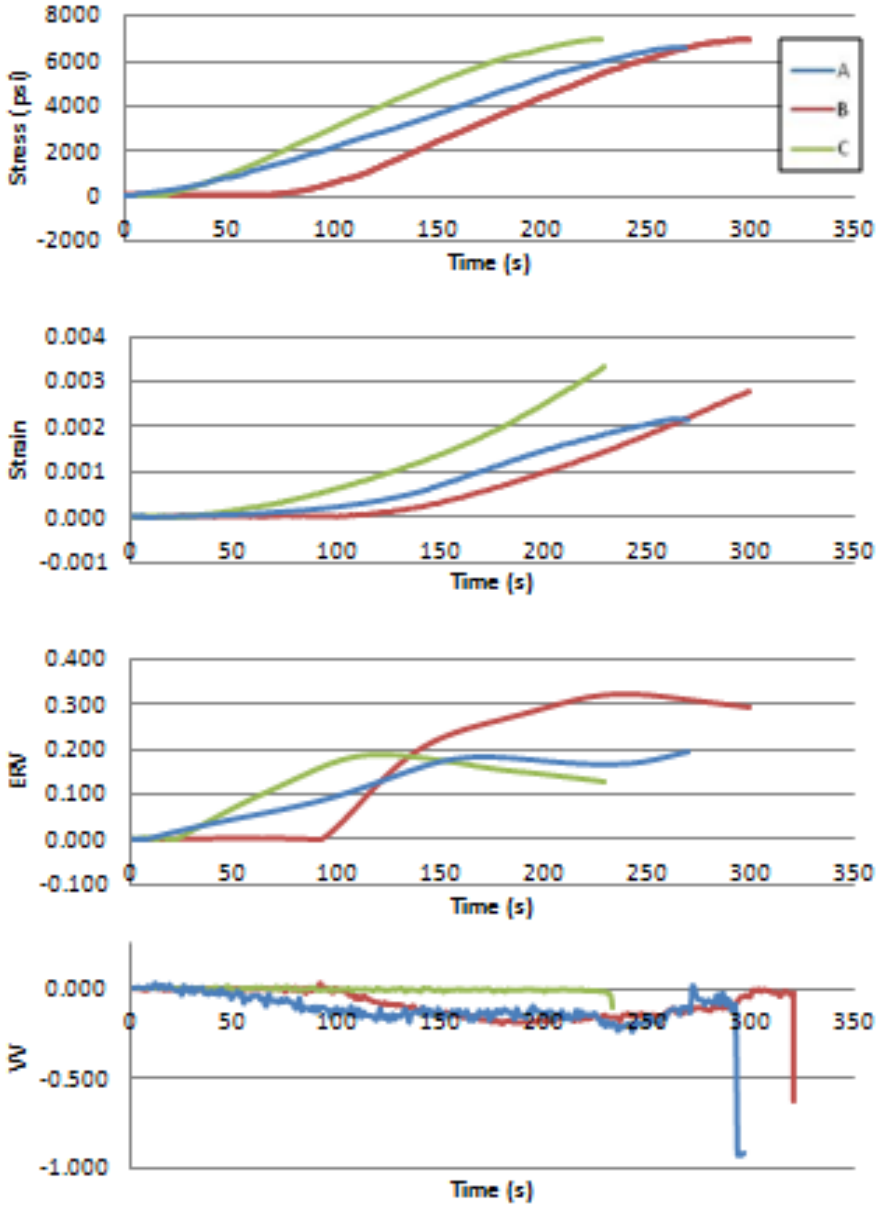

Fig. 6.7 Typical Stress, Strain, and ERV Results for Cylinders Tested in Compression at Room Temperature

While the trends are similar, there is considerable variation in the ERV values. Fig. 6.8 shows the mean ERV versus strain relationship for the 12 tested cylinders. The

standard deviation of the data is so large that a model would be impractical for use, but a model was developed for the data available.

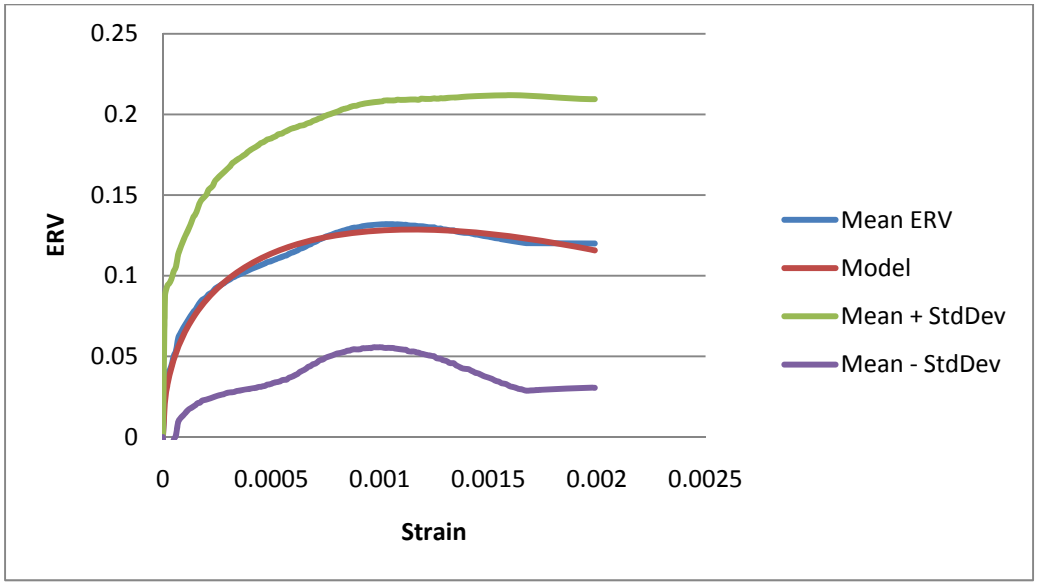

Fig. 6.8 Strain versus ERV for Group 1

Cornell's Creative Machines Lab developed a free mathematical software, Eureqa, which determines mathematical equations that describe sets of data in their simplest form (Schmidt and Lipson 2009). The mean ERV and strain data were entered into Eureqa and an equation was developed with a coefficient of determination of 0.985,

$$ERV = 7.59\sqrt{\varepsilon} - 112\varepsilon, \qquad \textbf{Equation 6.1}$$

where:

ERV: Electrical resistance variation,

ε: Strain.

The mathematical model is graphed in Fig. 6.8.

After testing, a calibration factor was developed to reduce the variation in the tested results. The calibration factor is based from the initial slope of the ERV versus strain

relationship. For each tested cylinder, the strain and ERV were recorded at a stress of 6.89 MPa (1.00 ksi). The calibration factor was determined as:

$$C = \frac{ERV_{c1}}{\varepsilon_{c1}}, \qquad \textbf{Equation 6.2}$$

where:

C: Calibration factor,

ERV_{c1}: Calibration ERV, the ERV at a stress of 6.89 MPa (1.00 ksi),

ε_{c1}: Calibration strain, the strain at a stress of 6.89 MPa (1.00 ksi).

Equation 6.2 was used to find the mean calibration factor for the data, which was 393. The calibration factor was added to Equation 6.1,

$$ERV_c = \frac{C}{393}\left(7.59\sqrt{\varepsilon} - 112\varepsilon\right). \qquad \textbf{Equation 6.3}$$

The raw data can be calibrated for comparison as:

$$ERV_c = \frac{393}{C} ERV, \qquad \textbf{Equation 6.4}$$

where:

ERV_c: Calibrated ERV.

The calibrated ERV standard deviation for each CNFA was calculated for the modeled behavior. Fig. 6.9 shows the modeled behavior plus and minus one standard deviation for the calibrated CNFAs. The average coefficient of variation reduced from 77.6% for the uncalibrated CNFAs to 9.8% for the calibrated CNFAs. This shows that in the future, CNFAs may be individually calibrated prior to embedment in concrete to achieve more consistent ERV results.

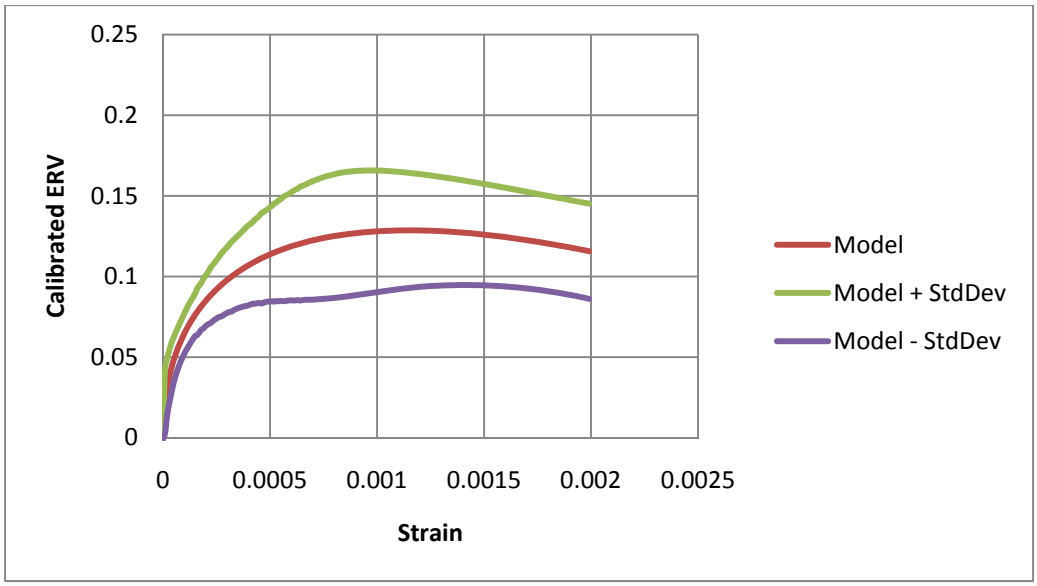

Fig. 6.9 Strain versus Calibrated ERV for Group 1

6.4.2 Group 2 Experimental Results

Since it was found that ERV is greatly affected by cold temperatures, a series of frozen cylinders was tested monotonically in compression. The mean temperature of each cylinder during testing is shown in Table 6.2. Please note that Cylinder F, while cold, was not frozen during testing. Cylinder C's temperature was nearly exactly at the freezing point and was considered frozen for the purposes of this experiment. The temperatures of the cylinders in Group 1 were also recorded for comparison purposes. The cylinders in Group 1 were all tested at approximately 22°C (72°F).

Table 6.2 Group 2 Cylinder Temperatures

Cylinder	Mean Temperature During Testing (°C)	Mean Temperature During Testing (°F)
A	-8.24	17.16
B	-8.64	16.44
C	0.978	33.8
D	-7.41	18.65
E	-5.44	22.2
F	6.55	43.8

Research in the 1960s proved that concrete behaves brittlely at low temperatures (Lentz and Monfore 1966; Monfore and Lentz 1962), and this phenomenon was observed during the cylinder tests. As shown in Fig. 6.10, the stress versus strain relationships for Group 1 exhibited an initial elastic modulus, strain softening, and failure between a strain of 0.002 and 0.003. The stress versus strain relationship for the cylinders tested in Group 2 is shown in Fig. 6.11. As a whole, the cylinders in Group 2 exhibited no strain softening and failed at similar stresses between a strain of 0.0015 and 0.002.

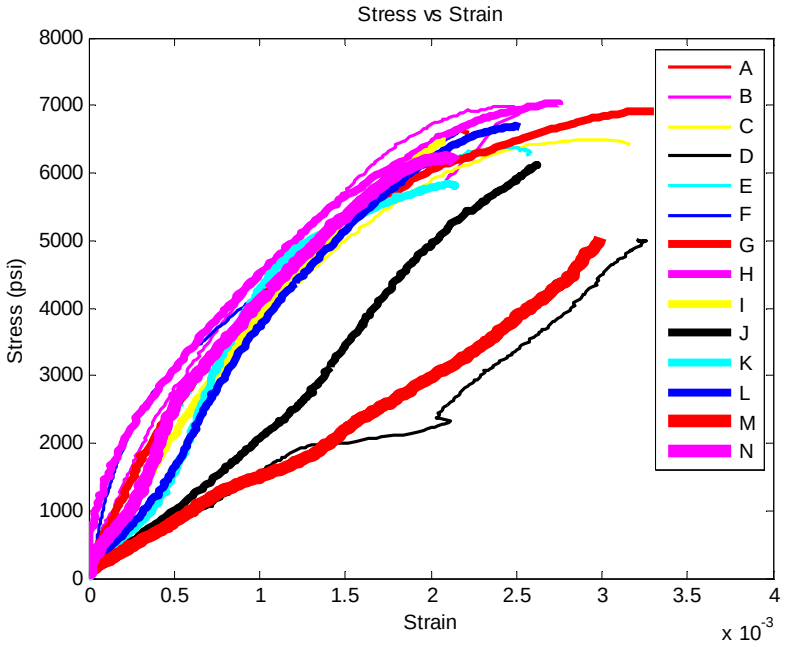

Fig. 6.10 Stress versus Strain for Group 1

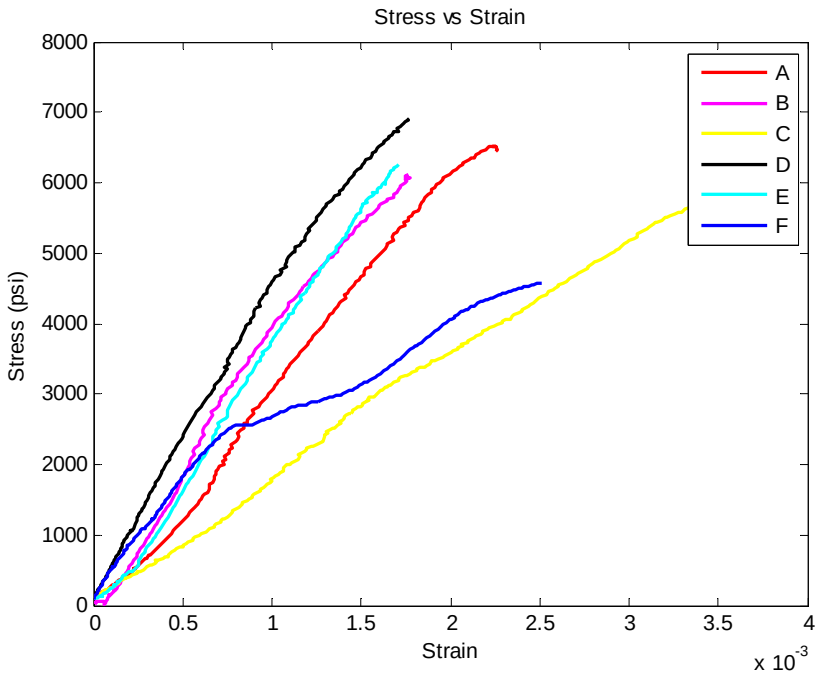

Fig. 6.11 Stress versus Strain for Group 2

A similar phenomenon was observed in the ERV versus strain relationship for Group 2. The ERVs were calibrated using the same method developed for Group 1. Fig. 6.12 shows the ERV versus strain relationships for the modeled behavior from Group 1 and the six CNFAs tested in Group 2. The relationships in Group 1 exhibited early softening behavior at a strain of about 0.0002. The five frozen cylinders maintained their original slopes until softening behavior began near a strain of 0.001. Cylinder F, which was cold but not frozen, behaved more like the modeled behavior from Group 1. Additional testing is required to extend the model to include strain and temperature effects.

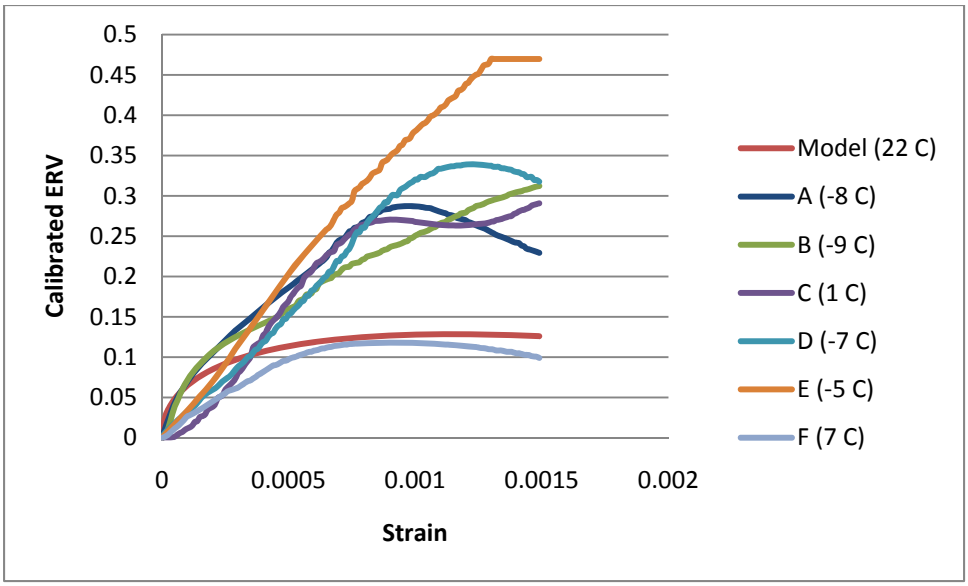

Fig. 6.12 Strain versus Calibrated ERV for Group 2

6.4.3 Group 3 Experimental Results

Group 3 consisted of three cylinders tested cyclically. Previous work has qualitatively shown that carbon fiber cement-based composites have the potential for structural health monitoring because when the strain versus time and electrical properties for a cyclic test were plotted together, the peaks and valleys in the data sets occurred simultaneously (Chung 1995, 2000; Howser et al. 2011). A notable example tested by Chung (Chung 2000) is shown in Fig. 6.13. Chung measured the change in fractional resistivity, stress, and strain in a small scale carbon fiber latex cement paste specimen. The specimen was tested cyclically in compression. Chung showed that while the electrical properties were able to detect the peaks and valleys in the strain, the electrical properties drifted during the experiment. Ideally, the embedded CNFAs will behave equally as well as the specimens made entirely of a carbon fiber cement composite material.

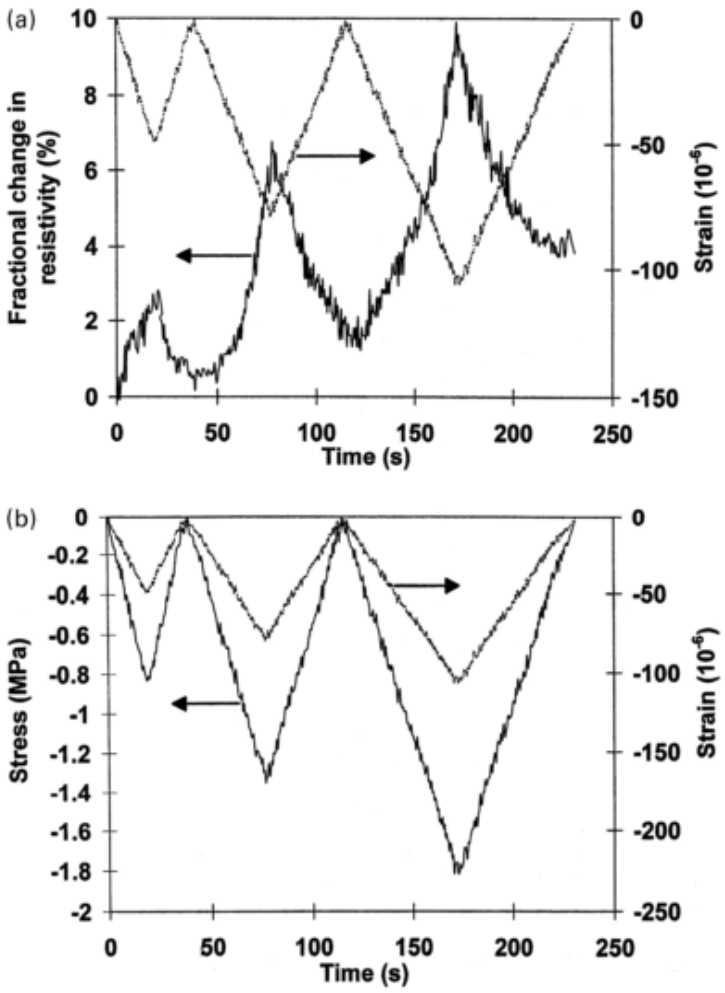

Fig. 6.13 Change in Fractional Resistivity, Stress, and Strain versus Time (Chung 2000)

Displacement-control was used to test the cylinders in Group 3. A base displacement of 0.0381 mm (0.0015 in.) was chosen. Two cycles were applied at n times the base displacement where n=1, 2, 3, etc. until failure. One cycle consists of loading the cylinder in compression to the desired displacement and returning the actuator to the zero displacement position. The loading procedure is shown graphically in Fig. 6.14.

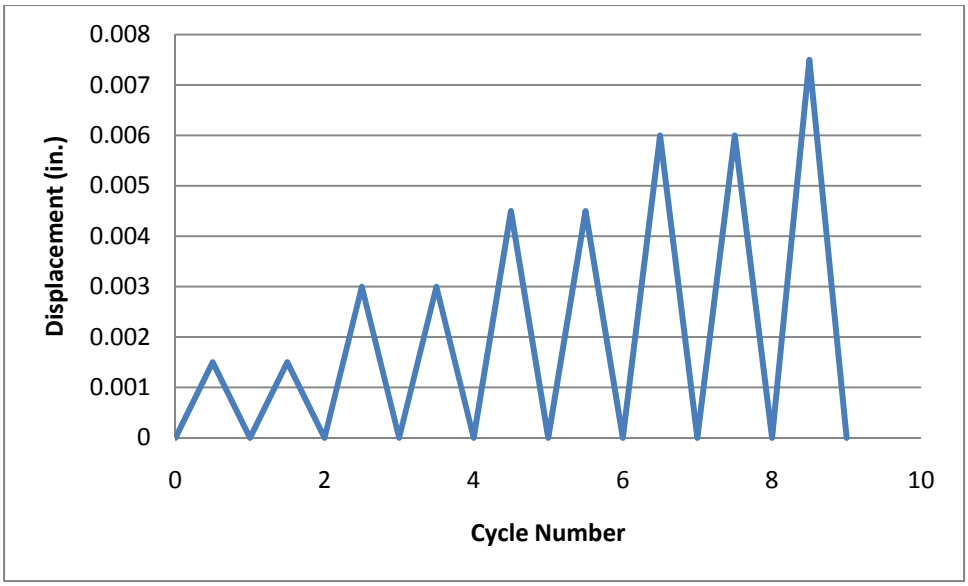

Fig. 6.14 Group 3 Loading Procedure

The results for the stresses, strains, and ERVs for Cylinders A, B, and C are shown in Fig. 6.15, Fig. 6.16, and Fig. 6.17, respectively. Qualitatively, the experiment was successful. The peaks and valleys of the stress, strain, and ERV coincide for all three cylinders. The CNFAs had a difficult time detecting the first two cycles in each test, but the strain was quite small for these cycles. The same drift behavior that was observed in Chung's experiment (Chung 2000) occurred in the present experiment.

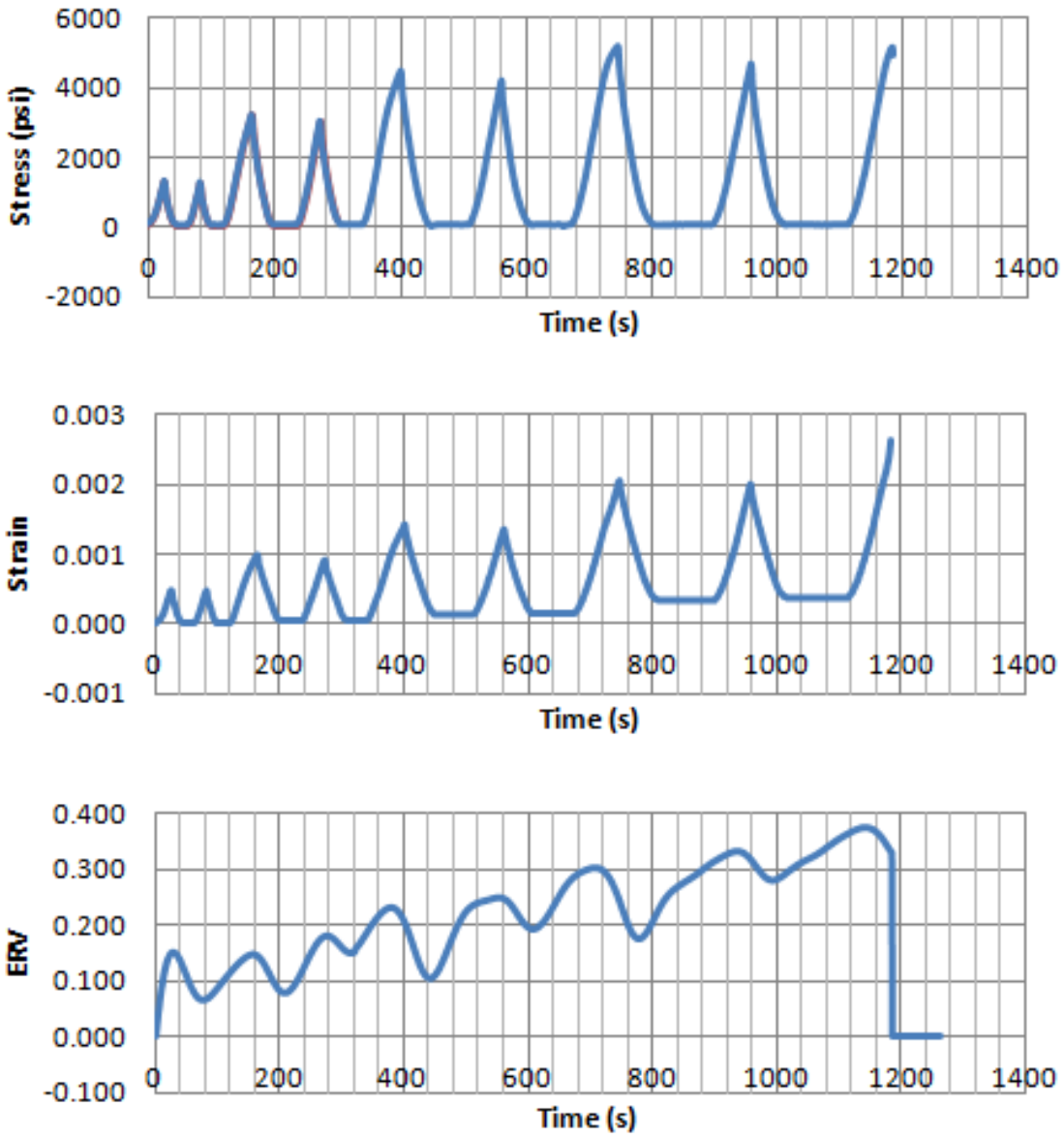

Fig. 6.15 Group 3 Cylinder A Stress, Strain, and ERV versus Time

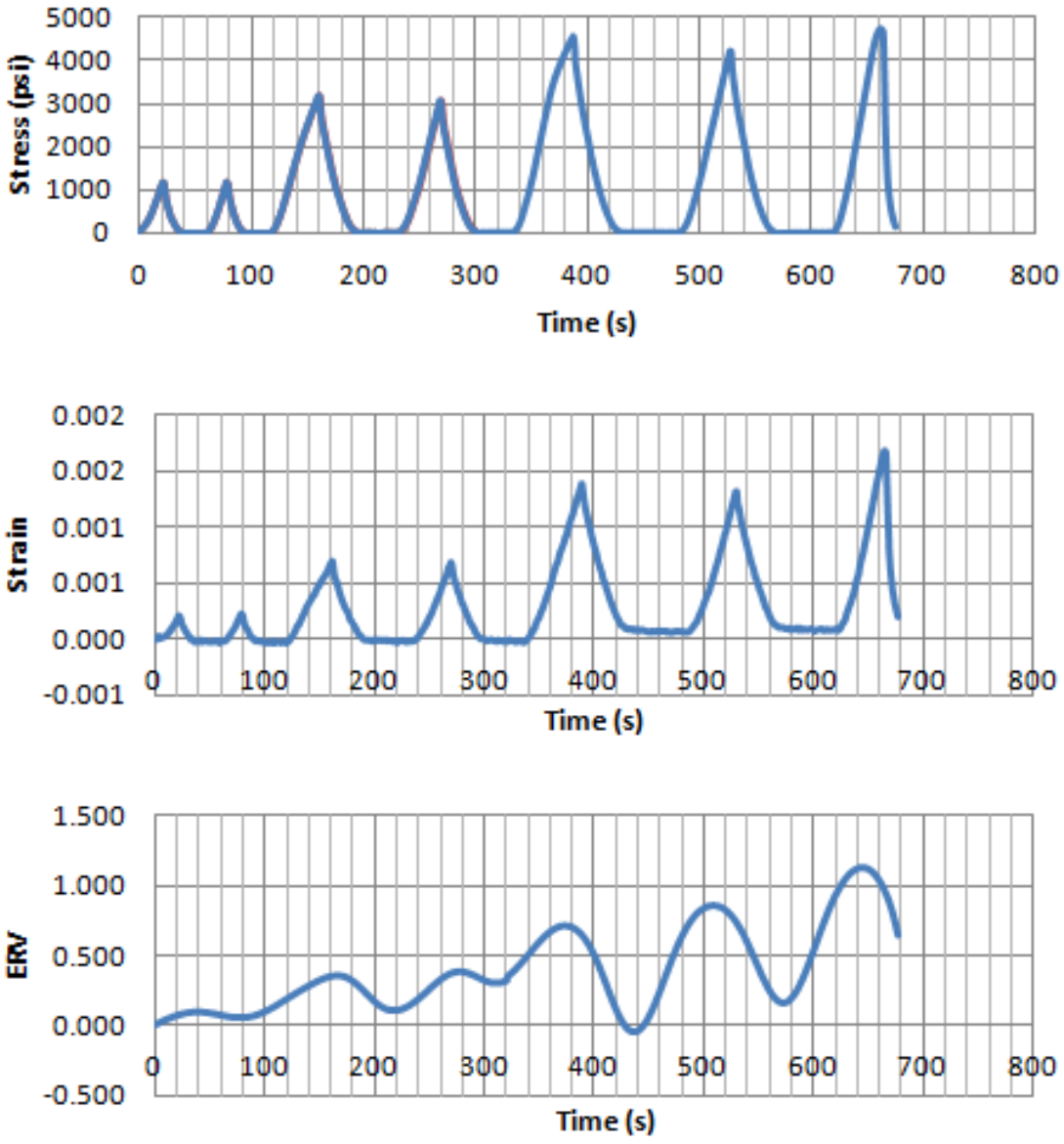

Fig. 6.16 Group 3 Cylinder B Stress, Strain, and ERV versus Time

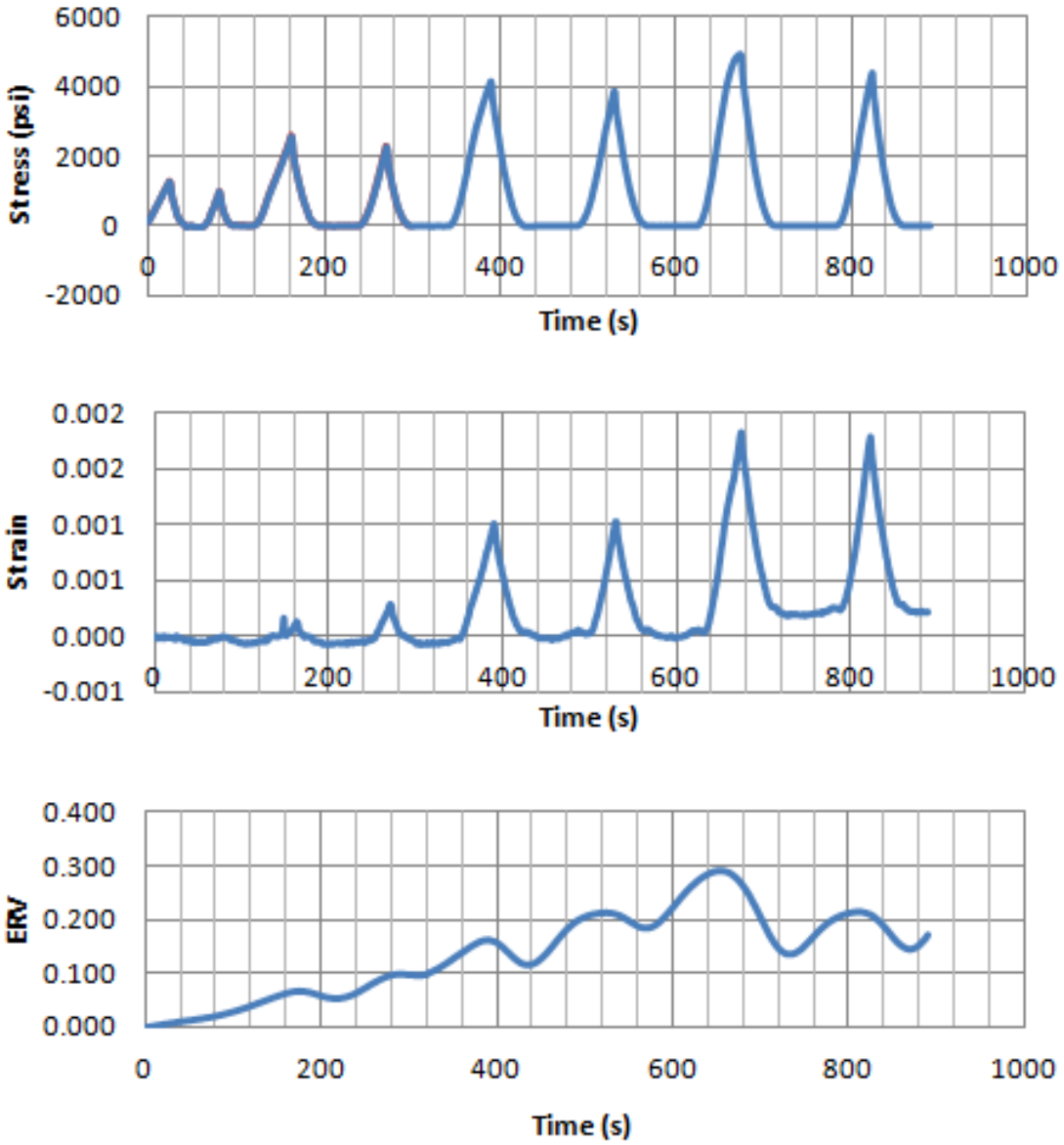

Fig. 6.17 Group 3 Cylinder C Stress, Strain, and ERV versus Time

While three specimens were not enough to create a comprehensive model, some simple modifications were made to the model found for Group 1 in an attempt to predict the cyclic behavior of embedded CNFAs. The model is shown graphically in Fig. 6.18.

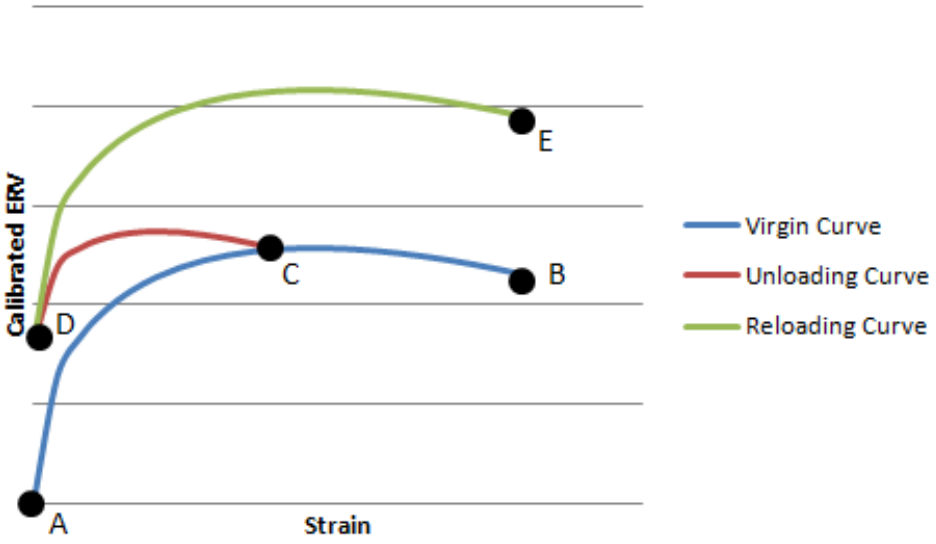

Fig. 6.18 Cyclic Compressive Strain versus Calibrated ERV Model

Following Fig. 6.18, if the embedded CNFA is loaded monotonically in compression from Point A to B, it will follow the blue virgin curve, which corresponds to Equation 6.3. If the CNFA is loaded and then unloaded, following Points A, C, and D, Section AC is modeled using Equation 6.3, and Section CD is modeled as

$$R_u = ERV_t - \frac{2}{3}\frac{C}{393}\left(7.59\sqrt{\varepsilon_t} - 112\varepsilon_t\right), \qquad \textbf{Equation 6.5}$$

where:

R_u: Unloading turning point factor,

ERV_t: Calibrated ERV at the turning point,

C: Calibration factor calculated from Equation 6.2,

ε_t: Strain at turning point,

$$ERV_u = \frac{2}{3}\frac{C}{393}\left(7.59\sqrt{\varepsilon} - 112\varepsilon\right) + R_u, \qquad \textbf{Equation 6.6}$$

where:

ERV_u: Calibrated unloading ERV,

ε: Strain.

If the CNFA is reloaded after being unloaded, such as from Point D to E, the section is modeled as:

$$R_r = ERV_t - \frac{C}{393}\left(7.59\sqrt{\varepsilon_t} - 112\varepsilon_t\right), \qquad \textbf{Equation 6.7}$$

where:

R_r: Reloading turning point factor

$$ERV_r = \frac{C}{393}\left(7.59\sqrt{\varepsilon} - 112\varepsilon\right) + R_r, \qquad \textbf{Equation 6.8}$$

where:

ERV_r: Calibrated reloading ERV.

All subsequent loading and reloading is modeled using Equations 6.5 through 6.8.

The three cyclically tested CNFAs were modeled using the cyclic model with satisfactory results. Fig. 6.19 and Fig. 6.20 show the calibrated and modeled ERV for Cylinder A versus time and strain, respectively. Fig. 6.21, Fig. 6.22, Fig. 6.23, and Fig. 6.24 show the same relationships for Cylinders B and C, respectively.

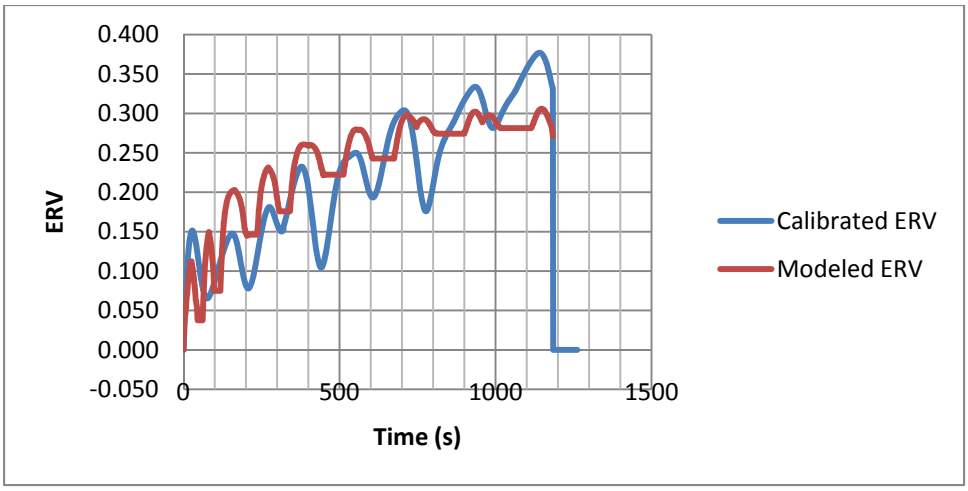

Fig. 6.19 Group 3 Cylinder A Calibrated and Modeled ERV versus Time

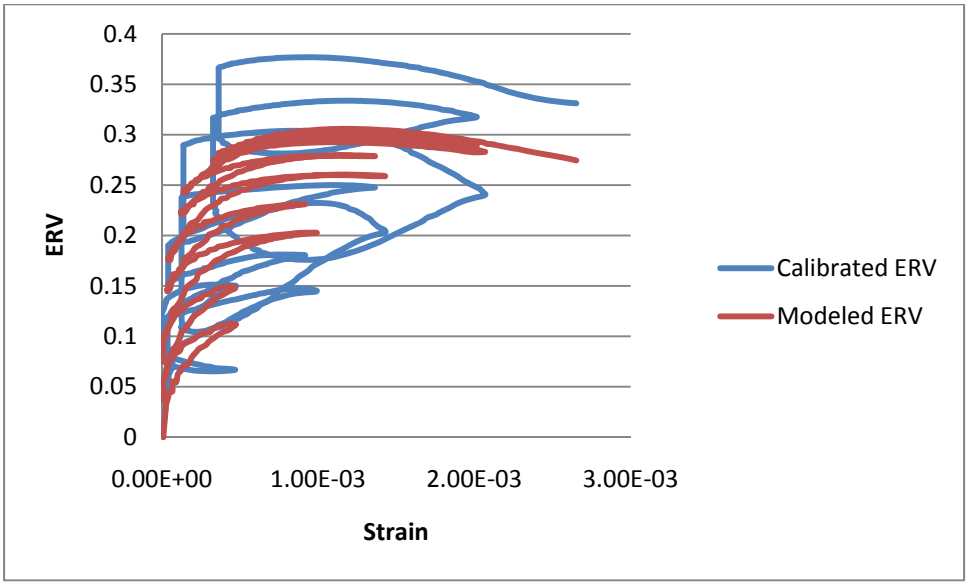

Fig. 6.20 Group 3 Cylinder A Calibrated and Modeled ERV versus Strain

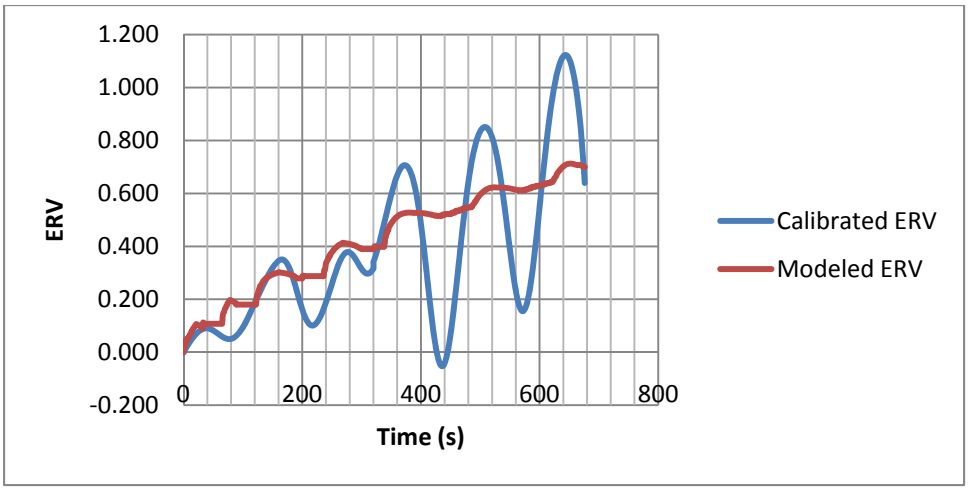

Fig. 6.21 Group 3 Cylinder B Calibrated and Modeled ERV versus Time

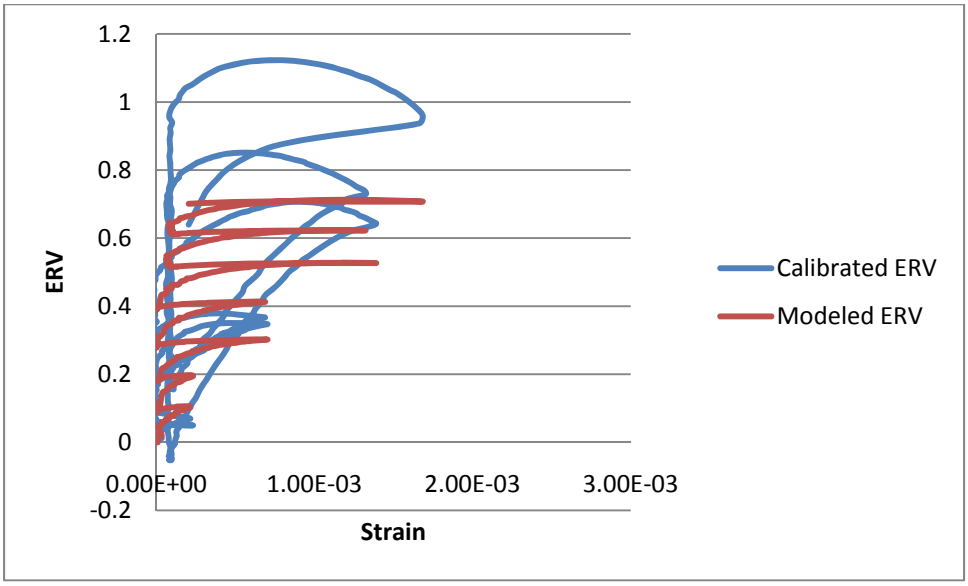

Fig. 6.22 Group 3 Cylinder B Calibrated and Modeled ERV versus Strain

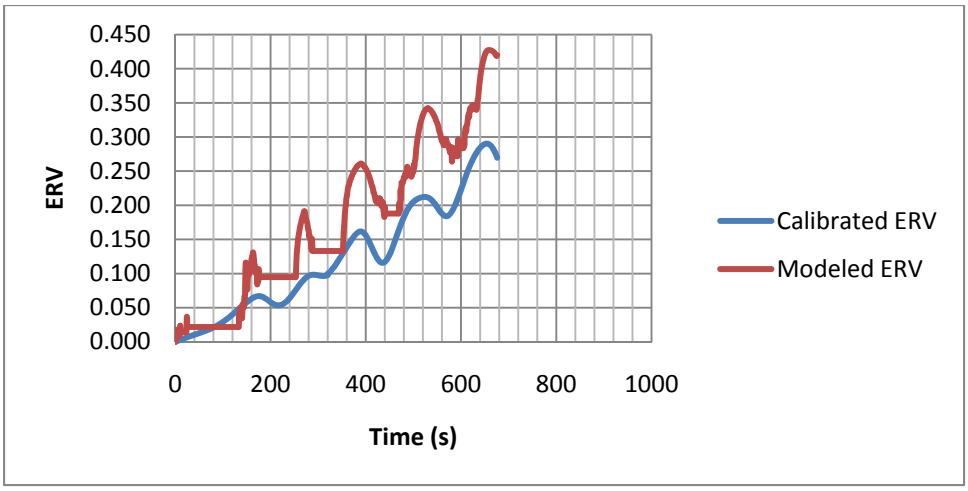

Fig. 6.23 Group 3 Cylinder C Calibrated and Modeled ERV versus Time

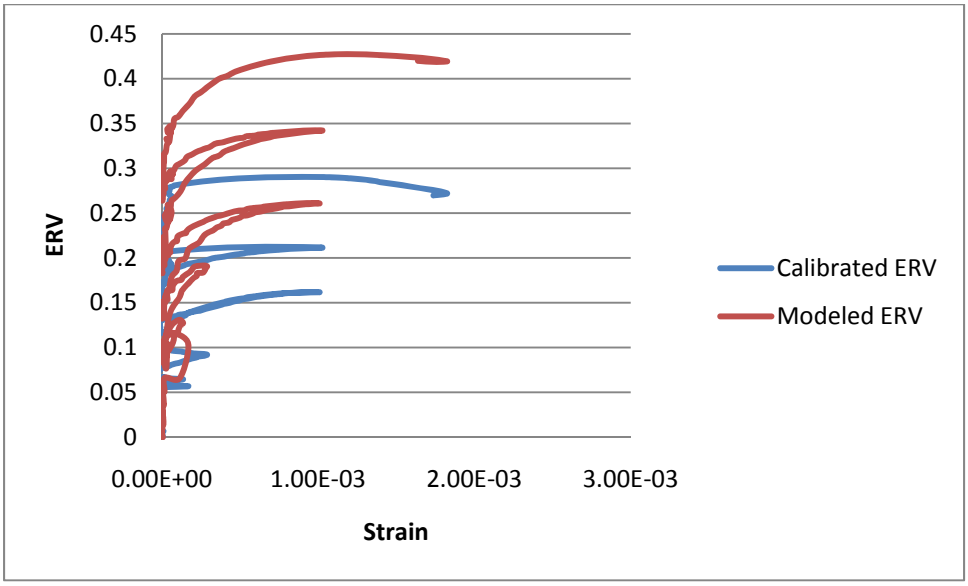

Fig. 6.24 Group 3 Cylinder C Calibrated and Modeled ERV versus Strain

6.5 Summary and Future Work

Three groups of cylinders with embedded carbon nanofiber aggregates (CNFAs) were tested in compression. The first group was tested in monotonic compression at room temperature. The second group was frozen then tested monotonically. The third group was tested cyclically at room temperature. The following conclusions were made from the study:

- A qualitative assessment of the electrical data from a CNFA embedded in a cylinder can show when loading began on the cylinder, a strain of approximately 0.001, and failure.
- While the raw electrical resistance variation (ERV) values have a large coefficient of variation from the mean ERV values, a calibration factor can be applied to the ERV value to obtain a reasonable coefficient of variation. A model was developed to estimate the ERV versus strain relationship.
- Frozen cylinders behave brittlely. The ERV versus strain behavior is similar to the stress versus strain behavior in the lack of strain softening for frozen cylinders.
- Qualitatively, cyclic stress and strain can be assessed from the ERV versus time relationship. The peaks and valleys of all three relationships coincide during cyclic loading. A model was developed to estimate the cyclic ERV versus strain relationship.

Future work for this project includes:

- The calibration factor developed for this study was calculated post-embedment and testing. A calibration method should be developed for use pre-embedment.
- Many cylinders should be tested monotonically at various temperatures to develop a comprehensive monotonic ERV versus strain model.
- Many cylinders should be tested cyclically to develop a cyclic ERV versus strain model. The use of a frequency-response based feedback control

system should be explored. The observed drift behavior may be eliminated through the use of feedback control.

CHAPTER 7
CARBON NANOFIBER AGGREGATE SMALL-SCALE BEAM MONITORING STUDY

7.1 Introduction

A system of embedded carbon nanofiber aggregates (CNFAs) was used for the structural health monitoring of a small-scale beam tested monotonically. The primary purpose for developing carbon nanofiber (CNF) composites is for strain monitoring. Because of the high cost associated with CNFs, a CNFA was developed. The CNFA is a 16.39 cm^3 (1.00 $in.^3$) cubic specimen of CNF mortar. The CNF mortar is self-sensing and can be used to determine the damage in the CNFAs.

7.2 Test Specimens

A small scale-beam was designed for the purpose of testing CNFAs in a reinforced concrete structure. The cross-section of the beam was 152.4 mm (6.00 in.) square and contained 3 #3 longitudinal rebar in the tension region and 2 #2 rebar in the compression region. The beam also contained #2 stirrups with a typical spacing of 63.5 mm (2.50 in.). The stirrups in the central portion of the beam, where there was no shear, were placed to hold the CNFAs in place. The beam was 533 mm (21.0 in.) long. The beam cross-section and elevation view are shown in Fig. 7.1 and Fig. 7.2, respectively. The beam was instrumented with six CNFA as shown in Fig. 7.1 and Fig. 7.2. The calculations for the beam can be found in Appendix A.

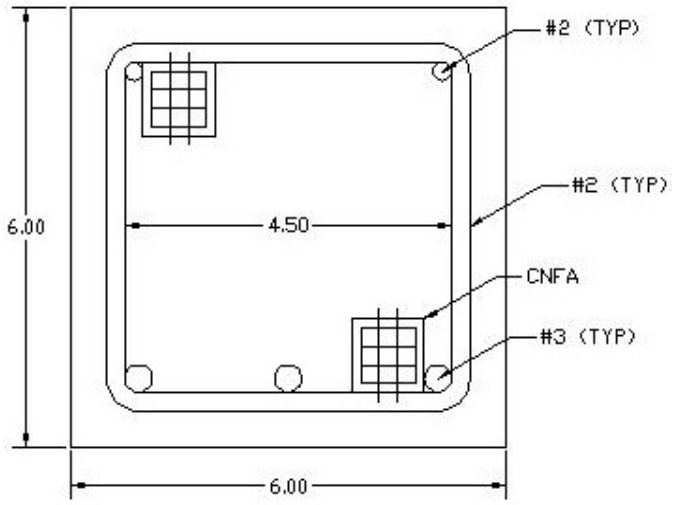

Fig. 7.1 Beam Cross-Section (units in in.)

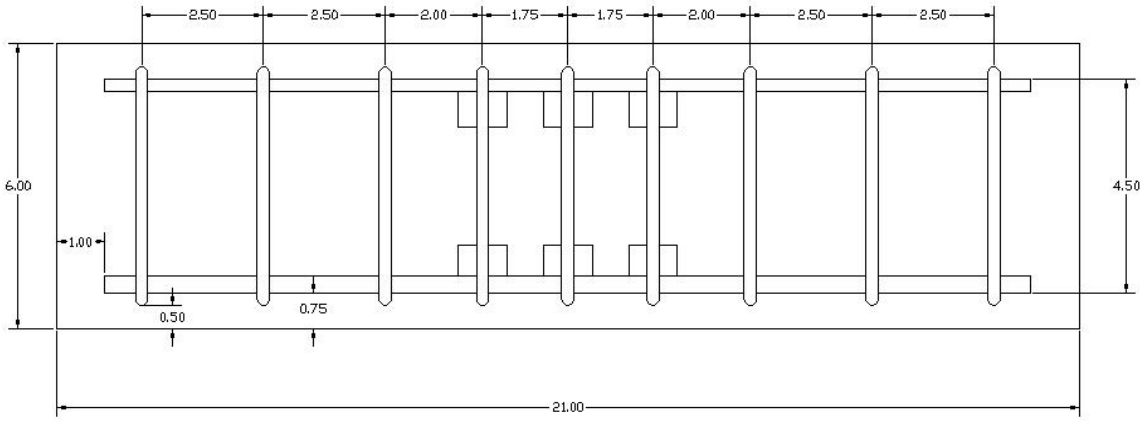

Fig. 7.2 Beam Elevation View (units in in.)

7.3 Specimen Construction and CNFA Instrumentation

Because of the small rebar size, the stirrups were bent by hand and welded to the longitudinal reinforcement. The rebar adjacent to the CNFA locations were coated with epoxy so that the electrical properties of the rebar did not affect the electrical properties of the CNFAs. Fig. 7.3 shows the rebar cage. After the rebar cage was constructed, CNFAs were tied into place using zip ties. Fig. 7.4 shows the installed CNFAs and the rebar cage within the formwork. Self-consolidating concrete (SCC) was used for the

beam because of close rebar spacing. SCC is not as prone to honeycombing as normal concrete.

Fig. 7.3 Beam Rebar Cage

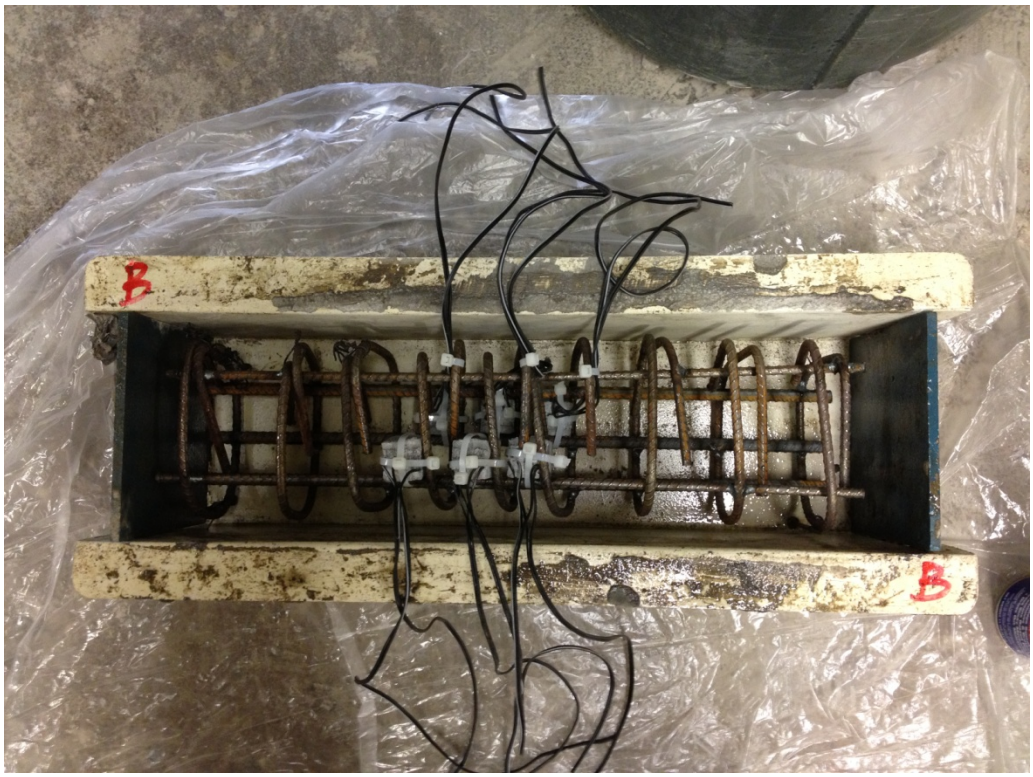

Fig. 7.4 Installed CNFAs and Beam Rebar Cage in Formwork

7.4 Experimental Setup

To measure the electrical resistance, the outer wires of the 6 CNFAs were connected in series with a 5.6 kΩ resistor and a 10 V power supply, as shown in blue in Fig. 7.5. The voltage drops across the inner wires of the CNFAs and resistor were measured using the data acquisition system dSpace, as shown in red in Fig. 7.5. There was an impedance problem within the data acquisition system, so differential amplifiers were placed between each component of the circuit and the data acquisition system, as shown in Fig. 7.5.

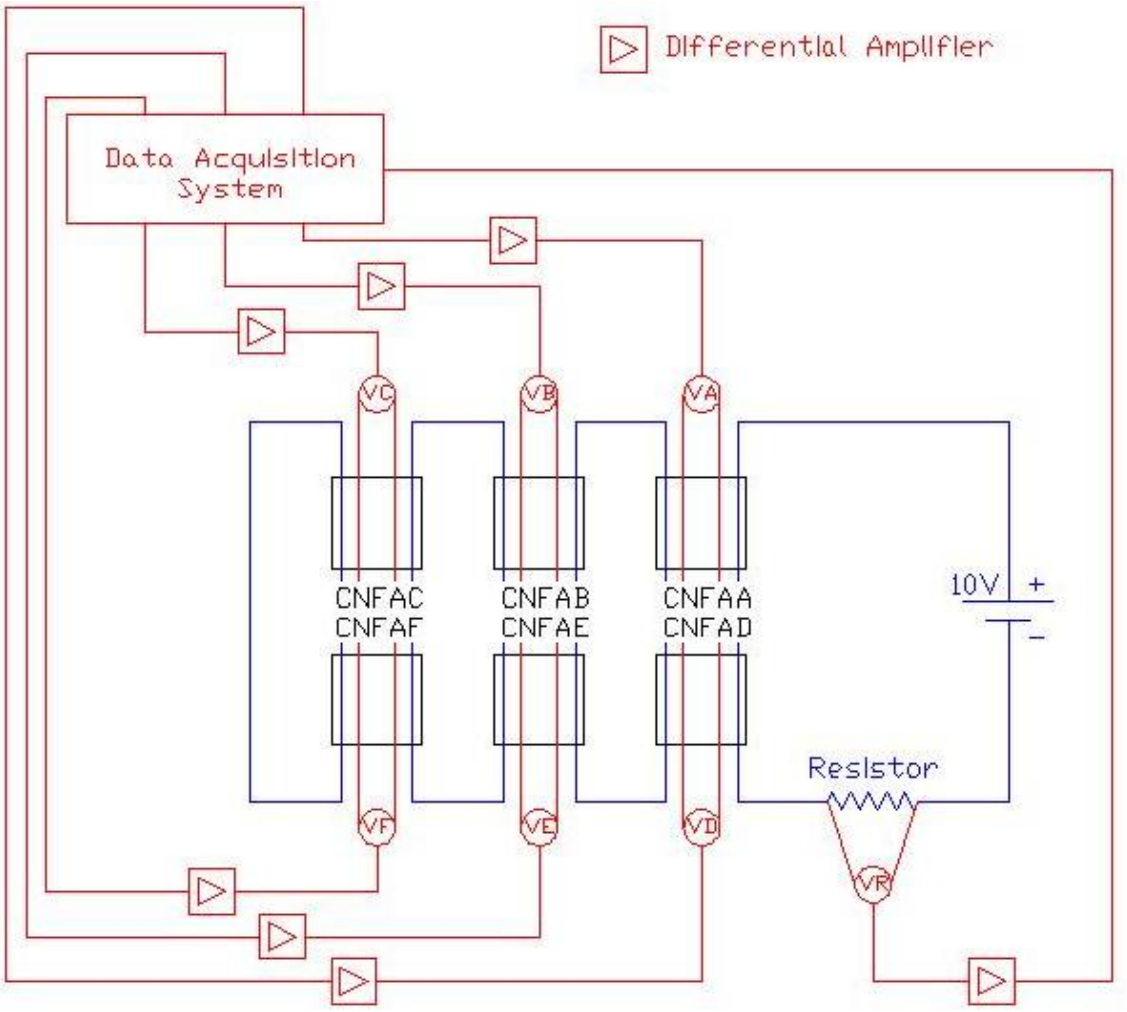

Fig. 7.5 Electrical Circuit and Connection to Data Aquisition System for Beam Experiment

The differential amplifier circuit is shown in Fig. 7.6. A differential amplifier is a circuit that computes the differences of two voltages and multiplies it by a constant. If all four of the resistors have equal resistances, then the output voltage will equal the difference of the two input voltages. The differential amplifiers, consisting of all equal resistors and 741 operational amplifiers, are shown in Fig. 7.7.

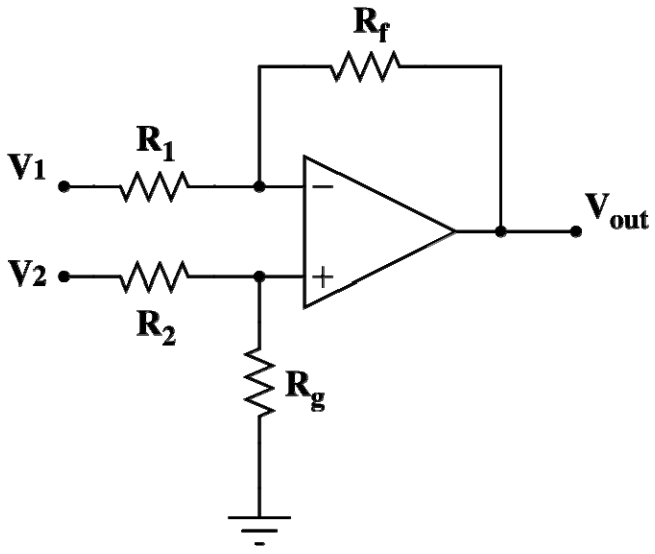

Fig. 7.6 Differential Amplifier Circuit

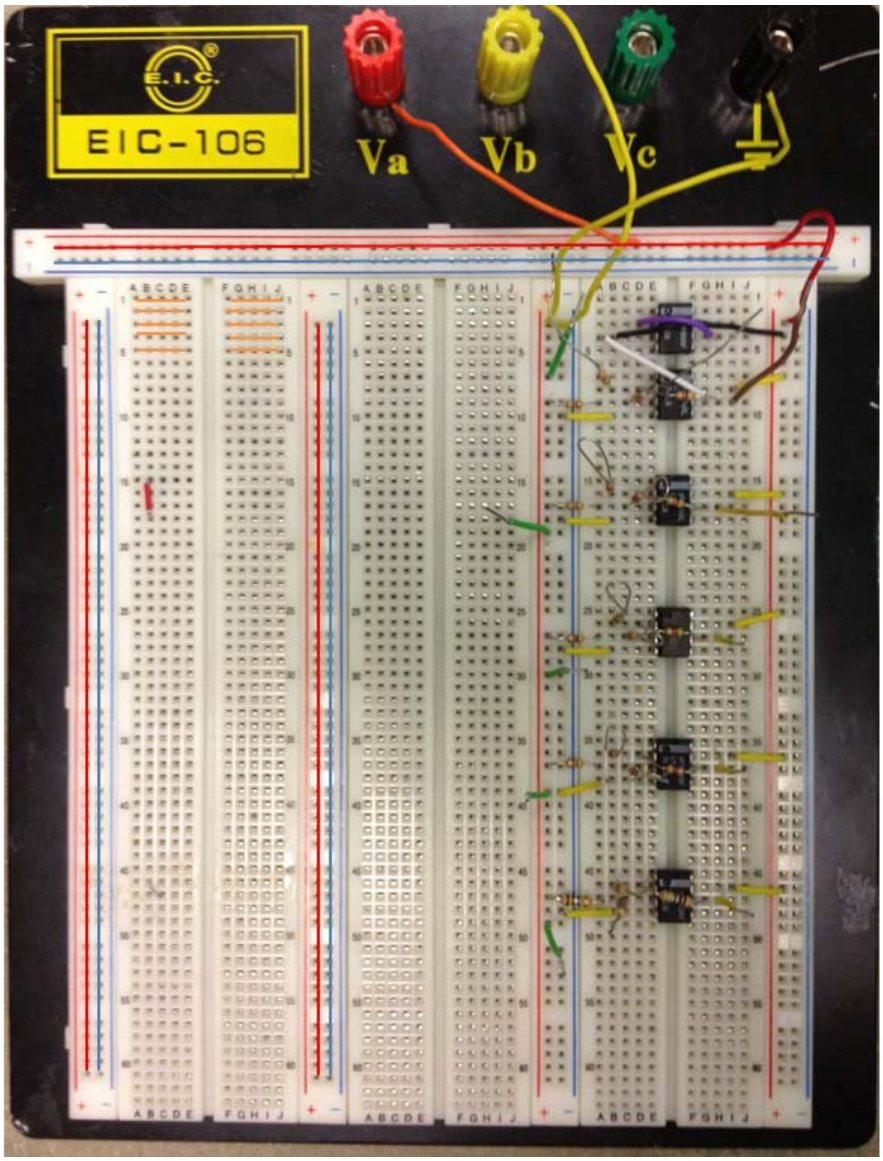

Fig. 7.7 Differential Amplifiers

The beam was tested in a Tinius Olsen Hydraulic Tester using the four-point bending method depicted in Fig. 7.8. The four-point bending method was chosen because the moment is constant between the two loading points, where three CNFAs were placed in both the compression and tension region. In Fig. 7.8, the span L is 457 mm (18.00 in.) and P is the total force. The force was measured from the Tinius Olsen

Hydraulic Tester. The displacement was monitored using two linear variable differential transformers (LVDTs). The experimental setup is shown in Fig. 7.9.

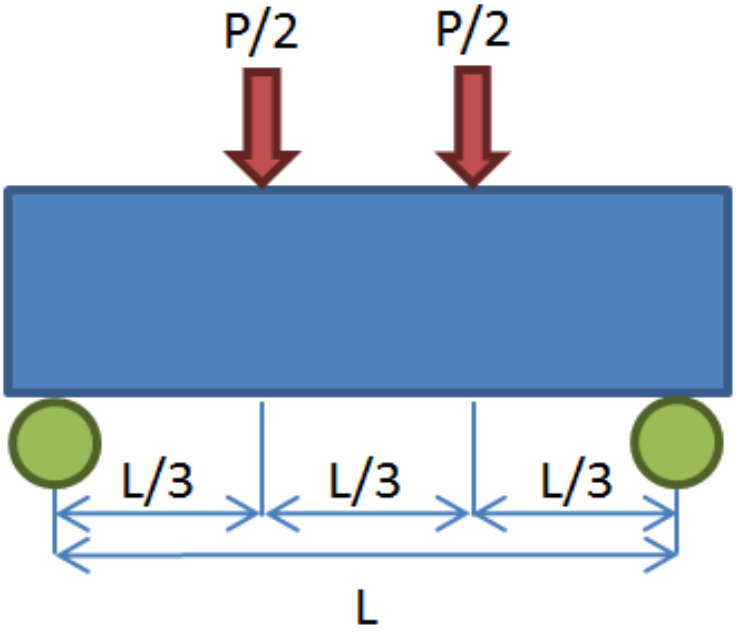

Fig. 7.8 Four Point Bending Method

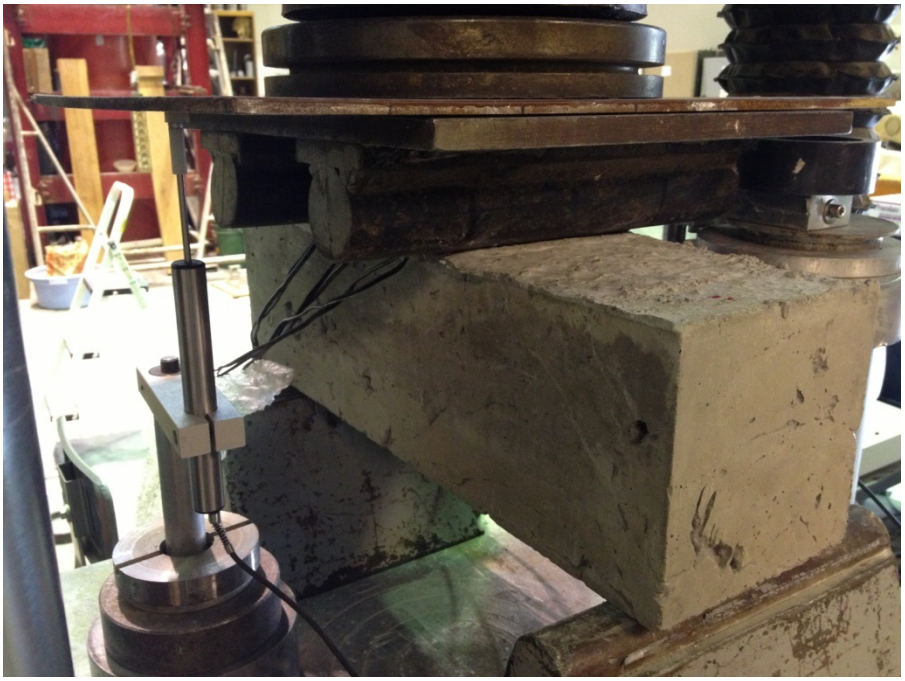

Fig. 7.9 Beam Experimental Setup

7.5 Experimental Results

The beam was expected to fail in flexure/crushing similarly to the previously tested small-scale beam shown in Fig. 7.10; however, the concrete strength was 70% higher than expected and the beam failed in shear, as shown in Fig. 7.11. Fig. 7.12 shows the force versus displacement relationship of the beam.

Fig. 7.10 Previously Tested Beam with Flexural and Crushing Failure Modes

Fig. 7.11 Tested Beam with Shear Failure Mode

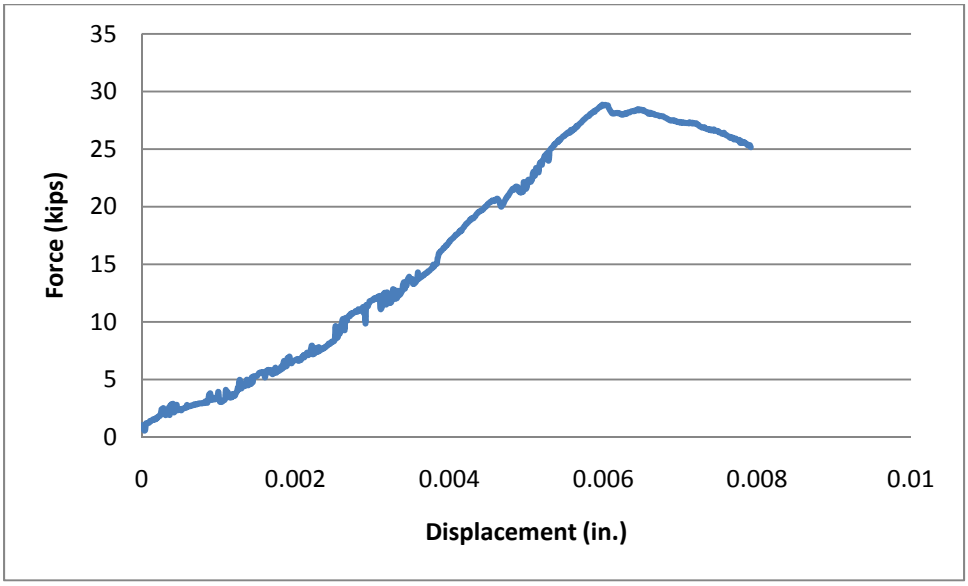

Fig. 7.12 Beam Force versus Displacement

The sensors were embedded in the flexure critical region rather than the shear critical region, so the collected data was not ideal. For simplicity, the strains were calculated using Euler-Bernoulli beam theory (Timoshenko 1953). The flexural strains

were very low at failure, and the CNFAs are less stable at low strains. The ERVs were calibrated based on their initial ERV versus strain relationship, as suggested in Chapter 6. Fig. 7.13 shows the calibrated ERV versus strain relationship. The calibration factor specifies that the calibration factor should be calculated at a stress of 6.89 MPa (1.00 ksi); however, the three CNFA in the compression region, CNFAs A, B, and C, did not reach a stress of 6.89 MPa (1.00 ksi) during the test. Their maximum stress was 3.29 MPa (478 psi). They were calibrated at a stress of 2.07 MPa (300 psi). The strain in the compression region was so small that no conclusions could be determined on the appropriateness of the compression model. The three CNFA in the tension region, CNFAs D, E, and F, were calibrated at 6.89 MPa (1.00 ksi). They did not match the compression model well, which implies that the tension and compression behavior of the CNFAs is different. This was expected since concrete is not isotropic. There was not enough data from the test to create a tension model.

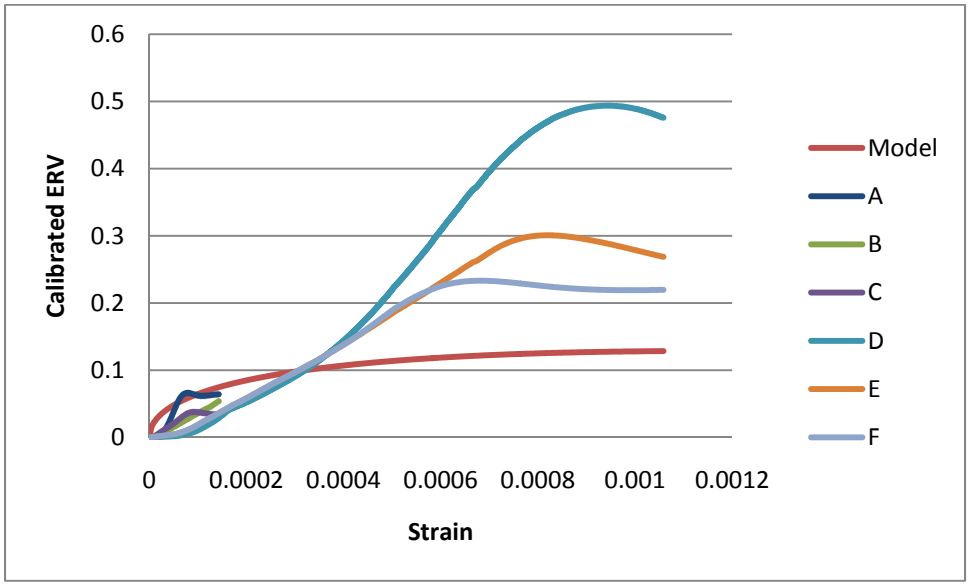

Fig. 7.13 Beam Calibrated ERV versus Strain

The load carrying capacity of the beam began to decrease after a sudden large crack formed at one of the loading points, near CNFA A. Fig. 7.14 shows the crack with all of the loading equipment in place. Fig. 7.15 shows the crack and its proximity to CNFA A (the wires closest to the crack), which was embedded 12.7 mm (0.50 in.) below the surface of the concrete.

Fig. 7.14 Crack at Loading Point with Loading Equipment in Place

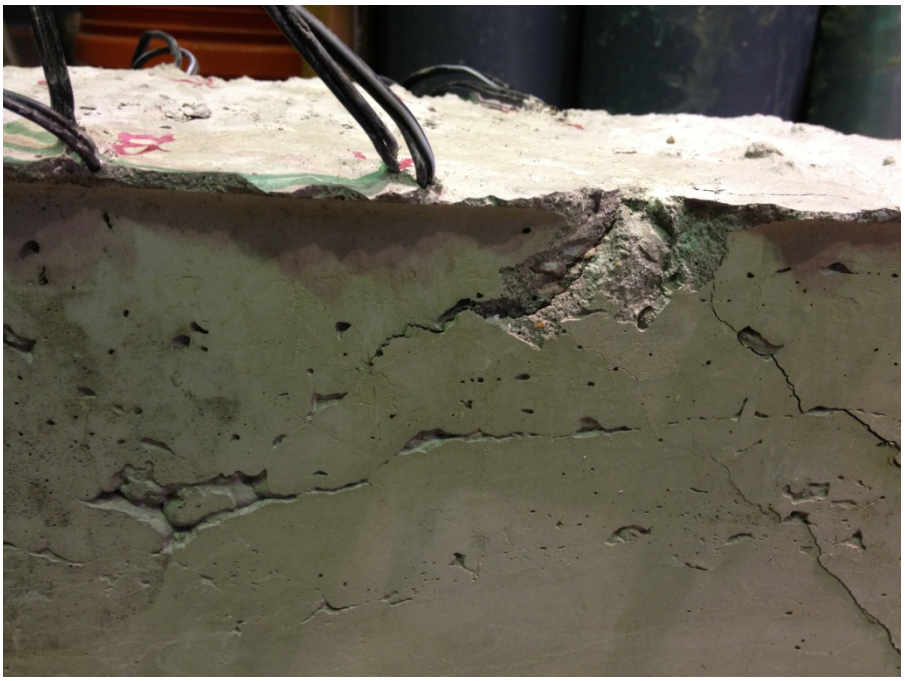

Fig. 7.15 Crack at Loading Point

At the exact time that the crack suddenly opened, the ERV in CNFA A suddenly dropped. This occurred simultaneously with the peak recorded load, as shown in Fig. 7.16. This proves that CNFAs are capable of detecting localized, catastrophic damage.

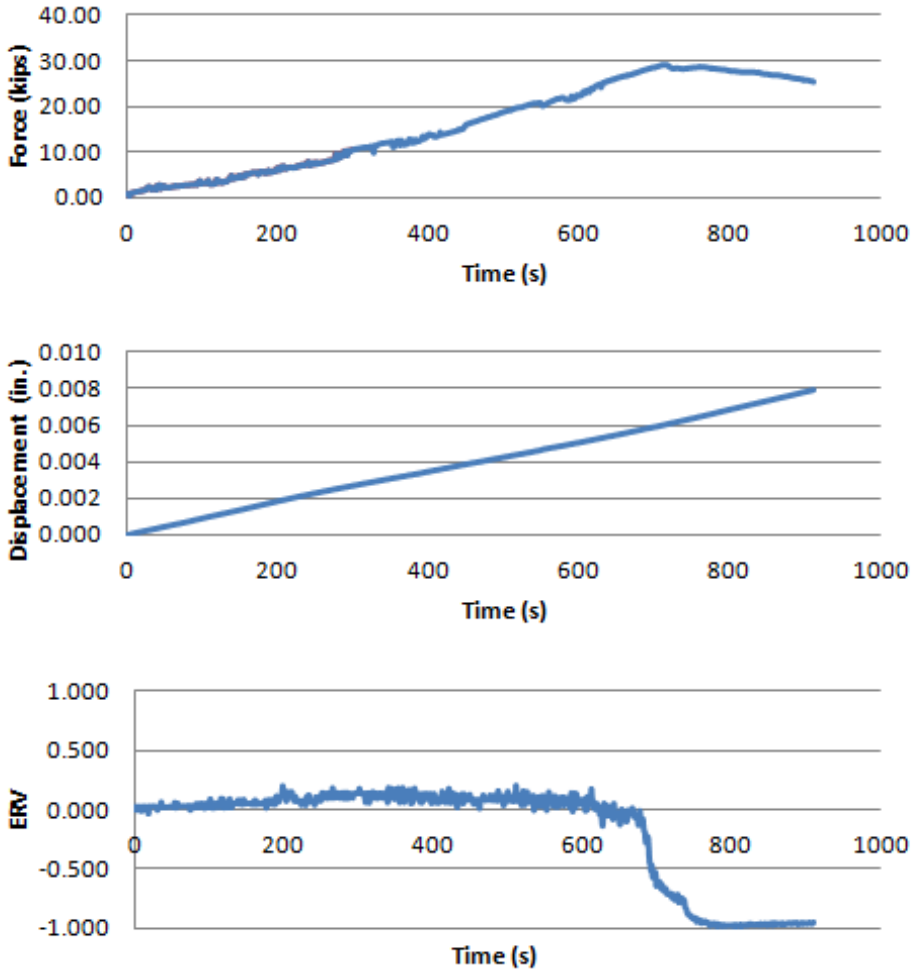

Fig. 7.16 Beam Force, Displacement, and ERV of CNFA A versus Time

7.6 Summary and Future Work

A small-scale reinforced concrete beam with six embedded carbon nanofiber aggregates (CNFAs) was tested using the four-point bending method. The following conclusions were made from the study:

- CNFAs behave differently if they are tested in tension rather than compression. This was expected since concrete is not isotropic.
- CNFAs are capable of detecting localized catastrophic damage in reinforced concrete structures.

Future work in this area of study includes:

- Flexure-critical beams should be tested so that a model can be developed for CNFAs in tension.
- The comprehensive compression model discussed in the future work section of Chapter 6 should be compared to CNFAs in the compression region of reinforced concrete beams.

CHAPTER 8
CARBON NANOFIBER AGGREGATE FULL-SCALE COLUMN MONITORING STUDY

8.1 Introduction

The primary purpose for developing carbon nanofiber (CNF) composites in this study is for strain monitoring. Because of the high cost associated with CNFs, a CNF aggregate (CNFA) was developed. The CNFA is a 16.39 cm^3 (1.00 $in.^3$) cubic specimen of CNF mortar. The CNF mortar is self-sensing and can be used to determine the damage in the CNFAs. The CNFAs can be embedded in reinforced or prestressed concrete structures and used to determine the localized strain in a structure. For this study, a system of embedded CNFAs was used for the structural health monitoring of a full-scale column excited with a reversed cyclic load.

8.2 Test Specimens

A series of shear- and flexure-critical reinforced concrete (RC) columns were designed at the University of Houston (UH) for the purpose of studying the applicability of using CNF cement-based composites for structural health monitoring in full-scale structures. The columns were constructed and are currently (as of July 2013) in the process of being tested at Tongji University (TU) in Shanghai, China; therefore, the results shown in this dissertation will be limited to one of the flexure-critical columns to prove that the CNFAs can be used for structural health monitoring.

Since the column was constructed internationally at TU, European rebar were used throughout the project. Table 8.1 shows the geometric and material properties of the rebar used. The cross-section of the column was 450 mm (17.7 in.) square and contained 14 #25 longitudinal rebar, providing a longitudinal reinforcement ratio of 2.91% by volume of concrete. The column also contained #8 stirrups with a spacing of 100 mm (3.94 in.). This corresponds to the maximum spacing specified by the American Concrete Institute (ACI) for columns in seismic regions. This maximum spacing is defined as the distance from the extreme compression fiber to the centroid of the longitudinal tension reinforcement divided by four (ACI Committee 318 2011). This resulted in a transverse reinforcement ratio of 0.356% by volume of concrete. See Fig. 8.1 for the column cross-section. The column was 3.13 m (10.27 ft.) tall, resulting in an aspect ratio of 7.75. The column was rigidly connected to a 900 mm (35.4 in.) by 1525 mm (60.0 in.) by 500 mm (19.7 in.) foundation. The foundation was reinforced with 20 #25 bars in the loading direction and #8 stirrups spaced at 150 mm (5.91 in.). The foundation and column elevation is shown in Fig. 8.2, and the foundation plan view is shown in Fig. 8.3. The column was instrumented with 12 CNFAs, among other sensors, as shown in Fig. 8.1 and Fig. 8.2. The calculations for both the column and foundation can be found in Appendix B.

Table 8.1 European Rebar Sizes Used in Column Construction

European Size	Yield Strength MPa (ksi)	Mass per Unit Length kg/m (lb./ft.)	Nominal Diameter mm (in.)	Cross-Sectional Area mm^2 ($in.^2$)
8	235 (34.1)	0.395 (0.265)	8.00 (0.315)	50.3 (0.0780)
25	335 (48.6)	3.86 (2.59)	25.0 (0.984)	491 (0.761)

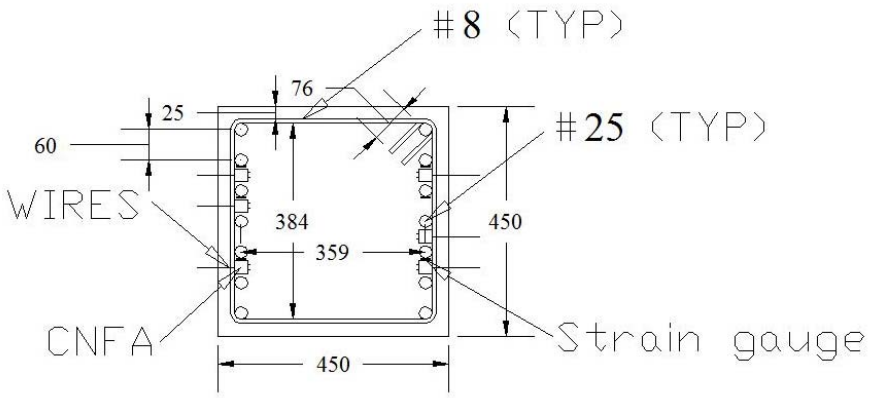

Fig. 8.1 Column Cross-Section (units in mm)

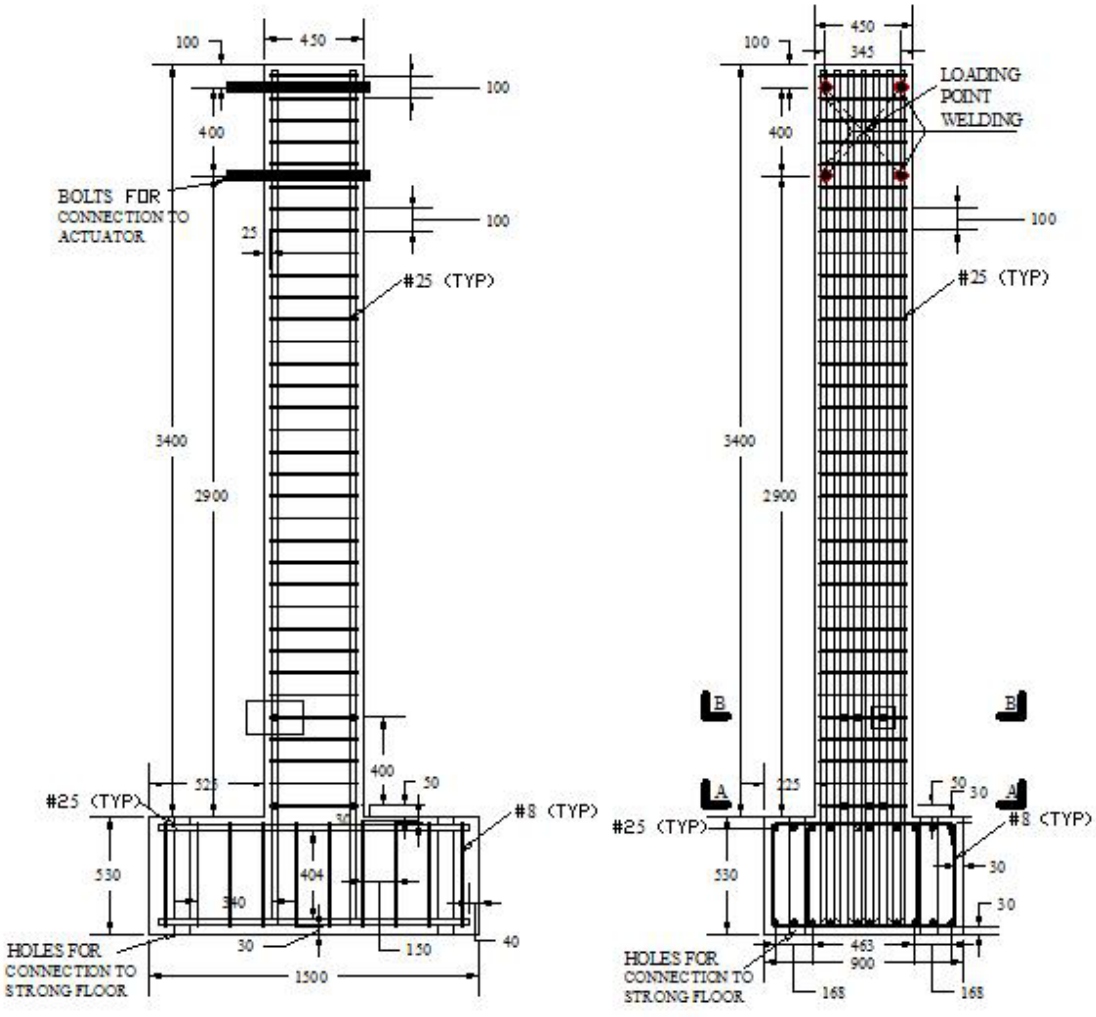

Fig. 8.2 Column and Foundation Elevation Views (units in mm)

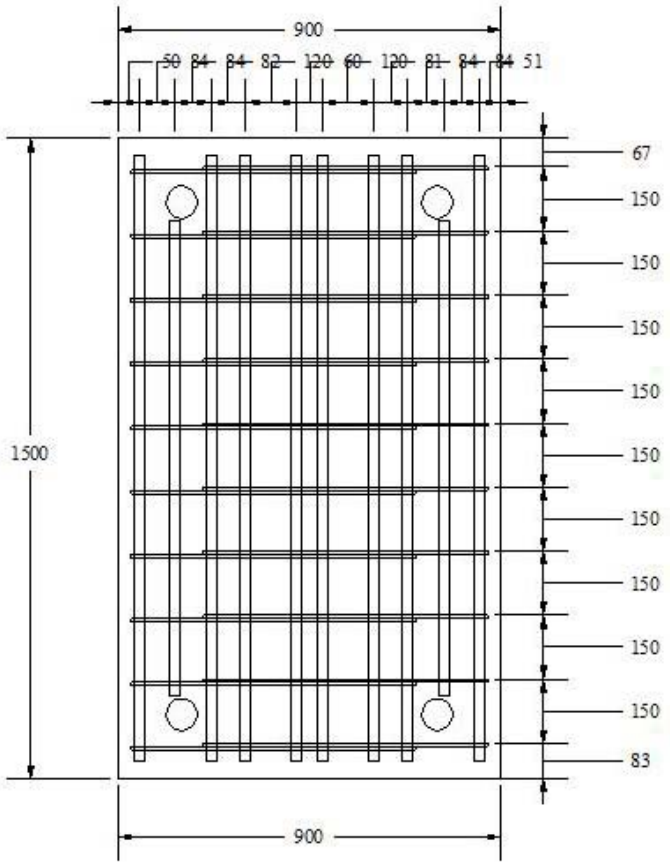

Fig. 8.3 Foundation Plan View (units in mm)

8.3 Specimen Construction and Internal Sensor Instrumentation

At TU, several of the foundations for the series of columns were poured simultaneously. Fig. 8.4 shows column rebar cages and foundations for four flexure-critical and four shear-critical columns. All but one of the flexure-critical columns are outside the scope of this dissertation. After the rebar cages were built and the foundations poured, the column was instrumented with internal sensors. The rebar adjacent to the CNFA locations shown in Fig. 8.1 and Fig. 8.2 were painted with epoxy

so that the electrical properties of the rebar would not affect the electrical properties of the CNFAs. The CNFAs were fixed to the rebar using plastic zip ties. Fig. 8.5 shows an installed CNFA. The column was also instrumented with strain gauges and thermocouples as shown in orange and blue respectively in Fig. 8.6.

Fig. 8.4 Column Rebar Cages and Foundations

Fig. 8.5 Installed CNFA

Fig. 8.6 Installed Thermocouples (Blue) and Strain Gauges (Orange)

8.4 Loading Procedure

An open-source finite element analysis (FEA) program, Open System for Earthquake Engineering Simulation (OpenSees) (McKenna and Fenves 1999) was used to model the column subjected to a monotonic push-over load. The results from the model, shown in Fig. 8.7, predicted that the yield point should occur at approximately a load of 150 kN (33.7 kips) and a displacement of 20 mm (0.787 in.).

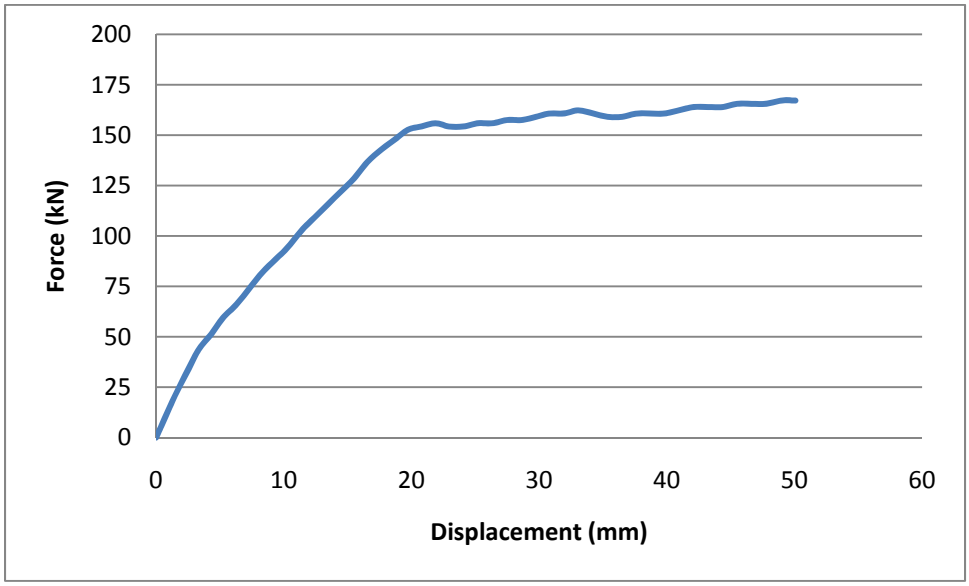

Fig. 8.7 Predicted Column Behavior Under a Monotonic Load

Based from the FEA results, a loading procedure was developed as follows:

1. An incremental load was chosen by dividing the yield load by 6 and multiplying by 0.8. This resulted in an incremental load of 20.0 kN (4.50 kips).
2. Using force-control, three cycles of the incremental load times n were applied to the column where n=1, 2, 3, 4, 5, and 6. One cycle consisted of loading the column to the desired load in the positive direction, loading the

column to the desired load in the negative direction, and returning to zero load. The cycles were applied at a rate of 0.1 Hz.

3. To ensure that the yield point was not missed, the loading procedure was switched from force-control to displacement-control. The displacement was increased in the positive direction until yielding.
4. The yield point corresponded to a ductility of μ=1. Three cycles were applied at each ductility level, μ=1.1, 1.2, 1.3, etc., until the force of the envelope curve equaled 80% of the maximum force recorded. One cycle consisted of loading the column to the desired ductility level in the positive direction, loading the column to the desired ductility level in the negative direction, and returning to zero displacement. The cycles were applied at a rate of 0.1 Hz.

8.5 Experimental Setup

To measure the electrical resistance, the outer wires of the six CNFAs were connected in series with a 10 kΩ resistor and a 10 V power supply, as shown in blue in Fig. 8.8. The voltage drops across the inner wires of the CNFAs and the resistor were measured using a data acquisition system, as shown in red in Fig. 8.8. There was an impedance problem within the data acquisition system, so differential amplifiers were placed between each component of the circuit and the data acquisition system, as shown in Fig. 8.8.

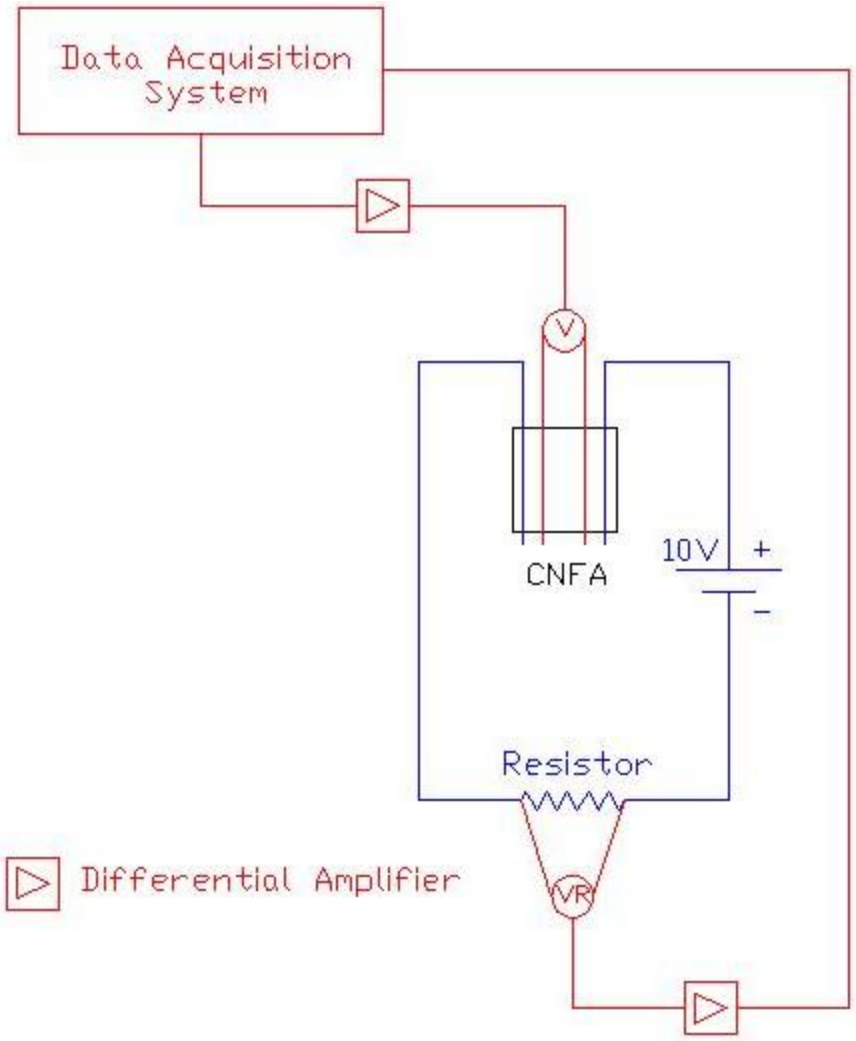

Fig. 8.8 Electrical Circuit and Connection to Data Aquisition System for Column Experiment

The differential amplifier circuit is shown in Fig. 8.9. A differential amplifier is a circuit that computes the differences of two voltages and multiplies it by a constant. If all four of the resistors have equal resistances, then the output voltage will equal the difference of the two input voltages. The differential amplifiers, consisting of all equal resistors and operational amplifiers, are shown in Fig. 8.10.

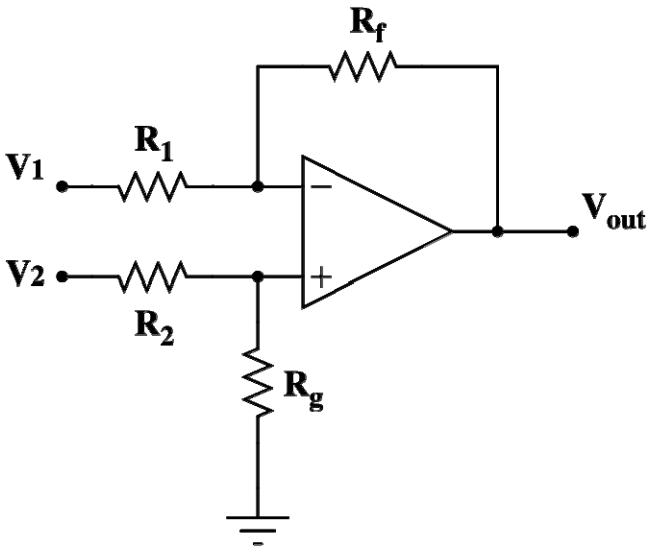

Fig. 8.9 Differential Amplifier Circuit

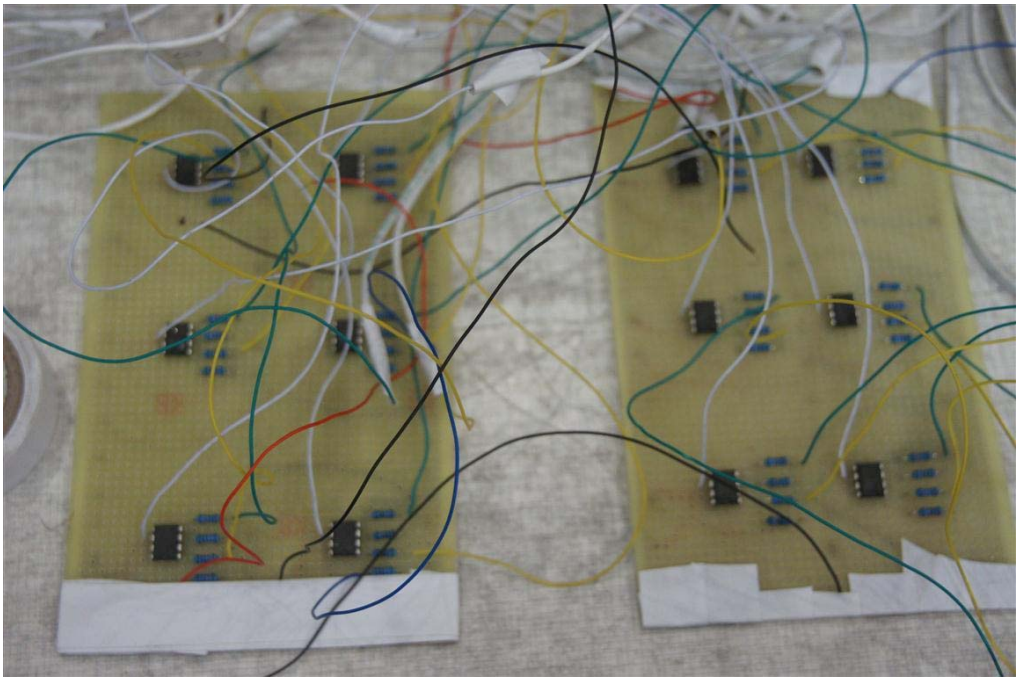

Fig. 8.10 Differential Amplifiers

The column foundation was bolted to the strong floor, and a horizontal actuator bolted to a strong wall provided the horizontal loading on the column. Displacement was

measured using linear variable differential transformers (LVDTs). The experimental setup is shown in Fig. 8.11.

Fig. 8.11 Column Experimental Setup

8.6 Experimental Results

Fig. 8.12 shows the force versus displacement curve for the tested column. The foundation of the column failed rather than the column, as shown in Fig. 8.13. Because of this failure mode, the column exhibited less ductility than was expected.

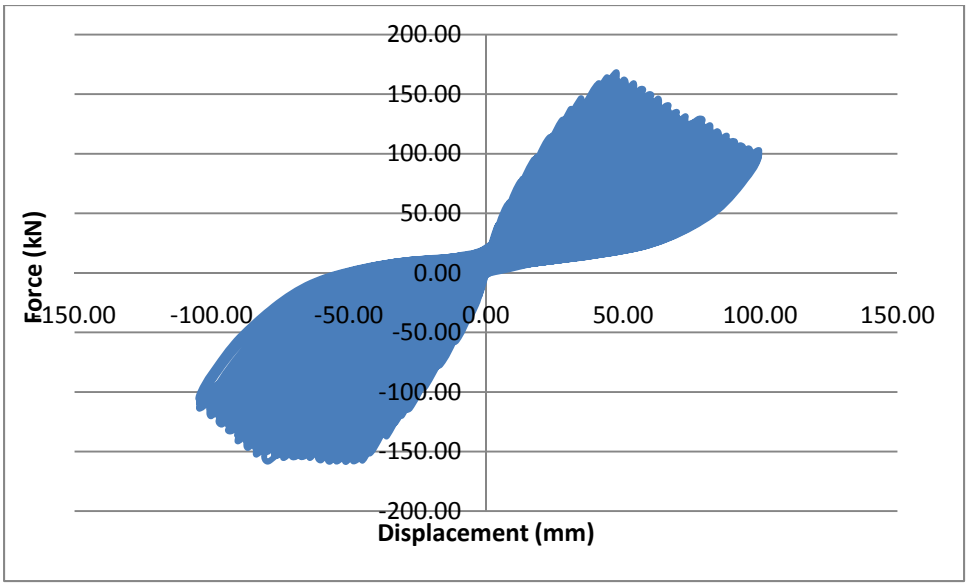

Fig. 8.12 Column Force versus Displacement

Fig. 8.13 Column Foundation Failure

When the internal instrumentation was installed, CNFAs and strain gauges were installed in pairs so that the strain and ERV could be directly compared. During the course of the test, three of the strain gauges failed prematurely. The CNFAs were installed in rows of three where each row should have the same strain value. At least one functional strain gauge was located on each row, so the strain values measured by the

functional strain gauges were averaged for each row to determine that row's strain. The internal sensor locations are shown in Fig. 8.14. The row designations are shown in Table 8.2.

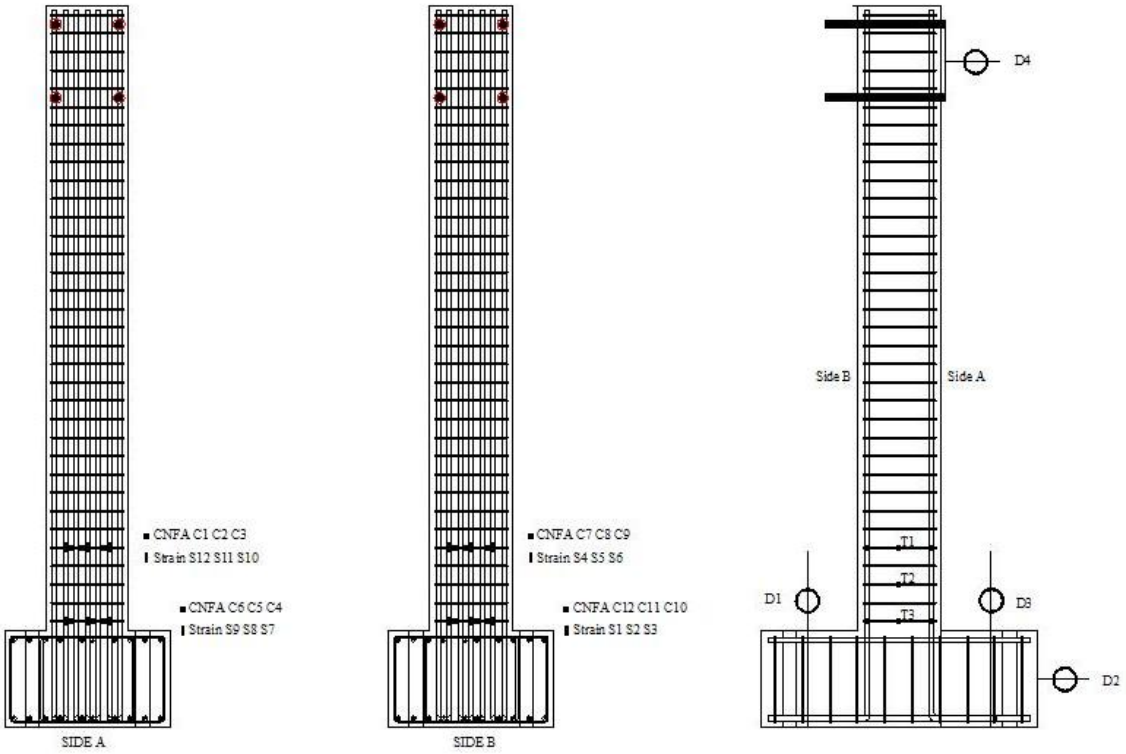

Fig. 8.14 Column Internal Sensor Locations

Table 8.2 Rows of Equal Strain and Associated CNFAs

Row	Associated CNFAs		
A	C1	C2	C3
B	C4	C5	C6
C	C7	C8	C9
D	C10	C11	C12

The force, strain and ERV behavior was compared for each row. Qualitatively, the CNFAs did an excellent job sensing the behavior of the columns. The CNFAs were not sensitive enough to sense the cyclic behavior of the 20 kN (4.50 kip) load, but with the exception of CNFA C9, each CNFA sensed every other cycle of the entire experiment.

CNFA C9 picked up most, but not all, of the cycles. The peaks and valleys of the force, strain, and ERV match for every other CNFA. There was an underlying drift behavior similar to the drift behavior observed in Chapter 6 in each signal. The drift appears to be random and could not be modeled. Fig. 8.15, Fig. 8.16, Fig. 8.17, Fig. 8.18 show the force, strain, and ERV behavior for Rows A, B, C, and D, respectively. Fig. 8.19 shows a typical strain verses ERV curve for one of the embedded CNFAs. The overall shape of the curve is similar to that shown in Chapter 6 for the cyclically tested cylinder.

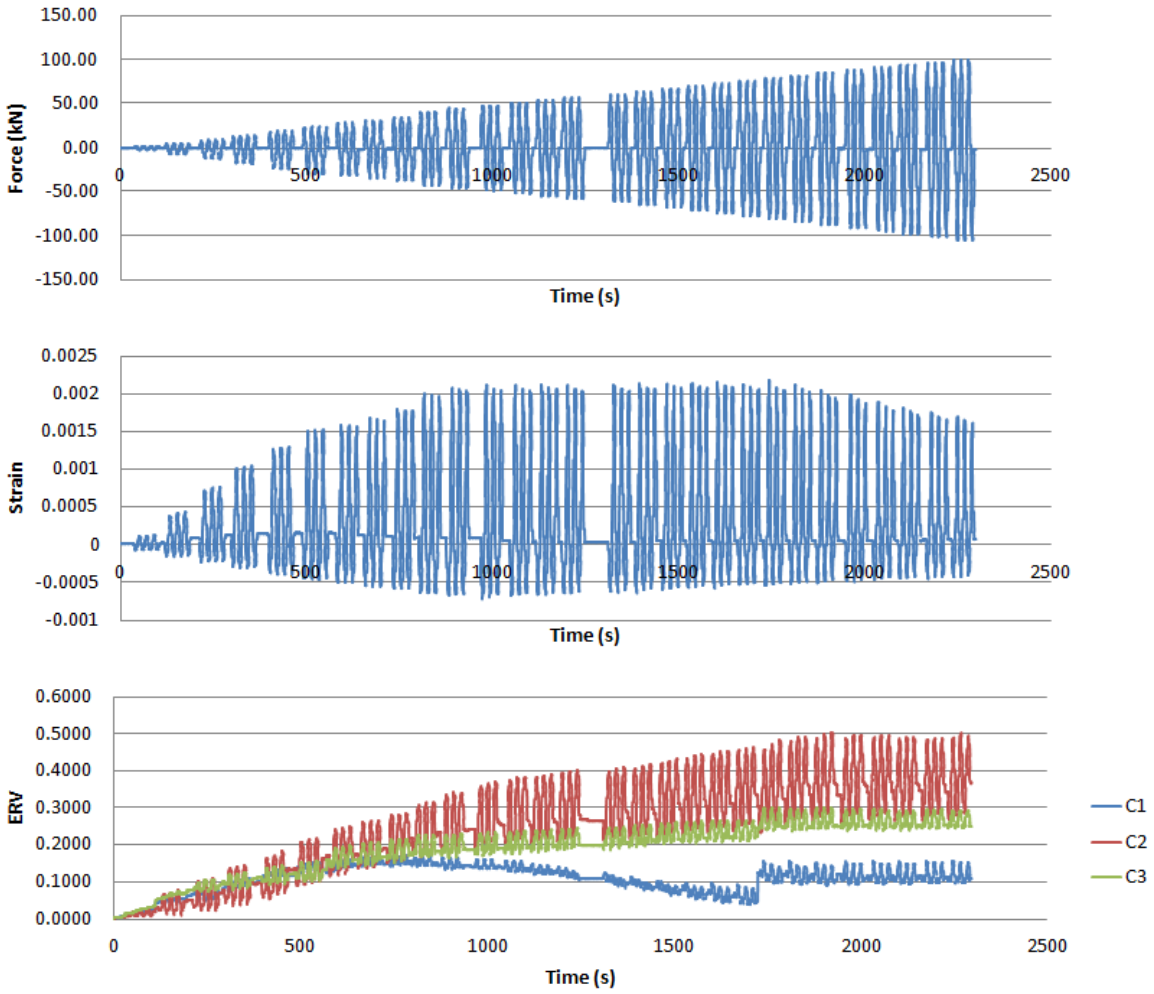

Fig. 8.15 Column Row A Force, Strain, and ERVversus Time

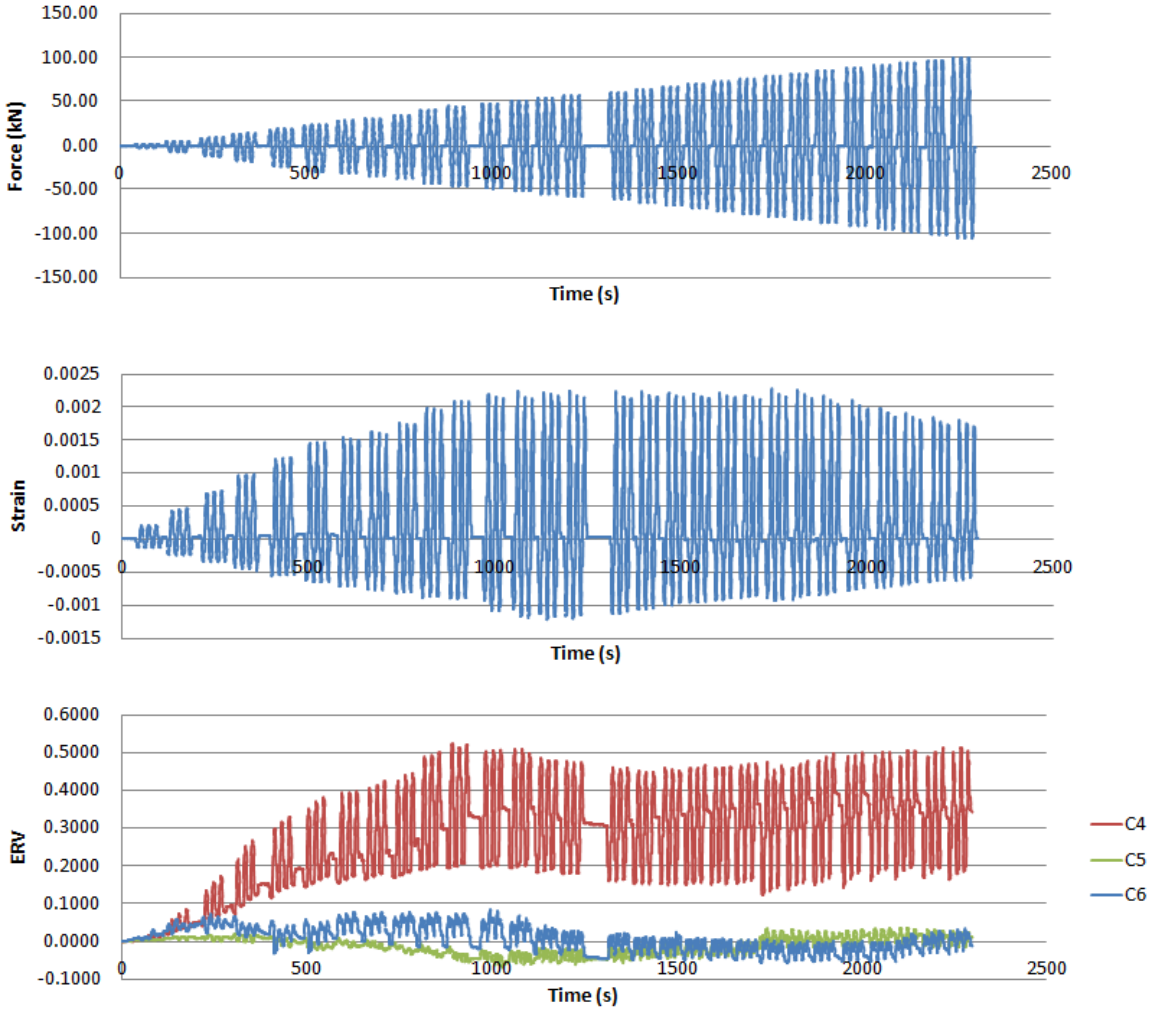

Fig. 8.16 Column Row B Force, Strain, and ERVversus Time

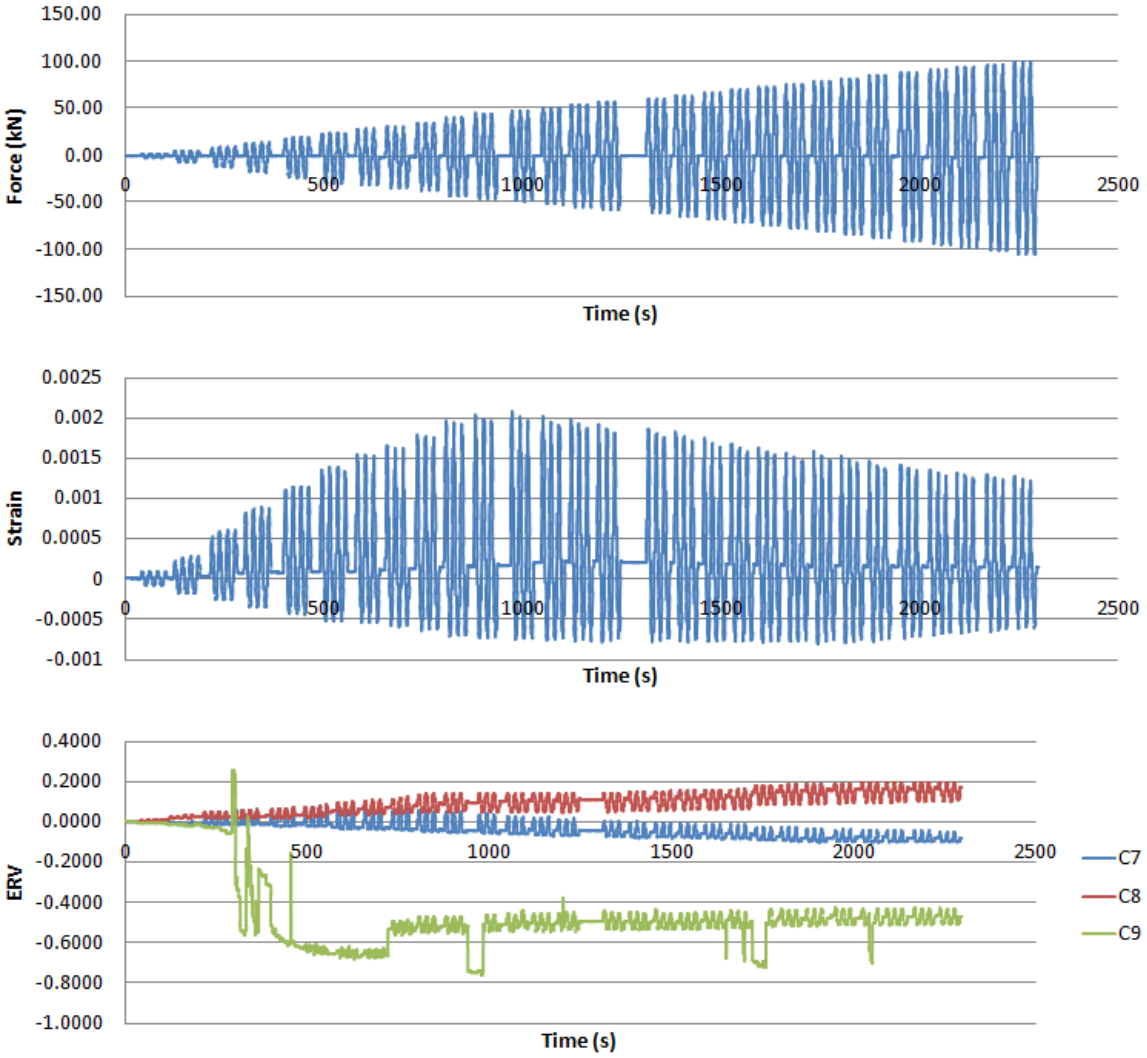

Fig. 8.17 Column Row C Force, Strain, and ERVversus Time

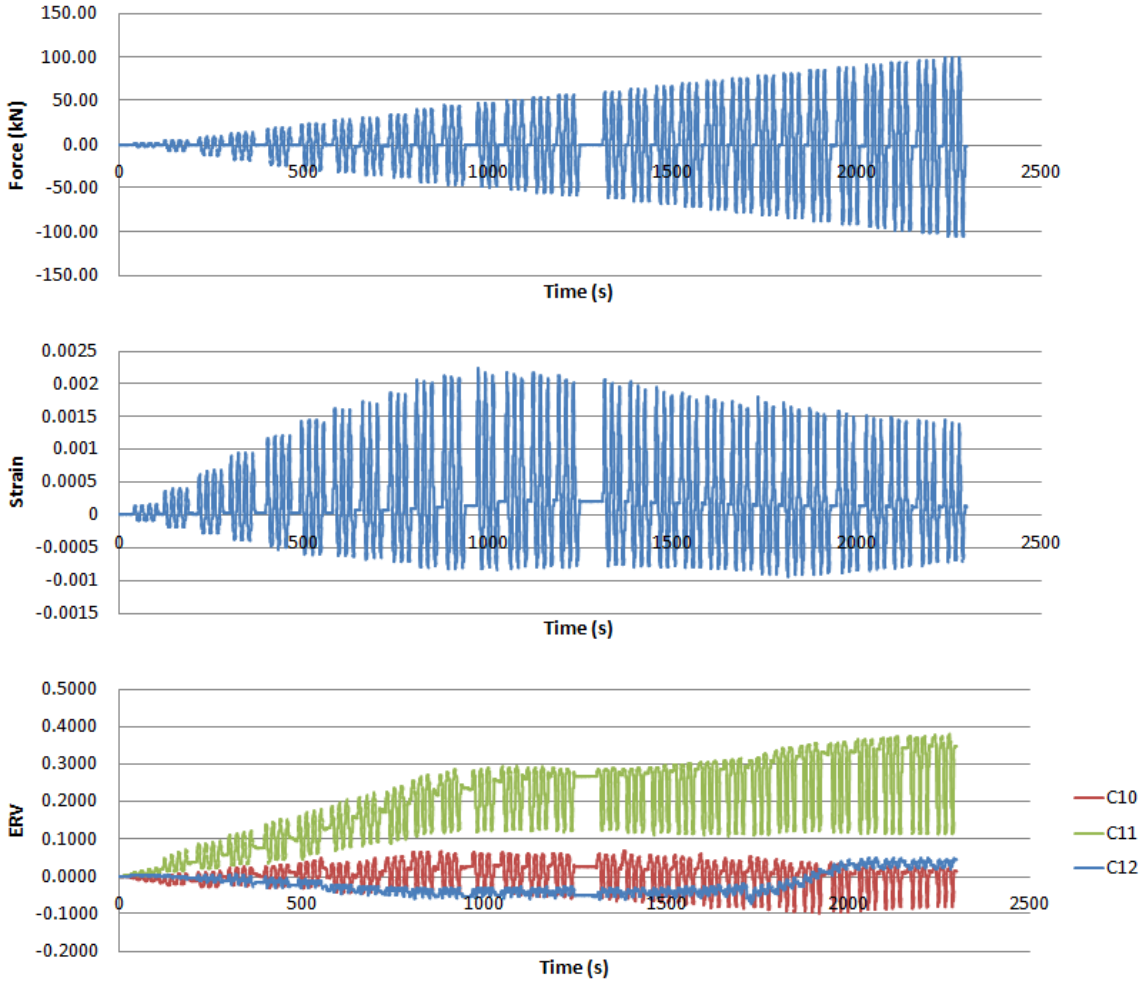

Fig. 8.18 Column Row D Force, Strain, and ERVversus Time

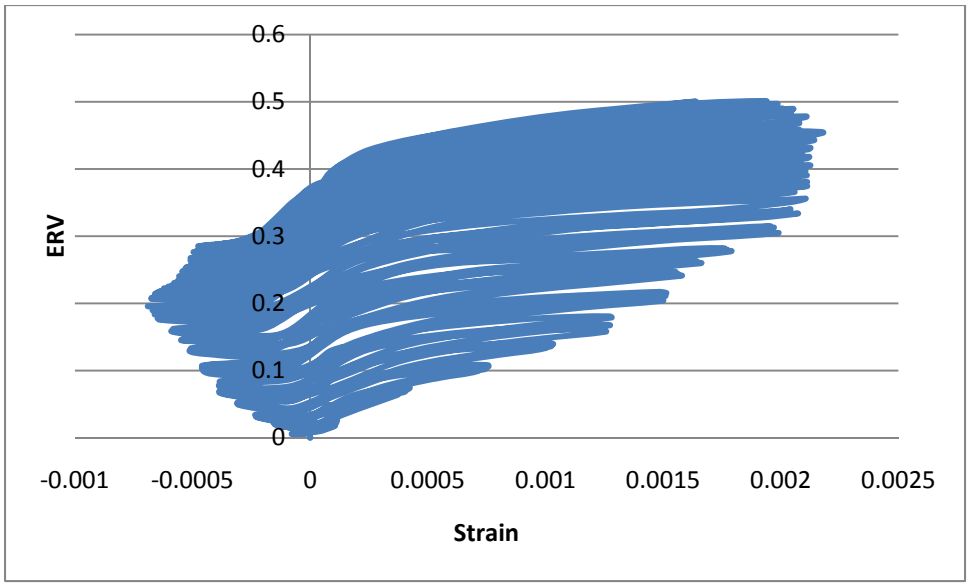

Fig. 8.19 Typical Stress versus ERV Relationship for CNFA Embedded in Column (CNFA C2 Shown)

8.7 Summary and Future Work

A full-scale reinforced concrete column with twelve embedded carbon nanofiber aggregates (CNFAs) was tested under reversed cyclic loads. The following conclusions were made from the study:

- Qualitatively, the CNFAs are capable of sensing complex strain histories.
- CNFAs are a robust sensor; while 3 of the strain gauges quit working during the experiment, all 12 CNFAs measured data throughout the entirety of the experiment.

Future work in this area of study includes:

- The underlying cause of the drift behavior should be determined so the CNFA cyclic behavior can be modeled.

- More full-scale tests should be completed so that a comprehensive CNFA model can be determined.
- The use of a frequency-response based feedback control system should be explored. The observed drift behavior may be eliminated through the use of feedback control.

CHAPTER 9
CONCLUSIONS AND FUTURE WORK

9.1 Introduction

Because of past success at the University of Houston (UH) demonstrating that self-consolidating carbon nanofiber concrete (SCCNFC) can be used as a strain sensor (Gao et al. 2009; Howser et al. 2011), a carbon nanofiber aggregate (CNFA) was developed. The CNFA is a 16.39 cm^3 (1.00 $in.^3$) cubic specimen of CNF mortar. The CNFA is self-sensing multifunctional sensor that can be used to monitor temperature, early-age properties, and strain. The CNFAs can be embedded in reinforced or prestressed concrete structures for structural health monitoring. The development of a CNFA is significant because it is possible to use the sensing capabilities of SCCNFC with a greatly reduced cost since only the CNFAs placed in the structure would contain carbon nanofibers (CNFs). SCCNFC costs nearly 20 times as much as normal concrete.

9.2 Conclusions and Future Work

9.2.1 Development of Carbon Nanofiber Aggregate

A carbon nanofiber aggregate (CNFA) was developed with self-sensing capabilities. The CNFA is a 2.54 cm by 2.54 cm by 2.54 cm (1.00 in. by 1.00 in. by 1.00 in) cube of mortar contain 0.70% carbon nanofibers (CNFs) by weight of cement. The electrical resistance is measured in the CNFAs through the embedment of four steel meshes and the use of the four-probe method. Preliminary testing was completed to prove that CNFAs

are multifunctional sensors capable of monitoring temperature, early-age properties, and strain in concrete structures.

The next steps in the development of the CNFA include:

- It is very difficult to align the meshes in the current formwork and the meshes sometimes become misaligned during casting. A better design would have vertical grooves cut into the side plates of the formwork. The meshes would slide down into the vertical grooves and be held perfectly aligned. This would result in a more consistently constructed CNFA.
- Other, more conductive, electrode materials should be explored for the meshes. These materials could include such materials as copper or nickel.
- Scanning electron microscope (SEM) pictures should be taken of the microstructure of the CNFAs. These should include pictures of the fibers post-testing to capture the pull-out behavior and pictures of the mesh-fiber interaction.
- Mortar was used as the material for the CNFA development so that the material properties matched the properties of the material in which it was embedded; however, cement based materials have some of the most variable material properties of any construction material. This variability translates to the electrical properties, making sensing difficult. Another material, such as a polymer, with similar elastic material properties may have better sensing capabilities due to more consistent material behavior.
- CNFAs should be exposed and calibrated to other stresses besides axial stress. If the study shows that their dominant behavior is in the axial-

direction, than the use of CNFAs oriented in three principal directions should be explored.

9.2.2 Temperature Monitoring

The response of embedded CNFAs was studied as they were exposed to temperatures varying from 20°C (-4°F) to 90°C (194°F). It was determined that CNFAs are a type of thermistor, a semiconductor that is capable of temperature sensing, and two models were derived that predict the thermal behavior of CNFAs. Future work includes testing many more specimens to make sure that the proposed model is appropriate. A wider temperature range should also be explored.

9.2.3 Early-Age and Hydration Monitoring

The response of CNFAs was studied as they were exposed to fresh concrete and pure water. The following conclusions were drawn from experimental data:

- Three waterproof coatings were tested for use with CNFAs. It was discovered that all three waterproof coatings failed, allowing water in the CNFAs. Later, when the waterproofed CNFAs were tested inside of concrete cylinders, the bond behavior was poor and the CNFAs could not be used for strain sensing.
- It was discovered that uncoated aggregates embedded in cylinders had the same behavior whether or not the cylinder was exposed to water. Since the uncoated CNFAs embedded in concrete are not sensitive to water, it was deemed that the waterproof coating was unnecessary.

- It was discovered that it was not necessary to oven dry the CNFAs before embedment since the uncoated CNFAs would become saturated with water upon embedment. The final resistances after embedment were on the same order of magnitude whether or not the CNFAs were oven dried before embedment.
- A more detailed, systematic study should be completed on the effects of moisture on the CNFAs.
- The electrical resistance variation (ERV) of the CNFAs becomes stable one to two days after embedment. Initial set occurs roughly one day after casting, so this phenomenon may be useful for early-age monitoring of concrete.

Future work in this area of research includes:

- Although it appears that waterproofing is not necessary, other waterproofing agents such as epoxies can be explored. These materials should have similar elastic properties to that of concrete so the sensor can still be used for strain monitoring.
- The early properties of embedded CNFAs should be tested with the purpose of observing any correlation between early strength and ERV.

9.2.4 Small-Scale Compressive Strain Monitoring

Three groups of cylinders with embedded CNFAs were tested in compression. The first group was tested in monotonic compression at room temperature. The second group

was frozen then tested monotonically. The third group was tested cyclically at room temperature. The following conclusions were made from the study:

- A qualitative assessment of the electrical data from a CNFA embedded in a cylinder can show when loading began on the cylinder, a strain of approximately 0.001, and failure.
- While the raw ERV values have a large coefficient of variation from the mean ERV values, a calibration factor can be applied to the ERV value to obtain a reasonable coefficient of variation. A model was developed to estimate the ERV versus strain relationship.
- Frozen cylinders behave brittlely. The ERV versus strain behavior is similar to the stress versus strain behavior in the lack of strain softening for frozen cylinders.
- Qualitatively, cyclic stress and strain can be assessed from the ERV versus time relationship. The peaks and valleys of all three relationships coincide during cyclic loading. A model was developed to estimate the cyclic ERV versus strain relationship.

Future work in small scale compressive strain monitoring includes:

- The calibration factor developed for this study was calculated post-embedment and testing. A calibration method should be developed for use pre-embedment.
- Many cylinders should be tested monotonically at various temperatures to develop a comprehensive monotonic ERV versus strain model.

- Many cylinders should be tested cyclically to develop a cyclic ERV versus strain model. The use of a frequency-response based feedback control system should be explored. The observed drift behavior may be eliminated through the use of feedback control.

9.2.5 Small-Scale Beam Strain Monitoring

A small-scale reinforced concrete beam with six embedded CNFAs was tested monotonically using the four-point bending method. The following conclusions were made from the study:

- CNFAs behave differently if they are tested in tension rather than compression. This was expected since concrete is not isotropic.
- CNFAs are capable of detecting localized catastrophic damage in reinforced concrete structures.

Future work on small-scale beam strain monitoring includes:

- Flexure-critical beams should be tested so that a model can be developed for CNFAs in tension.
- The comprehensive compression model developed using the small-scale compression tests should be compared to CNFAs in the compression region of reinforced concrete beams.

9.2.6 Full-Scale Column Strain Monitoring

A full-scale reinforced concrete column with twelve embedded CNFAs was tested under reversed cyclic loads. The following conclusions were made from the study:

- Qualitatively, the CNFAs are capable of sensing complex strain histories.

- CNFAs are a robust sensor; while 3 of the strain gauges quit working during the experiment, all 12 CNFAs measured data throughout the entirety of the experiment.

Future work on full-scale column strain monitoring includes:

- The CNFAs exhibited a seemingly random drift behavior. The underlying cause of the drift behavior should be determined so the CNFA cyclic behavior can be modeled.
- More full-scale tests should be completed so that a comprehensive CNFA model can be determined.
- The use of a frequency-response based feedback control system should be explored. The observed drift behavior may be eliminated through the use of feedback control.

REFERENCES

ACI Committee 318. (2011). *Building Code Requirements for Structural Concrete*. American Concrete Institute, Farmington Hills, Michigan.

ACI Committee 544. (1996). *State-of-the-Art Report on Fiber Reinforced Concrete Reported by ACI Committee 544*. American Concrete Institute, Farmington Hills, Michigan, 66.

Aoude, H., Cook, W. D., and Mitchell, D. (2009). "Behavior of Columns Constructed with Fibers and Self-Consolidating Concrete." *ACI Structural Journal*, 106(3), 349–357.

Bartos, P. (2006). "Nanotechnology in construction: A roadmap for development." *Nanotechnology of Concrete: Recent Developments and Future Perspective*, American Concrete Institute, Denver, CO, 1–14.

Baughman, R. H., Cui, C. X., Zakhidov, A. A., Iqbal, Z., Barisci, J. N., Spinks, G. M., G, W. G., Mazzoldi, A., de Rossi, D., Rinzler, A. G., Jaschinski, O., Roth, S., and Kertesz, M. (1999). "Carbon Nanotube Actuators." *Science*, 284, 1340–1344.

Baughman, R. H., Zakhidov, A. A., and de Heer, W. A. (2002). "Carbon nanotubes--the route toward applications." *Science*, 297, 787–92.

Bontea, D.-M., Chung, D. D. L., and Lee, G. C. (2000). "Damage in carbon fiber-reinforced concrete, monitored by electrical resistance measurement." *Cement and Concrete Research*, 30(4), 651–659.

Chang, C., Ho, M., Song, G., Mo, Y.-L., and Li, H. (2009). "A feasibility study of self-heating concrete utilizing carbon nanofiber heating elements." *Smart Materials and Structures*, 18(12), 127001.

Chen, B., Wu, K., and Yao, W. (2004). "Conductivity of carbon fiber reinforced cement-based composites." *Cement and Concrete Composites*, 26(4), 291–297.

Chen, P.-W., and Chung, D. D. L. (1993a). "Concrete reinforced with up to 0.2 vol% of short carbon fibres." *Composites*, 24(1), 33–52.

Chen, P.-W., and Chung, D. D. L. (1993b). "Carbon fiber reinforced concrete for smart structures capable of non-destructive flaw detection." *Smart Materials and Structures*, 2(1), 22–30.

Chen, P.-W., and Chung, D. D. L. (1996). "Concrete as a new strain/stress sensor." *Composites Part B: Engineering*, 27(1), 11–23.

Chen, P.-W., Fu, X., and Chung, D. D. L. (1997). "Microstructural and mechanical effects of latex, methylcellulose, and silica fume on carbon fiber reinforced cement." *ACI Materials Journal*, 94(2), 147–155.

Chung, D. D. L. (1995). "Strain sensors based on the electrical resistance change accompanying the reversible pull-out of conducting short fibers in a less conducting matrix." *Smart Materials and Structures*, 4, 59–61.

Chung, D. D. L. (1998). "Composite material strain/stress sensor." *US Patent 5,817,944*, United States of America.

Chung, D. D. L. (2000). "Cement reinforced with short carbon fibers: a multifunctional material." *Composites Part B: Engineering*, 31, 511–526.

Chung, D. D. L. (2004). "Self-heating structural materials." *Smart Materials and Structures*, 13(3), 562–565.

Chung, D. D. L. (2005). "Dispersion of short fibers in cement." *Journal of Materials in Civil Engineering*, 17(4), 379–3831.

Coleman, J. N., Khan, U., Blau, W. J., and Gun'ko, Y. K. (2006). "Small but strong: A review of the mechanical properties of carbon nanotube–polymer composites." *Carbon*, 44(9), 1624–1652.

Dume, B. (2007). "Nanofibres under control." *nanotechweb.org*, <http://nanotechweb.org/cws/article/tech/32055> (Oct. 8, 2012).

Feynman, R. (1960). "There's Plenty of Room at the Bottom." *Engineering and Science*, 23, 22–36.

Gaimster, R., and Foord, C. (2000). "Self-compacting concrete." *Concrete*, 34, 23–25.

Gao, D., Sturm, M., and Mo, Y. L. (2009). "Electrical resistance of carbon-nanofiber concrete." *Smart Materials and Structures*, 18(9).

Han, B., Zhang, L., and Ou, J. (2010). "Influence of water content on conductivity and piezoresistivity of cement-based material with both carbon fiber and carbon black." *Journal of Wuhan University of Technology-Mater. Sci. Ed.*, 25(1), 147–151.

Hilding, J., Grulke, E. a., George Zhang, Z., and Lockwood, F. (2003). "Dispersion of Carbon Nanotubes in Liquids." *Journal of Dispersion Science and Technology*, 24(1), 1–41.

Howser, R. N., Dhonde, H. B., and Mo, Y. L. (2011). "Self-sensing of carbon nanofiber concrete columns subjected to reversed cyclic loading." *Smart Materials and Structures*, 20(8), 085031.

Howser, R. N., and Mo, Y. L. (2013). "Development of Carbon Nanofiber Aggregate." *Structures Congress 2013*, American Society of Civil Engineers, Pittsburgh, Pennsylvania, 12.

Iijima, S. (1991). “Helical microtubules of graphitic carbon.” *nature*, 354(November 1991), 11–14.

Kang, I., Heung, Y. Y., Kim, J. H., Lee, J. W., Gollapudi, R., Subramaniam, S., Narasimhadevara, S., Hurd, D., Kirikera, G. R., Shanov, V., Schulz, M. J., Shi, D., Boerio, J., Mall, S., and Ruggles-Wren, M. (2006). “Introduction to carbon nanotube and nanofiber smart materials.” *Composites Part B: Engineering*, 37(6), 382–394.

Khayat, K. H., Hu, C., and Monty, H. (1999). “Stability of Self-Consolidating Concrete, Advantages, and Potential Applications.” *First International RILEM Symposium on Self-Compacting Concrete*, Stockholm, Sweden, 143–152.

Konsta-Gdoutos, M., Metaxa, Z., and Shah, S. (2010a). “Multiscale Fracture Characteristics of Cement Based Materials Reinforced with Carbon Nanofibers.” *ECF18, Dresden 2010*, 1–8.

Konsta-Gdoutos, M. S., Metaxa, Z. S., and Shah, S. P. (2010b). “Highly dispersed carbon nanotube reinforced cement based materials.” *Cement and Concrete Research*, Elsevier Ltd, 40(7), 1052–1059.

Lentz, A. E., and Monfore, G. E. (1966). “Thermal of Portland Aggregate Conductivities Cement Paste , and Concrete Down to Very Low Temperatures.” *Journal of the PCA Research and Development Laboratories*, 8(3), 27–33.

Li, G. Y., Wang, P. M., and Zhao, X. (2005). “Mechanical behavior and microstructure of cement composites incorporating surface-treated multi-walled carbon nanotubes.” *Carbon*, 43(6), 1239–1245.

Li, G. Y., Wang, P. M., and Zhao, X. (2007). "Pressure-sensitive properties and microstructure of carbon nanotube reinforced cement composites." *Cement and Concrete Composites*, 29(5), 377–382.

Li, H., Xiao, H., Yuan, J., and Ou, J. (2004). "Microstructure of cement mortar with nano-particles." *Composites Part B: Engineering*, 35(2), 185–189.

Li, H., Zhang, M., and Ou, J. (2006). "Abrasion resistance of concrete containing nano-particles for pavement." *Wear*, 260(11-12), 1262–1266.

Li, H., Zhang, M., and Ou, J. (2007). "Flexural fatigue performance of concrete containing nano-particles for pavement." *International Journal of Fatigue*, 29(7), 1292–1301.

Li, V. C. (2002). "Large volume, high □performance applications of fibers in civil engineering." *Journal of Applied Polymer Science*, 83, 660–686.

Liao, W. C., Chao, S. H., Park, S.-Y., and Naaman, A. E. (2006). *Self-Consolidating High Performance Fiber Reinforced Concrete: SCHPFRC. High Performance Fiber …*, 76.

Makar, J., and Beaudoin, J. (2004). "Carbon nanotubes and their application in the construction industry." *1st International Symposium on Nanotechnology in Construction*, National Research Council Canada, Paisley, Scotland, 331–341.

Makar, J., Margeson, J., and Luh, J. (2005). "Carbon nanotube/cement composites–early results and potential applications." *3rd International Conference on Construction Materials: Performance, Innovations and Structural Implications*, National Research Council Canada, Vancouver, British Columbia, Canada, 1–10.

McGee, T. (1988). *Principles and Methods of Temperature Measurement*. John Wiley & Sons, 203.

McKenna, F., and Fenves, G. L. (1999). "Open System for Earthquake Engineering Simulation."

Mondal, P., Shah, S. P., and Marks, L. (2007). "A reliable technique to determine the local mechanical properties at the nanoscale for cementitious materials." *Cement and Concrete Research*, 37(10), 1440–1444.

Monfore, G. E., and Lentz, A. E. (1962). "Physical Properties of Concrete at Very Low Temperatures." *Journal of the PCA Research and Development Laboratories*, 4(2), 33–39.

Naaman, A. E. (1985). "Fiber Reinforcement for Concrete." *Concrete International*, 7(3), 21–25.

Narayan, R. J., Kumta, P. N., Sfeir, C., Lee, D.-H., Choi, D., and Olton, D. (2004). "Nanostructured ceramics in medical devices: Applications and prospects." *Journal of the Minerals, Metals and Materials Society*, 56(10), 38–43.

Okamura, H., and Ozawa, K. (1995). "Mix-Design for Self-Compacting Concrete." *Concrete Library of the Japanese Society of Civil Engineers*, 25(6), 107–120.

Padmarajaiah, S. K., and Ramaswamy, A. (2002). "Comparative Study on Flexural Response of Full and Partial Depth Fiber-Reinforced High-Strength Concrete." *Journal of Materials in Civil Engineering*, American Society of Civil Engineers, 14(2), 130–136.

PCI TR-6-03. (2003). *Interim Guidelines for the Use of Self-Consolidating Concrete in Precast/Prestressed Concrete Institute Member Plants*. Precast/Prestressed Concrete Institute, Chicago, 165.

Roco, M. (2007). "National nanotechnology initiative-past, present, future." *Handbook on Nanoscience, Engineering and Technology*, CRC Press, Boco Raton, 3.1–3.26.

Salvetat, J.-P., Bonard, J.-M., Thomson, N. H., Kulik, A. J., Forró, L., Benoit, W., and Zuppiroli, L. (1999). "Mechanical properties of carbon nanotubes." *Applied Physics A: Materials Science & Processing*, 69(3), 255–260.

Sanchez, F., and Sobolev, K. (2010). "Nanotechnology in concrete – A review." *Construction and Building Materials*, Elsevier Ltd, 24(11), 2060–2071.

Schmidt, M., and Lipson, H. (2009). "Distilling Free-Form Natural Laws." *Science*, 324, 81–85.

Shah, S. (2010). "Fracture of concrete and reinforcement scale." *ECF18, Dresden 2010*.

Shah, S. P., and Naaman, A. E. (1976). "Mechanical Properties of Glass and Steel Fiber Reinforced Mortar." *ACI Journal Proceedings*, 73(1), 50–53.

Steinhart, J., and Hart, S. (1968). "Calibration curves for thermistors." *Deep Sea Research and Oceanographic Abstracts*, 15, 497–503.

Tanaka, K., Sato, K., Watanabe, S., Arima, I., and Suenaga, K. (1993). "Development and Utilization of High-Performance Concrete for the Construction of the Akashi Kaikyo Bridge." *ACI Special Publication 140*, 140, 25–52.

Thess, A., Lee, R., Nikolaev, P., Dai, H., Petit, P., Robert, J., Xu, C., Lee, Y. H., Kim, S. G., Rinzler, A. G., Colbert, D. T., Scuseria, G. E., Tomanek, D., Fischer, J. E.,

and Smalley, R. E. (1996). “Crystalline ropes of metallic carbon nanotubes.” *Science*, 273, 483–487.

Timoshenko, S. (1953). *History of strength of materials*. McGraw-Hill, New York.

Tzeng, Y., Huang, T., Chen, Y., Liu, C., and Liu, Y. (2004). “Hydration properties of carbon nanotubes and their effects on electrical and biosensor applications.” *New Diamond and Frontier Carbon Technology*, 14(3), 193–201.

Wei, B. Q., Vajtai, R., and Ajayan, P. M. (2001). “Reliability and current carrying capacity of carbon nanotubes.” *Applied Physics Letters*, American Institute of Physics, 79(8), 1172.

Woo, L. Y., Wansom, S., Ozyurt, N., Mu, B., Shah, S. P., and Mason, T. O. (2005). “Characterizing fiber dispersion in cement composites using AC-Impedance Spectroscopy.” *Cement and Concrete Composites*, 27(6), 627–636.

Yang, X., and Chung, D. D. L. (1992). “Latex-modified cement mortar reinforced by short carbon fibres.” *Composites*, 23(6), 453–460.

Yu, X., and Kwon, E. (2012). *Carbon Nanotube Based Self-sensing Concrete for Pavement Structural Health Monitoring*. Washington, DC, 40.

APPENDIX A—BEAM CALCULATIONS

Calculated by: Rachel Howser | Small Scale Beam Test | 1/5

Date: 05/06/2013

Material Properties

fc'=	27.6	MPa				
fc'=	4000	psi				
fy=	414	MPa	(Longitudinal)	fy=	414 MPa	(Shear)
fy=	60000	psi		fy=	60000 psi	

Geometric Properties

h=	152.4	mm
h=	6.0	in
bw=	152.4	mm
bw=	6.0	in
Ag=	h*bw	
Ag=	23226	mm^2
Ag=	36.0	in^2
L=	457	mm
L=	18.0	in

Select Reinforcement

Bar Size	D (mm)	A (mm^2)	A (in^2)	# of Bars	ρl
2	6.35	31.669	0.049	2	0.0027
3	9.525	71.256	0.110	3	0.0092

Long. Bar= 3 No. 3 on bottom

Tran. Bar= No. 2 at 63.5 mm spacing

2.5 in spacing

Spacing= 42.9 mm between longitudinal rebars

Spacing= 1.7 in between longitudinal rebars

Calculate Capacity

d= 128.6 mm

d= 5.06 in

a= $\frac{A_s f_y}{0.85 f_c' b}$

a= 24.75 mm

a= 0.975 in

β1= $1.09 - 0.008 f_c'$ (ACI 10.2.7.3)

β1= 0.89

c= $\frac{a}{\beta_1}$ (ACI 10.2.7.1)

c= 27.8 mm

c= 1.095 in

εt= $\frac{(d_t - c)}{c} 0.003$

εt= 0.01087 tension controlled

Mn= $A_s f_y \left(d - \frac{a}{2} \right)$

Mn= 10.28 kN-m

Mn= 7.58 kip-ft

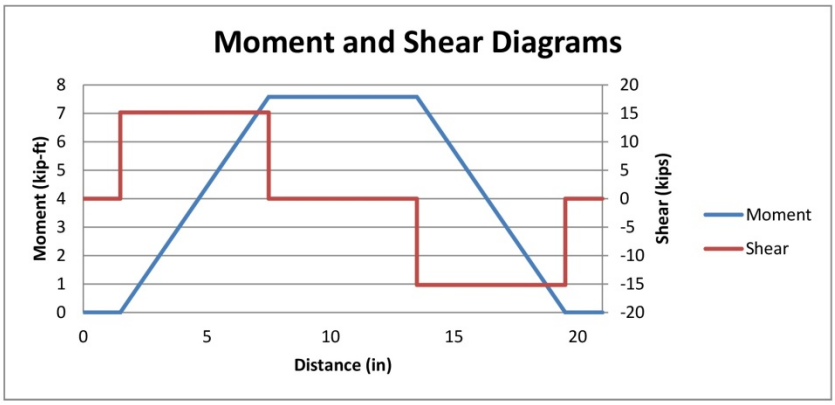

Vn= 134.9 kN

Vn= 30.32 kips

Determine Transverse Reinforcement Spacing
Confinement Requirements

s(max1)= $d/2$ (ACI 11.4.5.1)

s(max1)= 64.3 mm

s(max1)= 2.53 in

s(max2)= eight times the diameter of the smallest longitudinal bar

s(max2)= 76.2 mm

s(max2)= 3.00 in (ACI 21.3.4.2.b)

s(max3)= 24 times the diameter of the hoop bars

s(max3)= 152.4 mm

s(max3)= 6.00 in (ACI 21.3.4.2.c)

s(max4)= 305 mm

s(max4)= 12 in (ACI 21.3.4.2.d)

Shear Requirements

Vc=	$2\sqrt{f_c'}b_w d$			(ACI Eq. 11-3)
Vc=	17.09	kN		
Vc=	3.8	kips		
0.5ϕVc=	6.4	kN		(ACI 11.4.6.1)
0.5ϕVc=	1.44	kips		Stirrups Req'd
Av=	63.34	mm^2		
Av=	0.098	in^2		
s(max5)=	$\frac{A_v f_y}{0.75\sqrt{f_c'}b_w}$			(ACI Eq. 11-13)
s(max5)=	20.70	in		
s(max6)=	$\frac{A_v f_y}{50 b_w}$			(ACI 11.4.6.3
s(max6)=	19.63	in		
s (max7)=	$\frac{A_v f_y d}{V_n/\phi - V_c}$			(ACI Eq. 11-1, 11-2, and 11-15)
s (max7)=	2.63	in		

Choose Spacing

s=	64.3	mm		(minimum s(max))
s=	2.53	in		
s=	63.5	mm		(choose easily measurable number smaller than s)
s=	2.50	in		
ρt=	0.06627			
Vs=	$\frac{A_v f_y d}{s}$			(ACI Eq. 11-15)
Vs=	11.93	kips		
Vu=	$V_c + V_s$			
Vu=	15.8	kips	OK	
Vu=	70.2	kN		

Calculate the Maximum Deflection

Uncracked Moment of Inertia

Ec=	$57{,}000\sqrt{f_c'}$			(ACI 8.5.1)
Ec=	24855	MPa		
Ec=	3604997	psi		
Es=	199945	MPa		
Es=	29000000	psi		
n=	E_s/E_c			
n=	8.04			
As1=	1506	mm^2		
As1=	2.334	in^2		

As2= 446.2 mm^2
As2= 0.6916 in^2

Part	A (in^2)	y (in)	Ay (in^3)
Concrete	36.0	3.00	108.0
Top Steel	0.692	0.875	0.605
Bottom Steel	2.33	5.06	11.82
Total	39.0	8.94	120.4

yt= 78.4 mm
yt= 3.09 in

Part	A (in^2)	y (in)	I (in^4)	Ay^2 (in^4)
Concrete	36.0	-0.09	1296	0.264
Top Steel	0.692	-2.21	-	3.38
Bottom Steel	2.33	1.98	-	9.12
Total	39.0	-0.32	1296	12.77

Igt= 544749245 mm^4
Igt= 1309 in^4

Cracked Moment of Inertia

As1= 1720 mm^2
As1= 2.665 in^2
As2= 446.2 mm^2
As2= 0.6916 in^2

Part	A (in^2)	y (in)	Ay (in^3)
Concrete	6c	c/2	3c^2
Top Steel	0.692	c-0.875	0.692c-0.606
Bottom Steel	2.67	c-5.06	2.67c-13.51
Total	6c+2.99		3c^2+3.362c-14.12

c= 41.7 mm
c= 1.642 in

Part	A (in^2)	y (in)	I (in^4)	Ay^2 (in^4)
Concrete	9.8	0.82	26.5	6.64
Top Steel	0.692	0.77	-	0.406
Bottom Steel	2.67	-3.42	-	31.1
Total	13.2	-1.83	26.5	38.2

Icr= 26944733 mm^4
Icr= 64.7 in^4

Calculated by: Rachel Howser | Small Scale Beam Test | 5/5

Date: 05/06/2013

Cracking Moment

fr= $7.5\sqrt{f_c'}$

fr= 3.27 MPa

fr= 474 psi

Mcr= $\frac{f_r I_g}{y_t}$

Mcr= 22.51 kN-m

Mcr= 16.60 kip-ft Cracking moment is higher than Mn

Pcr= 90.04 kN

Pcr= 66.4 kips

Calculate Deflection

Δ= $\frac{5}{72}\frac{Ml^2}{EI}$

Δ= 0.488 mm

Δ= 0.01921 in

APPENDIX B—COLUMN AND FOUNDATION CALCULATIONS

Calculated by: Rachel Howser | Flexure-Critical Column | 1/8

Date: 05/06/2013

Material Properties

fc'=	30	MPa				
fc'=	4351	psi				
fy=	335	MPa	(Longitudinal)	fy=	235	MPa (Shear)
fy=	48588	psi		fy=	34084	psi

Geometric Properties

h=	450	mm
h=	17.7	in
Ag=	h^2	
Ag=	202500	mm^2
Ag=	314	in^2
L=	3130	mm
L=	123.2	in

Select Reinforcement

ρl=	0.028	OK	(Choose a value between 0.01 and 0.06)
Ast=	$\rho_l A_g$		
Ast=	5670	mm^2	

Bar Size	D (mm)	A (mm^2)	A (in^2)	# of Bars	ρl
8	8	50.265	0.078	113	0.0280
10	10	78.540	0.122	73	0.0283
12	12	113.097	0.175	51	0.0285
14	14	153.938	0.239	37	0.0281
16	16	201.062	0.312	29	0.0288
18	18	254.469	0.394	23	0.0289
20	20	314.159	0.487	19	0.0295
22	22	380.133	0.589	15	0.0282
25	25	490.874	0.761	12	0.0291

Long. Bar=	7	No.	25	on each face	14 bars total
Tran. Bar=		No.	8	at	100 mm spacing

Spacing= 34.7 mm between longitudinal rebars

Calculate Capacity

Pn=	156.7	kips	(10% of Capacity)
Pn=	696.8	kN	
Mn=	414.8	ft-kip	(From Interaction Diagram)
Mn=	562.4	m-kN	
Vas=	40.4	kips	(Assume Cantilever)
Vas=	179.7	kN	

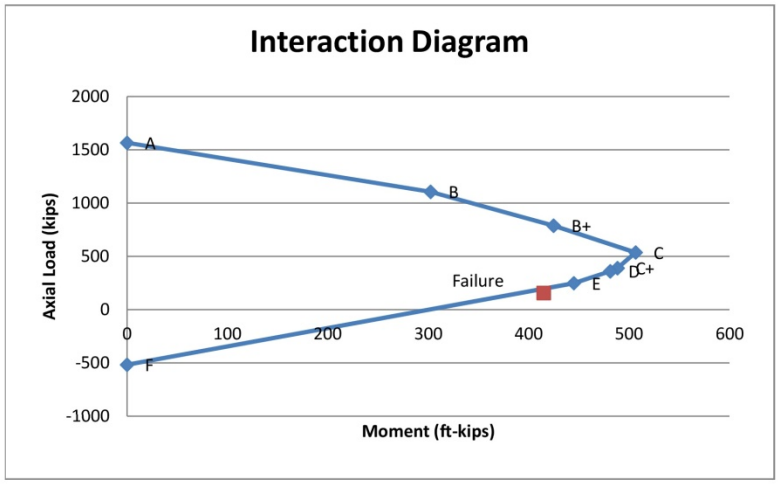

Figure 1: Column Interaction Diagram

Point	Pn (kips)	Pn (kN)	Mn (kip-ft)	Mn (kN-m)
A	1567	6968	0	0
B	1107	4924	302	410
B+	788	3505	425	576
C	537	2389	506	687
C+	390	1736	488	662
D	360	1600	481	652
E	249	1106	445	603
F	-518	-2302	0	0
Failure	157	697	415	562

From Figure 1, the moment at failure is 415 kip-ft, which corresponds to an axial load equal to 10% of the cross section capacity.

Determine Transverse Reinforcement Spacing

Confinement Requirements

s(max1)=	$d/4$			(ACI 21.3.4.2.a)
s(max1)=	3.98	in		
s(max2)=	eight times the diameter of the smallest longitudinal bar			
s(max2)=	7.87	in		(ACI 21.3.4.2.b)
s(max3)=	24 times the diameter of the hoop bars			
s(max3)=	7.56	in		(ACI 21.3.4.2.c)
s(max4)=	12	in		(ACI 21.3.4.2.d)

Shear Requirements

Vc=	$2\left(1+\frac{P_n}{2000A_g}\right)\sqrt{f_c'}b_w d$			(ACI Eq. 11-4)
Vc=	46.5	kips		
0.5ϕVc=	17.42	kips	Not OK	(ACI 11.4.6.1)
Av=	0.156	in^2		
s(max5)=	$\frac{A_v f_y}{0.75\sqrt{f_c'}b_w}$			(ACI Eq. 11-13)
s(max5)=	6.06	in		
s(max6)=	$\frac{A_v f_y}{50 b_w}$			(ACI 11.4.6.3
s(max6)=	6.00	in		
s (max7)=	$\frac{A_v f_y d}{V_n/\phi - V_c}$			(ACI Eq. 11-1, 11-2, and 11-15)
s (max7)=	11.42	in		

Choose Spacing

s=	3.98	in	(minimum s(max))
s=	101.0	mm	
s=	100	mm	(choose easily measurable number smaller than s)
s=	3.94	in	
ρt=	0.00356		
c=	3.23	in	(Found from interaction diagram calculations)
a=	123.23	in	
Vs=	$\frac{A_v f_y d}{s}$		(ACI Eq. 11-15)
Vs=	21.46	kips	

Vp= $P\frac{h-c}{2L}$

Vp= 9.21 kips

Vu= $V_c + V_s + V_P$

Vu= 86.3 kips OK

Vu= 383.7 kN

Complete Secondary Analysis

Since there are no flexural members in this system, assume k=1.

Pc= $\frac{\pi^2 EI}{(kl_u)^2}$ (ACI Equation 10-13)

EI= $\frac{0.4E_cI_g}{1+\beta_{dns}}$ (ACI Equation 10-15)

Ec= $57000\sqrt{f_c'}$ (psi) (ACI 8.5.1)

fc'= 4351 psi

Ec= 3759927 psi

Ec= 25924 MPa

Ig= $\frac{1}{12}bh^3$

b= 450 mm

b= 17.72 in

h= 450 mm

h= 17.72 in

Ig= 3417187500 mm^4

Ig= 8210 in^4

βdns= 1 (ACI 10.10.6.2)

EI= 1.77173E+13 kN-mm^2

EI= 6173669 k-in^2

ln= 3130 mm

ln= 123.2 in

Pc= 17849 kN

Pc= 4013 k

Pu= 696.8 kN

Pu= 156.7 k

δs= $\frac{1}{1-\frac{\sum P_u}{0.75\sum P_c}} \geq 1$ (ACI Equation 10-21)

δs= 1.055

The moment magnification factor is less than 5% and negligible.

Deflection Calculations

n=	E_s / E_c	
Es=	29000000	psi
Es=	199948	MPa
Ec=	3759927	psi
Ec=	25924	MPa
n=	7.71	
As=	5.33	in^2
As=	3436	mm^2
nAs=	41.08	in^2
nAs=	26502	mm^2
c=	3.23	in
c=	82.1	mm
Ac=	57.3	in^2
Ac=	36955	mm^2
yc=	1.617	in
yc=	41.1	mm
Ic(own)=	49.9	in^4
Ic(own)=	20769465	mm^4
Acyc^2=	149.7	in^4
Acyc^2=	62308395	mm^4
ys=	-12.68	in
ys=	-322.0	mm
Asys^2=	855.8	in^4
Asys^2=	356219510	mm^4
Icr=	1055.4	in^4
Icr=	439297370	mm^4
Δ=	$\frac{VL^3}{3EI}$	
V=	40.4	kips
V=	179.7	kN
L=	123.2	in
L=	3130	mm
Δ=	6.35	in
Δ=	161.3	mm

Find unfactored interaction diagram

γ=	0.796	
d1=	15.91	in
d2=	1.81	in
β1=	0.832	
εy=	0.00168	
Es=	29000	ksi
As1=	5.33	in^2
As2=	5.33	in^2

Equations used in calculation of interaction diagram:

εs1= $Z\varepsilon$

fs1= $\varepsilon_{s1}E_s \quad -f_y \le f_{s1} \le f_y$

c= $\dfrac{0.003}{0.003-\varepsilon_{s1}}$

a= $\beta_1 c$

εs2= $\left(\dfrac{c-d_2}{c}\right)0.003$

fs2= $\varepsilon_{s2}E_s \quad -f_y \le f_{s2} \le f_y$

Cc= $0.85f_c'ab$

Fs1= $f_{s1}A_{s1}$

Fs2= $(f_{s2}-0.85f_c')A_{s2}$

Pn= $C_c+F_{s1}+F_{s2}$

Mn= $C_c\left(\dfrac{h}{2}-\dfrac{a}{2}\right)+F_{s1}\left(\dfrac{h}{2}-d_1\right)+F_{s2}\left(\dfrac{h}{2}-d_2\right)$

Point A

P0= 1567 kips

Point B

Z=	0	
εs1=	0	
fs1=	0	ksi
c=	15.91	in
a=	13.24	in
εs2=	0.00266	
fs2=	48.6	ksi
Cc=	868	kips
Fs1=	0	kips
Fs2=	239.1	kips
Pn=	1107	kips
Mn=	302	ft-kips

Point B+

Z=	-0.5	
εs1=	-0.00084	
fs1=	-24.3	ksi
c=	12.44	in
a=	10.35	in
εs2=	0.00256	
fs2=	48.6	ksi
Cc=	678	kips
Fs1=	-129.4	kips
Fs2=	239.1	kips
Pn=	788	kips
Mn=	425	ft-kips

Point C

Z=	-1	
εs1=	-0.00168	
fs1=	-48.6	ksi
c=	10.21	in
a=	8.50	in
εs2=	0.00247	
fs2=	48.6	ksi
Cc=	557	kips
Fs1=	-258.8	kips
Fs2=	239.1	kips
Pn=	537	kips
Mn=	506	ft-kips

Point C+

Z=	-2	
εs1=	-0.00335	
fs1=	-48.6	ksi
c=	7.52	in
a=	6.26	in
εs2=	0.002279	
fs2=	48.6	ksi
Cc=	410	kips
Fs1=	-258.8	kips
Fs2=	239.1	kips
Pn=	390	kips
Mn=	488	ft-kips

Point D

Z=	-2.31	
εs1=	-0.00386	
fs1=	-48.6	ksi
c=	6.96	in
a=	5.79	in
εs2=	0.002221	
fs2=	48.6	ksi
Cc=	379	kips
Fs1=	-258.8	kips
Fs2=	239.1	kips
Pn=	359.7	kips
Mn=	481	ft-kips

Point E

Z=	-4	
εs1=	-0.0067	
fs1=	-48.6	ksi
c=	4.92	in
a=	4.10	in
εs2=	0.001898	
fs2=	48.6	ksi
Cc=	268.3	kips
Fs1=	-258.8	kips
Fs2=	239.1	kips
Pn=	248.6	kips
Mn=	444.8	ft-kips

Point F

Pnt=	-518	kips

Calculated by: Rachel Howser | Foundation Design | 1/4

Date: 05/06/2013

Material Properties

fc'=	30	MPa
fc'=	4351	psi
fy=	335	MPa
fy=	48588	psi

Footing Geometry:

b1=	1525	mm	b2=	900	mm
b1=	60.0	in	b2=	35.4	in
Thick.=	500	mm			
Thick.=	19.7	in			

Footing Loads:

Axial=	162	kN
Axial=	36.5	kips
Column=	179.22	kN
Column=	40.29	kips
Footing=	27.4	kN
Footing=	6.16	kips
Factored Pressure=	1.2(Dead Load)/b^2	
Factored Pressure=	0.190	kPa
Factored Pressure=	3.98	ksf

Check Two-Way Shear

Cover=	76.3	mm
Cover=	3.00	in
Average d=	(Thickness)-(Cover)-(#10 diameter)	
Average d=	415.7	mm
Average d=	16.37	in
Vu=	(Factored Pressure)(Critical Shear Area)	(ACI 11.11.1.2)
Vu=	300	kN
Vu=	67.4	kips
b0=	4(b+d)	
b0=	3463	mm
b0=	136.3	in

ϕVc(1)= $\phi 6\sqrt{f_c'}b_0 d$ (ACI 11-31)

ϕVc(1)= 662 kips

ϕVc(2)= $\phi\left(\frac{20d}{b_0}+2\right)\sqrt{f_c'}b_0 d$ (ACI 11-32)

ϕVc(2)= 486 kips

ϕVc(3)= $\phi 4\sqrt{f_c'}b_0 d$ (ACI 11-33)

ϕVc(3)= 442 kips

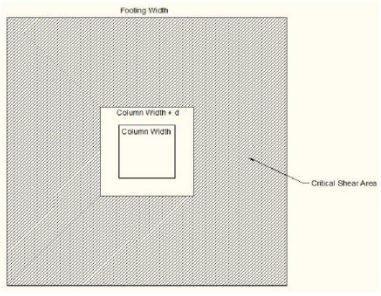

ϕVc(min)= 442 kips Footing is thick enough by: 85%

ϕVc(min)= 1964 kN

Check One-Way Shear

Vu=	(Factored Pressure)(Critical Shear Area)		
Vu=	35.4	kN	
Vu=	7.9	kips	
ϕVc=	$\phi 2\sqrt{f_c'}bd$		
ϕVc=	97.2	kips	OK
ϕVc=	432	kN	
ϕVc=	57.4	kips	OK
ϕVc=	255	kN	

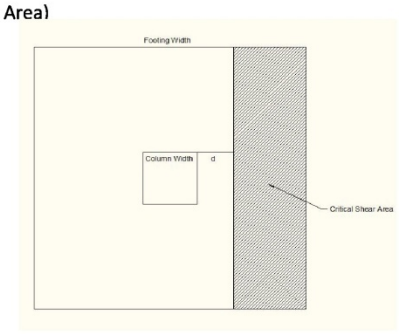

Check the flexural reinforcement

Mu=	(Factored Pressure)(Critical Height)(Critical Width)^2/2		
Mu=	30.9	kip-ft	
Mu=	41.9	kN-m	
j=	0.9	(Assumption)	
ϕ=	0.9	(Assumption)	
As=	$\frac{M_u}{\phi f_y jd}$		
As=	0.58	in^2	
As=	372	mm^2	
As (min)=	0.0018bh	(ACI 7.12.2.1)	
As (min)=	2.13	in^2	
As (min)=	1373	mm^2	

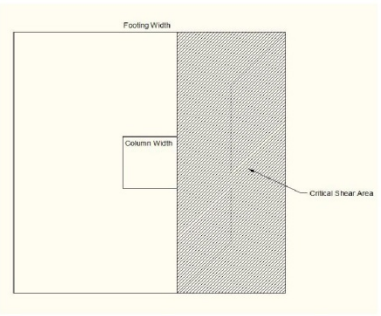

As=	2.13	in^2	(Max of As and As(min))
As=	1373	mm^2	
Max Spacing=	18	in	(ACI 7.12.2.2)
Max Spacing=	457	mm	
Use:	7	25	Bars in Each Direction
As=	5.33	in^2	OK
As=	3436	mm^2	
Spacing=	8.48	in	OK
Spacing=	216	mm	
a=	$\frac{A_s f_y}{0.85 f_c' b}$		
a=	1.165	in	
a=	30	mm	

a/d=	0.0712		Tension Controled
Mn=	$A_s f_y \left(d - \frac{a}{2} \right)$		
ϕMn=	306.3	kip-ft	OK
ϕMn=	415.3	kN-m	

Check the development length

Bar Length=	54.0	in	
Bar Length=	1372	mm	
β=	1	(Uncoated Reinforcement)	
λ=	1	(Normal Weight Concrete)	
ld=	$54.8 d_b \beta\lambda$		
ld=	53.937008	in	OK
ld=	1370	mm	

Design Column-Footing Joint

Bearing

A1=	313.9	in^2	
A1=	202500	mm^2	
A2=	2127	in^2	
A2=	1372500	mm^2	
Max Allow Bearing=	1509	kips	
Max Allow Bearing=	6713	kN	
Bearing=	99.5	kips	No Dowels Req'd for Bearing
Bearing=	443	kN	

Moment

Provide the same bars required in column. Determine development length.

ldh=	$\frac{0.02 f_y \beta\lambda}{\sqrt{f_c'}} d_b$		
ldh=	14.5	in	
ldh=	368	mm	
Factor=	0.56	(90 deg hook w/ adequate cover and stirrups)	
ldh=	8.12	in	
ldh=	206	mm	
distance available=	10.43	in	OK
distance available=	265	mm	

Design Location of Lift Points

Check to see if lift points can be added anywhere

Calculate cracking load

Mcr=	$\frac{f_r I_g}{y_t}$		
fr=	$7.5\sqrt{f_c'}$		

$7.5\sqrt{f_c'}$

fr=	494.73	psi
fr=	3.41	MPa
Ig=	38165	in^4
Ig=	0.0158854	m^4
yt=	9.84	in
yt=	0.25	m
Mcr=	159.9	k-ft
Mcr=	216.7	kN-m

Calculate maximum possible moment in section

Weight of Section=	6.16	k
Weight of Section=	27.4	kN
M (max)=	7.70	k-ft
M (max)=	10.45	kN-m

Since the maximum moment is less than the cracking moment, hooks can be placed anywhere.